2016

An investigation of skin tribology phenomena involved in tactile communication through braille and its associated psychophysical response during task-based discrimination

Matthew Aguirre Darden
Iowa State University

An investigation of skin tribology phenomena involved in tactile communication through braille and its associated psychophysical response during task-based discrimination

by

Matthew Aguirre Darden

A dissertation submitted to the graduate faculty

in partial fulfillment of the requirements for the degree of

DOCTOR OF PHILOSOPHY

Major: Mechanical Engineering

Program of Study Committee:
Christian J. Schwartz, Major Professor
Wei Hong
Adarsh Krishnamurthy
Seda McKilligan
Sriram Sundararajan

Iowa State University

Ames, Iowa

2016

DEDICATION

To my wife, Ellie, for her unending support, words of encouragement, patience and loving spirit that carried me every step of the way; and to my parents, Robert and Liz Darden, for their constant prayers and for instilling in me the will and drive to accomplish whatever I set my mind to.

TABLE OF CONTENTS

ACKNOWLEDGMENTS

I would like to extend my sincerest thanks to my committee chair, advisor, and mentor Dr. Cris Schwartz for all the guidance, wisdom, and advice he has shared with and taught me throughout my entire academic career. This dissertation would not be possible without him.

I would also like to thank my committee members Dr. Wei Hong, Dr. Adarsh Krishnamurthy, Dr. Sriram Sundararajan, and Dr. Seda Yilmaz for the time and willingness they have extended to help with my research endeavors.

I would also like to acknowledge my fellow INNOMAT colleagues Geetha Chimata and Mark Placette for their counsel and companionship throughout this journey; my collaborator Dr. Rob West from the Department of Psychology; and the Mechanical Engineering Department staff who were always willing to assist me: Deb Schroeder, Neely Lehman, Taylor Shire, Joel Buehler, and Craig Severson.

Finally, I want to thank the rest of my friends and family, all of whom have encouraged and pushed me to finally reach my goal.

ABSTRACT

Most individuals utilize all five senses, especially their sense of sight, to create a unique sensory experience depicting the surrounding environment. Unfortunately, individuals in the blind and visually impaired (BVI) community lack the sense of sight and rely primarily on tactile means to acquire valuable or potentially vital information, leading to the advent of tactile communication methods like braille. A key challenge in controlling the haptic experience of a surface is the lack of fundamental understanding of how various surface attributes, such as friction and texture, affect the tactile response. Oftentimes, braille users experience tactile confusion when scanning complex tactual codes such as tactile graphics or advanced mathematics commonly seen in the STEM fields, but coding standards and limitations in perceptive resolution reduce the opportunity for innovating or redesigning the language to aid the reader.

This dissertation aims to address confusion in tactile information transfer by identifying, characterizing, and developing an understanding of the skin-surface contact interactions experienced during braille reading in order to promote innovations in surface engineering and material design that can improve existing tactile communication methods. The authors first propose a method to directly observe an individual's cognitive response to tactile experiences through an "oddball paradigm" discrimination task using event-related potential (ERP) via electroencephalography (EEG), a technique that is common in visual and auditory psychological sensory studies. Results indicate that varying levels of friction and roughness from textured samples (i.e. sandpaper) elicit different magnitudes of cognitive activity, suggesting that this technique may prove to be a valuable tool in identifying and understanding the root causes of tactile confusion.

The second aspect of the research seeks to characterize the fundamental frictional forces that occur during braille reading by investigating the loading interactions as the fingerpad slides over a single braille dot and then progressively increasing the complexity of the topographies (i.e. dot spacing, orientation, count). Derived from Greenwood and Tabor, the authors develop and propose a multi-term friction model that predicts the adhesion and deformation frictional effects of a single feature during skin-on-dot sliding, identifying deformation as the dominant friction mechanism when a soft body slides over a spherical geometry. Incorporating both computational modeling and large-scale tribological tests under displacement-controlled sliding further decomposes the frictional loading mechanisms showing that surface tension and compression are driven by the elastic material's Poisson effect dependent on the bulk's position with respect to the dot feature. Here, loads in the vertical direction are governed by bulk material deformation due to contact pressure and loads in the lateral direction are governed by bulk material deformation due to both contact pressure and frictional shear.

CHAPTER 1: GENERAL INTRODUCTION

1.1 Motivation

The sense of touch is one of the most fundamental ways that individuals interact with their surrounding environments. Through tactile perception, objects are handled, manipulated, and interacted with; and these interactions provide components of necessary information to the user. Whereas touch is a single mode to acquiring information, it is not necessarily the most efficient avenue for information transfer. In addition to touch, each of the other senses such as sight, smell, hearing, and taste complement and assist one another, utilizing all sensory information in order to process and create a single experience. Unfortunately, some individuals are unable to make use of one or more of these senses, and this impairment can drastically affect the means with which one can acquire valuable or potentially vital information.

In the United States, approximately 1 out of every 5 citizens is afflicted by some form of physical or mental disability, and such disabilities have the potential to adversely affect one's quality of life in general, as well as his/her level of productivity when it comes to societal contributions and employment opportunities. In the blind and visually impaired (BVI) community, it is often the case where a non-sighted person may equal or surpass the intellectual performance of a sighted person, but such a disability presents challenges that the BVI population must overcome in order to compete with sighted individuals. Among BVI persons between the ages of 21-64, less than 45 percent held employment opportunities [1]. These challenges are even more prevalent in academic and employment areas that heavily rely on the visual domain, such as the science, technology, engineering, and mathematics (STEM) fields. Studying equations, graphs, charts, and images may be trivial for sighted individuals, but the BVI population must rely on less efficient tactile and auditory cues to acquire the exact same information. One of the most direct

ways that BVI individuals have access to written information is through the tactile system of Braille. Unfortunately, content-rich scientific graphics and complex mathematical equations are not easily reproduced and conveyed in a tactile manner such as Braille.

Assistive technologies in the BVI and tactile domain in general, are constantly changing and being further developed, but this approach is not systematic in execution. Little is known in the ability to identify and quantify the fundamental tribological interactions in skin-on-surface sliding, and further research must be pursued in order to truly develop, design, and engineer surfaces to more effectively provide and convey information through tactile means.

The following dissertation aims to better understand and characterize the tribological interactions of skin friction and skin-on-feature topographies in order to present an opportunity in advancing surface engineering and technologies that employ varying forms of tactile communication, particularly beneficial to the blind and visually impaired community.

1.2 Literature Review

1.2.1 Tactile perception and the somatosensory system

Perception is one of the most intriguing and complex aspects when examining human interactions with the outside world. Generally, perception is multimodal, where each of the five senses contributes to a single experience. Most often, visual and tactile cues cooperate in tandem, where the experience from one sensation affects the other [2].

Psychologists have been investigating the somatosensory system for decades, but from an engineering standpoint, little is known on how tribology and surface science contribute to the neural responses from tactile stimuli. Fundamentally, human anatomy governs how the brain interprets tactile information, but that is only one component in tactile interaction. Objects we come into contact with as well as environmental factors in general will further influence these

tactile signals the brain receives. Ultimately, one needs to consider what mechanisms within tactile interactions dominate perception. From a design perspective, what surface or mechanical properties affect how a product is perceived? From a communicative perspective, what information can be conveyed through tactile means, and how can this information be applied?

Skin is the largest organ in the human body and is the foundation of the sense of touch. Throughout its surface, skin is covered with a wide array of sensory receptor neurons, or afferent neurons. These afferents interpret all forms of tactile stimuli such as vibration, texture, temperature, or pain. Upon reception, these signals are encoded and transferred to the somatosensory cortex in the brain through a process called stimulus transduction. Mechanoelectric transduction is the predominant form of tactile perception where mechanical energy of a stimulus is detected by a sensory receptor and converted to electrical potential. The stimulus energy can occur in two forms: during heat transfer, or more commonly during skin displacement or deformation; and both forms cause the receptors to produce and transmit an electrical nerve impulse to the brain [3]. But in order for the stimulus to be recognized, the magnitude of the intensity must be large enough for the receptors to be activated.

Intensity thresholds vary for each person and even between different regions of the body for the same individual. Dating as far back as the 1950's, researchers have been investigating how somatosensory stimuli affect regional sensitivities, specifically with respect to warmth sensation compared to pain thresholds. Applying these thermal stimuli to varying sites such as the forearm, forehead, and back proved that each site is unique in its receptive behavior, and that each region exhibits resolution uniqueness across the pain threshold spectrum [4-8]. These studies further concluded that for low intensity stimuli, regional sensitivities greatly vary, but as intensity

approaches the pain threshold, regional sensation resolution and threshold uniqueness diminishes significantly.

In addition to thermal stimuli, mechanoreceptor afferents more frequently respond to skin displacement and deformation caused by skin-surface interactions. But instead of being limited by intensity magnitudes, the detection of skin displacement is more hindered by spatial resolution and afferent density, with respect to anatomical region. To investigate this avenue, studies have explored limitations of surface feature detection in relation to spatial resolution. Research examining these limitations tends to focus on object handling and surface perception, and consequently, it is more common for investigators to examine tactile sensitivities of skin on the hand and finger pad. Spatial resolution studies such as those by Van Boven et al. or Vega-Bermudez et al. have employed surfaces like mesh gratings and embossed letters of varying sizes in order to determine the skin's ability to discriminate between unique features. Each of these discrimination studies agreed with one another and concluded that for detection resolutions, feature spacing of at least 1.0mm was required in order for the two features to be determined as unique [9-11]. Subsequently, Van Boven et al. went on to perform a similar mesh study to determine if there is a significant difference in tactile acuity of blind subjects compared to sighted ones. Fascinatingly, the data showed that the blind subjects exhibited greater sensitivity to finer gratings, being able to detect sizes as small as 0.8 mm, leading one to conclude that blind subjects are able to adapt and hone the acuity of one sense (touch) to compensate the lack of another (sight) [10].

While it is known that afferents in the skin are sensitive to both heat transfer and skin deformation, studies have discovered that not all afferent neurons are identical, where certain types only respond to specific forms of stimuli. Four unique classes of mechanoreceptors have been recognized in different parts of the human skin: slowly adapting (SA) I and II, rapidly adapting

(RA), and Pacinian corpuscles (PC). Techniques such as microneurography allow researchers to observe mechanoreceptor responses under tactile stimuli such as embossed letters or even braille characters. According to such investigations, SAI afferents are the most significant contributors to form perception, pattern recognition and spatial resolution [11-14]. RA afferents were found to detect form to a much lesser degree than that of SAI, but have been found to be responsible for detection of stick-slip on the skin. It should be noted that each of these receptor's acuity is dominated by static stimulation, or bulk deformation of the skin. SAII and PC bundles exhibit noisy behavior under static stimuli, and they likely play little role in spatial resolution and form detection; but like the rest, have their own distinct purposes. SAII receptors respond to skin deformation and stretch, but this has not been directly correlated to form perception. This is suspected to occur due to their low afferent density, for if the nerve bundles are coarsely scattered, their spatial resolution is not fine enough to detect small scale deformations. Lastly, oscillatory stimuli in humans, as well as monkeys have shown that deep tissue nerve endings, namely PC afferents, have been shown to respond greatly under high frequency vibration [15].

While the PC afferents are largely responsible for interpreting vibrational stimuli, research has shown that such vibrations, depending on frequencies and amplitudes, can drastically affect the behavior of the other afferents. Gescheider et al. and Manfredi et al. used oscillatory apparatus to apply localized vibrational stimuli to subjects' finger pads to observe the relationship between input frequencies and afferent response for each of the classes [16, 17]. They found that a vibrational stimulus of approximately 200-300 Hz, the resonant frequency of skin and maximum sensitivity of Pacinian corpuscles, generates wave propagation throughout the skin which radically enhances afferent perception and sensitivity. This heightened sensitivity effectively desensitizes

the other afferents by making them highly susceptible to noisy inference and inhibits their ability to perform their default functions.

Anatomically, the somatosensory system is highly complex, and it depends on multiple receptors located throughout the skin that each performs specific functions. As seen above, intensity thresholds and deformation sensitivities play major roles in how the body interprets tactile signals from the outside world. Under certain conditions, the receptors can interfere with one another, further hindering an individual's tactile acuity. Such biological unpredictability presents significant problems for researchers who aim to develop models that effectively predict somatosensory behavior, yet a tactile system consists of two components: the subject, and the object or surface in contact with the subject. While the subject may be highly variable, the opposing surface has finite properties and parameters. If tribological conditions remain constant, a given surface should elicit the same tactile perception in a repeatable manner for a given individual. This statement is ideal when it comes to product design, but to effectively employ this tactic, the skin-surface interaction must be quantitatively characterized.

1.2.2 Tribology and mechanical properties

To successfully understand how a surface affects tactile perception, it is essential to understand the fundamental tribology of how two surfaces interact with one another during contact and sliding. In the 1960's, Greenwood and Williamson developed one of the foundational models to predict basic surface-on-surface contact behavior. Here, the theories focus on interactions between nominally flat surfaces, and these surface interactions are described at the microscopic level. One major assumption this theory makes is that these surfaces are not in fact flat, but that they are composed of rigid asperities of certain heights and radii of curvature. During the contact of two surfaces under normal loading, asperities on both faces will contact one another, and

adhesive forces will generate secondary bonding at each asperity interface. Once motion commences, these bonds will resist said motion, producing a tangential resistive force. Eventually, the secondary bonds will break due to the input sliding force exceeding the bonding strength, but they will reform once a new interface is formed. This process repeats indefinitely until either sliding stops, or the surfaces are removed from one another. The coefficient of friction (COF) between two surfaces sliding against one another is largely dependent on contact area created at the interface [18]. The main issue that arises from the Greenwood-Williamson model is that the only frictional component considered is due to material adhesion because it is also assumed that asperity deformation does not occur.

The Greenwood-Williamson framework has been expanded upon as more complexity is considered. One major addition is that there are in fact two contributors to the resulting coefficient of friction: an adhesion term, as well as a deformation component. Chang et al., and eventually others such as Horng et al. have iteratively derived frictional models further incorporating the intricacies of asperity adhesion as well as elastic and plastic deformation during the sliding of rough surfaces in contact [19, 20]. These models assume that asperities adhere to one another and deform during sliding. The deformation recovery that follows bond breakage exhibits hysteretic behavior that contributes to shear forces between surfaces. In the case of polymeric materials, Chernyak et al. theorized that adhesive linkages formed between chain ends and solid materials exhibit viscoelastic behavior and deform before breaking [21]. Each of these theories is tremendously important when it comes to applications involving highly polished surfaces such as low-wear bearings, but this sort of material design focuses on surface science at the microscopic level. In this case, COF between any two materials would be independent of any macroscopic features or texture applied to a surface. Consequently, these models are not valid approaches to

modeling the sliding interaction of skin across textured surfaces with complex geometries, and one must assume that models for larger-scale macroscopic surface features must be investigated.

1.2.3 Skin tribology and the influence of friction on perception

In order to be able to model skin-surface interactions, and eventually perception, tribologists have been performing investigations to determine which surface parameters are important in understanding skin-surface coefficient of friction. As noted by Greenwood, Williamson among others, the coefficient of friction is dependent on surface asperity adhesion as well as their deformation, and these are governed by the total contact area created at the sliding interface. Of note, these assumptions only applied to contact of hard sliding counterfaces, but studies performed by Han et al. investigated the question whether coefficient of friction is dependent on contact area in the case of a soft body sliding over a smooth, rigid surface. By observing the total contact area of a sliding human fingerpad at different sliding angles (and in turn contact area), two conclusions were drawn from this study. Firstly, Han's work remains consistent with data that show the inverse relationship between normal loading and coefficient of friction [22], notably for skin on rigid surfaces, and has since been validated by other investigators [23-26]. Secondly, this confirms that the Greenwood-Williamson theory of contact area and adhesion governing COF also applies to skin, and by extension similar elastomers [23, 27]. But simply modeling skin as a soft bulk sliding over a smooth surface is insufficient in determining the tactile effect of macroscopic surface properties.

Coefficient of friction is believed to be a major contributor to perception, but to this point, it has been exclusively governed by contact area and molecular adhesion. Each of these can be quantified, but only on the microscopic level. The next step is for research to observe how skin behaves as a deformable solid during interactions with macroscopic surface topographies. It is

believed that in addition to the adhesive mechanism of friction playing a major factor in the coefficient of friction on soft body sliding, soft body deformation and hysteresis contribute to frictional interactions as a soft bulk slides over and conforms to macroscopic surface features [28, 29]. To investigate such, the topographies must be easily quantifiable so that these interactions can be properly measured and evaluated. One of the simplest textures with which to identify geometric parameters for contact behavior is a series of ridge and groove combinations. Several studies have been performed to investigate the role of these surface features on friction. Independently, Taylor et al. and Bobjer et al. investigated textured aluminum samples with predefined ridge and groove parameters and compared their coefficients of friction to a subject's perceived roughness of the sample. For the tests, sliding always took place perpendicularly to the ridges, but based on the data acquired, neither found a correlation between the measured COF and perceived roughness. Incidentally, the feature dimensions, more specifically the groove widths, of each sample played a significant role in affecting perceived roughness. Larger groove widths permitted increased fingertip penetration, and thus increased perceived roughness. Increased ridge widths, or land surface, yielded smoother perceptions [30, 31]. Bobjer complemented his "dry surface" experiment by repeating it with lubrication, to better understand how films and contaminants affect COF and perceived roughness. This inclusion applies findings from others such as Sivamani et al., Gitis et al., and Gwosdow et al. who discuss the importance of environmental control in frictional sliding, for moisture and the environment as a whole can greatly impact surface-surface contact, especially when considering skin tribology mechanics [32-35]. For lubricants and contaminants, Bobjer included the likes of human sweat, paraffin oil, glycerol, and lard. Each of the environmental conditions were compared to a control dry condition, and like with Taylor's

experiment, subjects were asked to express their level of discomfort with respect to each of the textured samples under each condition.

Based on Bobjer's ridge/groove lubrication study, surface quality can be implemented to greatly impact coefficient of friction, as well as perceived coarseness. Dry sliding on smooth surfaces facilitates the largest contact area, and therefore the highest coefficient of friction as opposed to motion over a textured surface. But the introduction of a lubricant reverses this effect entirely. Film build-up between skin and the surface prevent the surface from drawing close to one another, minimizing contact area and negating adhesive bonding. This effect was observed for all textured samples, where the secondary governing factor was still the groove spacing parameter. Alternatively, sweat created stick-slip situations that in fact increase coefficient of friction when compared to a "dry" normal condition [31]. Smith et al. hypothesize that increased groove and ridge spacing independently activate the mechanoreceptors discussed in the previous section. This combination of high-amplitude, low-frequency stimulations activate the different afferents in the skin and produce necessary vibrotactile signals that the brain interprets as perceived roughness [36]. These findings are instrumental for designers concerned with applications involving grip, where there is a greater chance of introducing contaminants into the system. If friction needs to be maximized but contaminants may be likely, the surface must be designed to account for this to ensure that functionality will not be compromised.

The above studies are extremely important for the conclusions they have drawn, and the contributions they offer to the industry. However, they are somewhat limited in scope when it comes to their applicability, as well as the tactile attributes considered. In the realm of polymer manufacturing, one of the most prominent skin-polymer interactions is with that of polymer textiles [37-41]. Textiles and fabrics are used in myriad applications and are encountered in

countless situations each day. Materials such as automotive interiors, athletic apparel, or medical grade gauze and wrapping all are all designed for a specific tactile purpose, be it to emulate more expensive material, wick away sweat while remaining comfortable for the user, or to minimize abrasion and protect an individual's skin. Some of these design goals are objective, such as ensuring consumer health and minimizing adverse effects [42], but frequently, assessment of a product is highly subjective and uniquely dependent on the user. The iterative design process requires that subjective issues can be clearly defined and normalized among evaluators so that while their opinions may be different than one another, acquired data will be useful to assess a product's reception as a whole.

In the 1970's, Herbert Stone developed an evaluation technique called Quantitative Descriptive Analysis (QDA), and while it was originally designed for food and flavor assessment, it has subsequently been applied to a multitude of sensory evaluation studies. This technique employs a panel of experts who are familiar with a specific class of product that convenes to identify a set of attributes/descriptors to be appraised. These experts explicitly define each attribute with an agreed upon meaning as well as "high" and "low" values for each descriptor. If required, these attributes may then be used to train additional evaluators for larger sample populations [43]. This technique then establishes a quantitative scale that researchers can use to collect subjective data that would otherwise be unquantifiable. With QDA, a product's softness, abrasiveness, degree of prickle, etc. can then be accurately evaluated for a large sample population and statistically examined to further benefit sensory analysis.

This ability to quantify sensory attributes has further driven researchers to investigate the relationships between a product's material and surface properties and the tactile descriptors that it elicits, particularly in the realm of textile-based products. Darden et al. investigated the role of

coefficient of friction of fingertip sliding on a wide spectrum of polymer fabrics and how it affected four tactile attributes that each of the samples provoked [44]. Considering materials such as nylon-6, velvet, satin, and various weaves of cotton, tactile descriptors such as abrasiveness, slipperiness, fuzziness, and sensible texture were all evaluated. While a specific relationship between any of the attributes and measured coefficient of friction was not found due to statistical insignificance, the sample evaluators maintained consistency with one another across all four descriptors. And this proved that when applied correctly, QDA can effectively quantify sensory descriptors. Bertaux et al. performed a different study specifically examining the effect of sock composition on the wearer's comfort level during physical activities such as running or hiking. In addition to subjectively monitoring the subjects' comfort level, coefficients of friction were measured in a skin-sock simulator (much like Derler [38]), and environmental conditions such as moisture level and temperature were monitored as well. From the study, it was concluded that coefficient of friction is inversely related to the user's comfort level, and this could be controlled by modifying the socks' fiber content [45]. This study is a perfect example showing that when analysis techniques are correctly integrated with one another, sensorial, physiological, and design aspects can all be implemented to benefit one another in the optimization process.

1.2.4 Tactile communication

It is widely known that interacting with surfaces through tactile means can produce any number of sensory perceptions. A less obvious role of the somatosensory system is that it is vital in receiving tactile information that the brain would not be able to otherwise acquire. Sometimes, there are situations where visual or auditory cues are unavailable, and tactile means are required to convey specific information to the user. For example, cellular phones implement vibrational feedback to alert the user that a call is incoming; number pads on touch-tone phones and television

remotes provide location information so users can manipulate them in dark environments; and toggle buttons on electronics extend and depress to inform the user of its current state, whether activated or deactivated. Each of these design considerations were employed for a specific purpose, and to provide the user with a degree of convenience.

One of the most common and vital areas where tactile communication is essential relates to those who are blind or visually impaired (BVI), for these individuals rely entirely on their senses of hearing and touch to decode their environment. Where sighted individuals receive written language through visual text, BVI individuals read through their means of touch, via the tactile language, braille. It is understood that the BVI use their hands and fingers to perceive and decode braille, but there have been and continue to be research studies that investigate what exactly is occurring in the somatosensory system of the BVI, and what that allows touch to compensate for and completely replace the sense of sight. Phillips et al. first discovered that the SA1 mechanoreceptors and Merkel-cell end organs are the main contributors in one's ability to distinguish spatial form, and they investigated the use of braille cells to prove this. These receptors permit the fingertips to perceive the number and orientation of the dots involved, and the brain can then discriminate between individual braille patterns and interpret them into the intended meaning [13]. As previously mentioned, individuals who experience early onset blindness have been shown to adapt and eventually exhibit greater tactile acuity in these receptors [10].

Subsequent investigations have revolved around limitations of braille, and factors that impact an individual's reading rate and rate of comprehension. Individuals of all ages can become blind for any number of reasons, and regardless of age, that individual must eventually learn to read braille. Based on the user's experience, there are in fact many methods to reading braille. Inexperienced readers may use only one finger at a time, and slowly pan across the characters, or

more experienced readers may use two hands simultaneously, allowing him or her to perceive and comprehend the text at a faster rate. Davidson et al. performed a study to learn how braille reading proficiency specifically affected haptic scanning, and in turn, one's reading rate [46]. For the tests, subjects were asked to read simple, low-level sections of prose, as well as more complex and higher-level sections. All the while, the author recorded the subject's hand movements, noting moments where the subject pauses on certain cells. The scanning method implemented was also observed. Interestingly, the methods used throughout the subjects varied drastically. Some used a single hand, while others kept their left and right fingers together during scanning, or both hands scanning cells independently. It was also observed that lower proficiency readers tended to rely solely on the right hand when compared to those of higher proficiency, and they also paused on certain cells more often. Higher proficiency readers preferred to scan the text with both hands, but that tandem did not increase the individual's reading rate. The results from this study draw attention to the fact that the manner of reading braille varies widely among subjects, and becoming more proficient can only help so much in optimizing reading rates and the quality of information acquisition.

In accordance with Carver's definition of reading as "the process of looking at visually presented words, letters, or other language symbols to gain information or knowledge" [47], Wetzel et al. investigated both print and braille reading rates based on individual tasks: oral reading, silent reading, and studying [48]. For oral reading, the subject was timed as he/she orally presented the information read; for silent reading, the subjects were told to read to themselves, and afterwards were requested to recall the narrative; and for studying, the subjects were primed in advance and given as much time as needed to read and learn the material. As expected, the print readers completed the tasks more quickly than the braille readers in all three categories, but

between tasks, both print and braille readers adjusted their rates according to the tasks requested. The rates for silent reading task increased for subsequent trials because the subject had been cued for the summary at the end, and the rates for studying subsequently decreased, for they too knew what to expect for future trials.

Two extremely important conclusions can be drawn from this study. Firstly, and most glaring, braille readers are unable to keep pace with sighted individuals when comparing information transfer and reading rates. This disparity places BVI individuals at a competitive disadvantage when it comes to obtaining any form of written information, and it would become even more disparate when introducing complex content such as that found in the science, technology, engineering, or mathematics (STEM) fields. Secondly, reading rate procedures used by researchers such as Wetzel et al. are quite subjective and noisy, and simply measure reading rate without any method to truly observe and measure one's reading comprehension.

1.2.5 Quantifiably observing neural activity and perception

In order to circumvent latency issues such as those experienced by Wetzel, researchers have gravitated to directly observing stimuli-based neural activity using several different imaging techniques. Some common techniques to observe neural activity are functional magnetic resonance imaging (fMRI), positron emission tomography (PET), and electroencephalography (EEG), and each technique has its own benefits and drawbacks.

Functional magnetic resonance allows researchers to look "inside" the brain, through the implementation of magnetic fields to observe blood flow throughout. When areas of the brain are activated, highly oxygenated blood flows to those regions, and the machine detects the high oxygen levels, displaying which specific locations of the brain are being used. This technique is

entirely noninvasive, making it preferable patients of extreme ages, or those who may require special assistance. Unfortunately, fMRI does not detect measure the magnitudes of neuronal activity or how many are actually firing, only the specific location based on oxygenated blood flow [49].

Using positron emission tomography is drastically different than that of fMRI, but it is functionally similar. For this imaging technique, a patient is injected with a radioactive chemical, or tracer. This tracer, sometimes glucose, is attracted to cells that are using a lot of energy, such as cancer cells. When it comes to neuroscience, PET can also be used to observe blood flow throughout the brain because glucose is drawn toward freshly oxygenated red blood cells. This technique is commonly used in diagnosing conditions such as epilepsy, stroke, or dementia, but it is gradually becoming incorporated to somatosensory observation. Unlike fMRI, PET is highly invasive for other reasons in addition to the tracer. It can also be extremely time consuming, and may require the patient fast or remain inactive for periods of time prior to examination [50].

When it comes to implementing neural imaging for the purposes of investigating tactility and perception, very little has been studied, but this field will grow once the usefulness of these techniques for somatosensory applications becomes more widespread. Using PET, Sadato et al. discovered a very perplexing aspect of the human brain. He was interested in observing the neural behavior in sighted and braille reading blind subjects as they performed tactile discrimination tasks [51]. The tasks called for the subject to determine whether two stimuli exhibited identical features such as width, angle, or specific character pattern. During these tests, the subject's brain activity was monitored by a PET device. The data showed that for the blind subjects, the discrimination tasks elicited an increase in regional cerebral blood flow (rCBF) in the primary visual cortex, whereas a decrease of rCBF was shown for the sighted individuals.

This suggests that for blind subjects, the visual cortex, which is primarily reserved for visual cues, may be activated by other sensory modalities, and can promote nonvisual functions It should be noted that each of the blind subjects experienced early onset blindness and the visual cortex activation was not as a result of the individual generating mental imagery in response to the tactile stimuli. This is very important in recognizing the plasticity of the brain and its ability to adapt for further sensory learning. PET is very useful in determining which parts of the brain undergo the most activation, but one drawback with it is that it does not show exactly what sort of activity is occurring, just simply the use of (in this case) the somatosensory system to some capacity.

The technique that shows the most promise with respect to somatosensory observation is a modified form of EEG called event-related potential (ERP). It is used to observe specific neural responses to an applied sensory, cognitive, or motor stimulus. This method allows researchers to apply a given stimulus and observe the desired neural responses in real time. Langley et al. implemented ERP to observe the temporal stamp of familiarity and recognition due to visual cues [52]. As of now, little to no research has focused on investigating real-time neural responses with respect to tactility and skin tribology. It would greatly benefit the field to incorporate this technique to show that the brain's somatosensory response to skin tribology can be monitored in real time, temporally identifying an individual's moment of tactile perception, discrimination, and recognition.

1.3 Research Objectives and Dissertation Organization

1.3.1 Research Objectives

The research work for the dissertation was conducted to address several of the above issues. The overall objectives of this research were:

1. To investigate the ability to measure and observe human psychophysical response to tactile stimuli in order to understand how the skin's tribological interactions affect perception.

2. To characterize the fundamental tribological interactions and skin friction involved in reading the braille language, namely the impact of a single braille feature on that of coefficient of friction of skin sliding during braille reading.

3. To develop and propose a multi-term frictional model that predicts the adhesion and deformation frictional effects of a single spherical feature during skin-on-dot-sliding.

4. To determine the frictional effects of simple braille characters (a dot pair's orientation and spacing) on skin-on-braille coefficient of friction.

5. To validate empirical skin-on-braille and large-scale tribometer testing with computational modeling in order to predict both the loading and frictional behavior of more complex skin-on-dot tribological interactions.

6. To compare the tribological behavior and topographical parameters of perceptively unique and like tactile graphics to develop an association between tactility and surface engineering.

1.3.2 Dissertation organization

The chapters in this dissertation are organized according to the chronological order in which the experiments were conducted. Chapter 2 presents the work relevant to research objective '1'; Chapter 3 discusses the work relevant to objectives '2'-4'; Chapter 4 builds on research objective '2' and more specifically addresses objective '5'; and the work in Chapter 5 pertains to research objective '6'. Specifically, Chapter 2 investigates the viability of implementing

electrophysiological techniques (commonly used in the psychology domain) to monitor and detect tactile perception and its relationship to simple tactile stimuli. Chapter 3 investigates the tribological interactions of skin-on-braille sliding (and the effect of feature spacing on coefficient of friction) and proposes a multi-term model to describe the frictional behavior and tribological interactions within. Chapter 4 both computationally and empirically validates the behavior observed in Chapter 3 through the implementation of a large-scale representation of a finger sliding on a braille dot feature. Chapter 5 investigates the effect of surface topography and tribological interactions on tactual exploration of tactile graphics. Chapter 6 summarizes conclusions from all the different studies described in this dissertation as well as discusses potential directions for future work.

1.4 References

[1] United States. Bureau of the, C., Disabilities affect one-fifth of all Americans proportion could increase in coming decades. Disabilities affect one fifth of all Americans. 1997, Washington, D.C.]: Washington, D.C. : U.S. Dept. of Commerce, Economics and Statistics Administration, Bureau of the Census.

[2] Touch and blindness : psychology and neuroscience / edited by Morton A. Heller and Soledad Ballesteros, ed. M.A. Heller and S. Ballesteros. 2006, Mahwah, N.J.: Mahwah, N.J. : Lawrence Erlbaum Associates.

[3] Pfaff, D.W., Neuroscience in the 21st Century. 2013: Springer Science+Business Media, LLC.

[4] Kojo, I. and A. Pertovaara, The effects of stimulus area and adaptation temperature on warm and heat pain thresholds in man. International journal of neuroscience, 1987. 32(3-4): p. 875-880.

[5] Stevens, J.C., L.E. Marks, and D.C. Simonson, Regional sensitivity and spatial summation in the warmth sense. Physiology & Behavior, 1974. 13(6): p. 825-836.

[6] Yarnitsky, D. and J.L. Ochoa, Warm and cold specific somatosensory systems. Psychophysical thresholds, reaction times and peripheral conduction velocities. Brain : a journal of neurology. 114 (Pt 4): p. 1819.

[7] Yarnitsky, D., et al., Heat pain thresholds: normative data and repeatability. Pain, 1995. 60(3): p. 329-332.

[8] Kenshalo, D.R., T. Decker, and A. Hamilton, Spatial summation on the forehead, forearm, and back produced by radiant and conducted heat. Journal of Comparative and Physiological Psychology, 1967. 63(3): p. 510-515.

[9] Van Boven, R.W. and K.O. Johnson, The limit of tactile spatial resolution in humans: grating orientation discrimination at the lip, tongue, and finger. Neurology. 44(12): p. 2361.

[10] Van Boven, R.W., et al., Tactile spatial resolution in blind Braille readers11EDITED BY THOMAS J. LIESEGANG, MD. American Journal of Ophthalmology, 2000. 130: p. 542.

[11] Vega-Bermudez, F., K.O. Johnson, and S.S. Hsiao, Human tactile pattern recognition: active versus passive touch, velocity effects, and patterns of confusion. Journal of neurophysiology. 65(3): p. 531.

[12] Johnson, K.O. and S.S. Hsiao, Neural mechanisms of tactual form and texture perception. Annual review of neuroscience, 1992. 15: p. 227.

[13] Phillips, J.R., R.S. Johansson, and K.O. Johnson, Representation of braille characters in human nerve fibres. Experimental brain research. Experimentelle Hirnforschung. Expérimentation cérébrale, 1990. 81(3): p. 589.

[14] Loomis, J., On the tangibility of letters and braille. Perception & Psychophysics. 29(1): p. 37-46.

[15] Talbot, W.H., et al., The sense of flutter-vibration: comparison of the human capacity with response patterns of mechanoreceptive afferents from the monkey hand. Journal of neurophysiology. 31(2): p. 301.

[16] Gescheider, G.A., S.J. Bolanowski, and K.R. Hardick, The frequency selectivity of information-processing channels in the tactile sensory system. Somatosensory & motor research, 2001. 18(3): p. 191.

[17] Manfredi, L.R., et al., The Effect of Surface Wave Propagation on Neural Responses to Vibration in Primate Glabrous Skin (Effect of Surface Waves on Neural Responses). PLoS ONE. 7(2): p. e31203.

[18] Greenwood, J.A. and J.B.P. Williamson, Contact of Nominally Flat Surfaces. Proceedings of the Royal Society of London. Series A, Mathematical and Physical Sciences. 295(1442): p. 300-319.

[19] Chang, W.R., An elastic-plastic model for the contact of rough surfaces. Journal of tribology, 1987. 109(2): p. 257.

[20] Horng, J.-H., et al., A study of surface friction and particle friction between rough surfaces. Wear, 2009. 267(5): p. 1257-1263.

[21] Chernyak, Y.B. and A.I. Leonov, On the theory of the adhesive friction of elastomers. Wear, 1986. 108(2): p. 105-138.

[22] Wolfram, L.J., Friction of skin. Journal of the Society of Cosmetic Chemists, 1983. 34(8): p. 465-476.

[23] Darden, M.A. and C.J. Schwartz, Investigation of friction mechanisms during the sliding of elastomers against hard parallel-ridge textures. Tribology International, 2013. 63(0): p. 2-7.

[24] Buchholz, B., L.J. Frederick, and T.J. Armstrong, An investigation of human palmar skin friction and the effects of materials, pinch force and moisture. Ergonomics. 31(3): p. 317.

[25] Seo, N.J. and T.J. Armstrong, Friction coefficients in a longitudinal direction between the finger pad and selected materials for different normal forces and curvatures.(Report). Ergonomics. 52(5): p. 609-616.

[26] Derler, S. and L.C. Gerhardt, Tribology of skin: review and analysis of experimental results for the friction coefficient of human skin. Tribology Letters, 2012. 45(1): p. 1-27.

[27] Han, H.Y., A. Shimada, and S. Kawamura, Analysis of friction on human fingers and design of artificial fingers. p. 3061-3066.

[28] Greenwood, J.A. and D. Tabor, The Friction of Hard Sliders on Lubricated Rubber: The Importance of Deformation Losses. Rubber Chemistry and Technology, 1960. 33(1): p. 129-141.

[29] Greenwood, J.A., H. Minshall, and D. Tabor, Hysteresis Losses in Rolling and Sliding Friction. Proceedings of the Royal Society of London. Series A, Mathematical and Physical Sciences, 1961. 259(1299): p. 480-507.

[30] Taylor, M.M., Tactile roughness of grooved surfaces: A model and the effect of friction. Perception and Psychophysics, 1975. 17(1): p. 23.

[31] Bobjer, O., S.-E. Johansson, and S. Piguet, Friction between hand and handle. Effects of oil and lard on textured and non-textured surfaces; perception of discomfort. Applied Ergonomics, 1993. 24(3): p. 190-202.

[32] Gitis, N. and R. Sivamani, Tribometrology of Skin. Tribology Transactions. 47(4): p. 461-469.

[33] Sivamani, R.K., et al., Coefficient of friction: tribological studies in man – an overview. Skin Research and Technology. 9(3): p. 227-234.

[34] Sivamani, R.K., et al., Friction coefficient of skin in real-time. Skin Research and Technology, 2003. 9(3): p. 235-239.

[35] Gwosdow, A.R., et al., Skin Friction and Fabric Sensations in Neutral and Warm Environments. Textile Research Journal. 56(9): p. 574-580.

[36] Smith, A., et al., Role of friction and tangential force variation in the subjective scaling of tactile roughness. Exp Brain Res. 144(2): p. 211-223.

[37] Bueno, M.-A., et al., Tribological investigation of textile fabrics. Wear, 1996. 195(1): p. 192-200.

[38] Derler, S., U. Schrade, and L.C. Gerhardt, Tribology of human skin and mechanical skin equivalents in contact with textiles. Wear, 2007. 263(7–12): p. 1112-1116.

[39] Hatch, K.L., N.L. Markee, and H.I. Maibach, Skin Response To Fabric. A Review of Studies and Assessment Methods. Clothing and Textiles Research Journal. 10(4): p. 54-63.

[40] Kenins, P., Influence of Fiber Type and Moisture on Measured Fabric-to-Skin Friction. Textile Research Journal. 64(12): p. 722-728.

[41] Soufflet, I., M. Calonnier, and C. Dacremont, A comparison between industrial experts' and novices' haptic perceptual organization: a tool to identify descriptors of the handle of fabrics. Food Quality and Preference, 2004. 15(7): p. 689-699.

[42] Davis, L.L., et al., Dermatological Health Problems Attributed by Consumers to Contact With Textiles. Home Economics Research Journal. 18(4): p. 311-322.

[43] Stone, H., et al., Sensory Evaluation by Quantitative Descriptive Analysis, in Descriptive Sensory Analysis in Practice. 2004, Food & Nutrition Press, Inc. p. 23-34.

[44] Darden, M.A. and C.J. Schwartz, Investigation of skin tribology and its effects on the tactile attributes of polymer fabrics. Wear, 2009. 267(5): p. 1289-1294.

[45] Bertaux, E., et al., Textile, physiological, and sensorial parameters in sock comfort.(Report). Textile Research Journal. 80(17): p. 1803-1810.

[46] Davidson, P.W. and et al., Haptic Scanning of Braille Cells by Low- and High-Proficiency Blind Readers. Research in Developmental Disabilities, 1992. 13(2): p. 99-111.

[47] Carver, R.P., Reading rate: A review of research and theory. 1990: Academic Press.

[48] Wetzel, R. and M. Knowlton, A Comparison of Print and Braille Reading Rates on Three Reading Tasks. Journal of Visual Impairment & Blindness, 2000. 94(3): p. 146-54.

[49] Smith, K., fMRI 2.0: functional magnetic resonance imaging is growing from showy adolescence into a workhorse of brain imaging.(NEWS FEATURE). Nature. 484(7392): p. 24.

[50] Granov, A., L. Tiutin, and T. Schwarz, Positron Emission Tomography, ed. L. Tiutin and T. Schwarz. 2011, Dordrecht: Dordrecht Springer.

[51] Norihiro, S., et al., Activation of the primary visual cortex by Braille reading in blind subjects. Nature. 380(6574): p. 526.

[52] Langley, M.M., An event-related potential investigation of the neural representations that support familiarity-based picture recognition. 2010, Digital Repository @ Iowa State University.

CHAPTER 2: A COGNITIVE TRIBOMETER? USING BRAIN ACTIVITY TO DISCERN TACTILE DIFFERENCES AMONG SURFACES WITH VARIED FRICTIONAL CHARACTERISTICS

Abstract

A key challenge in controlling the haptic experience of a surface is the lack of fundamental understanding of how various surface attributes, such as friction and texture, affect the tactile response. Coefficient of friction is frequently used as a metric to characterize the skin-surface interaction, but it is not clear how important friction is to haptics. This becomes especially vital to understanding how to improve existing tactile communication methods such as braille. The authors propose a method to directly observe an individual's cognitive response to tactile experiences using event-related potential (ERP) via electroencephalography (EEG), a technique that is common in visual and auditory psychological sensory studies. EEG-ERP utilizes electrodes placed across the scalp to regionally detect and record neural impulses in response to given stimuli. In this work, eight subjects participated in two tasks: 1) discrimination between textured and non-textured surfaces, with different roughness and friction coefficients; and 2) attempted matching of like surfaces among three distinctly different sandpapers (ASTM-P100, P320, and P2500) and one smooth acrylic sample. Both phases of the study involved the textures being slid tangentially across the subjects' index fingerpads. EEG-ERP signals for responses were analyzed for each task, and distinct behavior was observed in the parietal lobe, which is largely responsible for sensory information, when the subjects sensed differences between textures. Furthermore, very precise event onset times were able to be determined from the EEG-ERP data. Fingertip coefficients of friction against each texture sample were shown to be distinct from each other, thus showing a correlation to the distinct differences observed in the cognitive data. These results indicate that

varying levels of friction and roughness elicit different magnitudes of cognitive activity, suggesting that this technique may prove to be a valuable tool in the tribological haptics research.

2.1 Introduction

Skin is the largest organ in the human body, and it is the foundation of the sense of touch. Throughout its surface are a wide array of sensory receptor neurons, or mechanoreceptors, and these neurons encode tactile stimuli such as vibration, temperature, and texture and transfer that information to the brain via mechanoelectric transduction [1]. At its core, tactility is driven by skin tribology, the fundamental interaction of skin and a counter-surface under contact and sliding. During a tactile interaction, the skin's mechanoreceptors stretch and deform around microscopic and macroscopic surface features, eliciting a tactile response, but one key challenge in controlling the haptic experience is the lack of a basic understanding of how various surface attributes such as friction and texture affect a given tactile response. Psychologists have been investigating the somatosensory system for decades, but from a mechanical perspective and tribological standpoint, little is known on how skin-surface tribology and surface science contribute to neural responses to tactile stimuli.

With the ability to quantify perception and directly measure neurological response to tactile stimuli in real-time, researchers can identify how specific surface properties and topographies are perceived and what tactile attributes they elicit. More importantly, understanding the relationship between tactility and surface engineering techniques could drive the innovation and optimization of domains that solely rely on tactile response, such as tactile communication methods like braille. Through braille, blind and visually impaired (BVI) individuals depend on their sense of touch to experience their environment and obtain valuable information, and given such, these individuals are at a severe disadvantage if information is not transmitted effectively. Educators are finding that

readers are experiencing varying forms of tactile confusion when it comes to complex representations of mathematics and tactile graphics, which are commonly used in the STEM fields. The root causes of such confusions are unknown, and coding standards and limitations in perceptive resolution reduce the opportunity for innovating or redesigning the language to aid the reader, thus requiring more robust techniques in quantifying perception.

Coefficient of friction is believed to be a major factor in tactile perception, and studies have investigated its influence in predicting the tactile attributes of myriad surfaces such as textiles [2-6], paper media [7, 8], or ridged textured polymers [9, 10]. While material and surface properties are easily quantifiable, quantifying tactile perception is significantly more difficult due to variability between an individuals' subjectivity. Quantitative Descriptive Analysis is a commonly adapted technique that presents subjects with benchmark samples to use as reference when evaluating tactile attributes [11-13], but subjectivity remains a potential source of error. In order to circumvent subjectivity and latency issues of survey and judgement-based evaluations, researchers have begun implementing techniques that allow direct observation of tactile stimuli-based neural activity, such as functional magnetic resonance (fMRI) [14] and positron emission tomography [15, 16]. The drawback with these techniques is that while they are capable of determining regions of the brain that activate due to an introduced tactile stimulus, they cannot quantify the degree of which the brain responds to them. Electroencephalography (EEG) is capable of observing and quantifying the brain's response to an applied stimulus, but to this date, this technique has only been used to explore electrophysiological response to visual and auditory cues [17]. While unexplored as a neural response evaluation technique for the tactile domain, event-related potential (ERP) through EEG has the potential to allow researchers to apply a tactile stimulus and observe and measure the subject's neural response, or tactile perception, in real-time.

The purpose of this investigation was to determine the viability of using an electrophysiological technique (event-related potential (ERP), via electroencephalography (EEG)) to observe and detect the human brain's cognitive response to the tactile experience. This technique is commonly implemented in observing psychophysical response to visual or auditory cues, but has not been incorporated into the tactile domain. The first phase of the study was to characterize the frictional behavior of the human fingerpad sliding across the tactile stimuli to ensure that frictional uniqueness existed amongst all samples. Identifying sample uniqueness then allowed for electrophysiological response tests to be performed in order to observe and detect the psychophysical response to decision-making during tactile discrimination tasks: 1) an oddball paradigm in which the subject is asked to identify when a stimulus deviates from the expected control, and 2) a matching task in which the subject is asked to identify whether a presented pair is similar or dissimilar.

2.2 Materials and Methods

2.2.1 Sample selection

Four tactually unique samples were selected for the coefficient of friction and EEG-ERP studies: three commercially available sandpapers and one roughened acrylic (matte finish). The three sandpapers were defined as textured samples, and the acrylic was defined as the non-textured, control sample. The sandpapers selected were FEPA-P100, P320, and P2500, and were noted as Coarse, Medium, and Fine, respectively due to their distinctly different perceived textures.

2.2.2 Skin-friction analysis for tactile stimuli

The four samples were cut into 25.4 mm X 76.2 mm (1 in. x 3 in.) strips and longitudinally mounted onto a 3.175 mm (1/8 in.) thick aluminum plate and attached onto a piezoelectric three-axis dynamometer (Fig. 2.1).

Fig. 2.1 Arrangement of the four textured samples mounted to the Kistler 9254 three-axis dynamometer: coarse texture (FEPA P100 top left), fine texture (FEPA-P2500, top right), medium texture (FEPA-P320, bottom left), fine texture (FEPA-P2500, top right), and control texture (bare acrylic, bottom right).

The coefficient of friction of a fingertip sliding against a sample was determined by recording the normal and shear forces produced during a finger swipe against a sample. These forces were measured with a piezoelectric three-force dynamometer and amplifier, and data were exported to a data acquisitioning system. Data were taken at a sampling rate of 1,000 Hz and written to files for subsequent processing and analysis. To ensure that environmental factors did not contribute to data variation, all finger swipes were performed in a 23.8 deg. C, 50% humidity environment, and hand cleanliness was also maintained between tests to reduce surface contamination.

For a given sample, the investigator used the left index finger and made three swipes across the length of the sample from left to right, and the data acquisition software simultaneously

recorded the normal and tangential loads applied during each swipe. Normal loading was controlled by the operator and maintained between 0.5-0.8 N for all passes. This loading was selected to simulate light sliding contact with a surface.

Data were collected for all samples in a random testing order dictated by the experimental design, where each sample was repeated three separate times. A swipe's coefficient of friction data was calculated by taking the instantaneous ratio of the tangential and normal loading. The force data, and subsequently the coefficient of friction data, from an individual swipe exhibited step function behavior. This step function was generated due to initial normal loading, driven during the sliding motion, and concluded upon end of motion and release. Therefore, a single mean coefficient of friction for a swipe was acquired by averaging the data across the step function's plateau. At three swipes per trial and three trials per sample, nine means were collected for each possible sample. These nine means were then analyzed using ANOVA and Tukey's post hoc analysis to determine how each texture type affected coefficient of friction.

2.2.3 Electrophysiological response to tactile stimuli during discrimination-based tasks

All electrophysiological testing and preliminary data analysis was performed under the guidance of EEG-ERP specialists from the Department of Psychology at Iowa State University.

2.2.3.1 Subjects

Seven right-handed undergraduate students were tested for EEG-ERP evaluations. The subject pool consisted of both males and females ranging from 18-22 years of age. Participants provided informed consent at the beginning of the testing session and received monetary compensation upon completion.

2.2.3.2 Sample preparation

For the ERP sessions, texture wands were constructed to apply the stimulus to the subject's index finger. In the case of the sandpapers, 25.4 mm X 76.2 mm (1 in. X 3 in.) strips were cut and adhered to the ends of 3.175 mm (1/8 in.) thick acrylic sticks. In the case of the control sample, the bare acrylic was roughened to a matte finish. A conductive copper film was placed at the leading edge of each sample to indicate to a touch sensor when contact was initiated with the given stimulus. This conductive signal was transferred via a coaxial cable on the reverse side of the wand. Additional tape was placed 76.2 mm (3 in.) below the stimuli to indicate to the operator where initial sliding contact would begin during each application. The four constructed stimuli can be seen in Fig. 2.2 below.

Fig. 2.2 The four texture wands for the ERP sessions; from top to bottom: Coarse, Medium, Fine, Control

2.2.3.3 Electrophysiological response data acquisition setup

The event-related potentials were recorded through the use of an electroencephalogram (EEG, bandpass 0.02-150 Hz, digitized at 500 Hz, gain 1,000, 16-bit A/D conversion). Data were collected from 68 tin electrodes sewn into an Electro-cap affixed to the scalp with conductive gel (Figure 2.3). Prior to each session, each subject was informed of the tasks to be performed and presented with an informed consent form to be signed and submitted. Once consent was given, the Electro-cap was fitted to the subject's head, and the subject was then brought to the appropriate room for data collection. Due to the EEG's extreme sensitivity to electrical noise, data collection took place in a custom-built Faraday cage, filtering out unwanted environmental noise.

Figure 2.3. The 68-channel electroencephalogram cap used during EEG-ERP testing, where each electrode detects the scalp's electrical activity and neural response with respect to specific regions of the brain.

As ERP data was analyzed about a specific stimulus event, a digital trigger was required to temporally pinpoint the exact moment the stimulus was applied. A custom tactile trigger was constructed by implementing an Atmel QT1010 Touch Sensor IC into a simple circuit powered by a 3V power supply. This conduction-driven sensor was integrated into the EEG system and activated each time the subject's finger came into contact with the copper strip on the stimulus wands pictured in Fig. 2.

2.2.3.4 Testing Procedure

Prior to the session, the subject was asked to thoroughly wash both hands to remove any possible dirt or contaminants. For the following tasks, the subject was asked to sit behind a blind partition, with the right hand placed through a small opening. A clean towel was provided in case the need arose for the subject to remove any sweat or contaminant from the hand or fingertip. The subject was asked to extend facing upward the index finger of the right hand, and to remain as still as possible for the duration of the task, to reduce the impact of motor control effects on the neural activity signal.

2.2.3.5 Task 1: Oddball paradigm

The first task asked the subject to respond whether or not the stimulus was a texture (any sandpaper: coarse, medium, or fine) as opposed to the control acrylic surface. If the stimulus was a texture, the subjects were not asked to identify what the specific texture was. In an "oddball" task, the subject is intended to expect a given stimulus, in this case, the control sample (NO texture). Consequently, out of 100 trials, the control sample was presented 70 times, and each type of sandpaper was presented 10 times. For each trial, the subjects' responses were recorded and evaluated, where only trials that yielded correct responses would be considered for analysis. Table 2.1 presents the response's categorical identifiers assigned to the events during post-processing,

where incorrect responses were not considered for data analysis. IDs 2 and 6 indicate incorrect responses of “false alarm” and “miss” respectively, and any trial marked with either was removed from consideration.

Table 2.1. Evaluated response identifiers used for labeling ERP events for Oddball task.

Stimulus	Response	ID
None	No	1
	Yes (FA)	2
Fine	Yes	3
Medium	Yes	4
Coarse	Yes	5
	No (Texture)	6

Each unique trial began with of the investigator connecting the appropriate stimulus wand to the tactile sensor’s coaxial connection. The wand was then held horizontally face down and lowered to come into contact with the subject’s index fingerpad under the static loading of the wand’s own weight. Contact was initiated at the first tape strip, and the wand was then dragged horizontally across the subject’s finger, simulating the finger sliding from left-to-right across the sample. The wand was then pulled across the fingertip until the trigger and stimulus were encountered. All four wands presented an initial control surface to calibrate the subject’s perception prior to the triggered stimulus event. Only one pass was permitted for a single trial, and a response of “texture” or “no texture” was recorded.

Prior to significance analysis, the data streams were scrubbed, such that ocular artifacts were filtered out to remove the impact of blinks and eye movement during the sessions. For each subject, similarly-categorized events were averaged over a time window (epoch) beginning 2.5 s

before the event began and ending 2.5s after it ended. Data were then analyzed with PCA (principal component analysis) and ANOVA to determine statistical significance between the neural responses of the control versus the textured samples. Throughout the session, data were collected for all 68 electrodes across the entire cap, but data analyses focuses on those on and around the brain's parietal and frontal lobes for their association with somatosensory and working memory related tasks. Additional statistical t-tests were performed to determine the significance of the signal deviation between the observed textured and non-textured neural responses.

2.2.3.6 Task 2: Matching task

The second task presented the subject with a tactile-memory related problem. To begin a given trial, the subject was presented with a 50.8 mm X 101.6 mm (2in. x 4in.) plate with one of the four stimuli. This plate, designated as the "target," was placed face up into the subject's extended right hand, and the right thumb was used to tactually examine the sample. The subject was permitted to examine it for as long as desired. Once familiar with the target, one of the four stimulus wands was applied to the face-up extended index finger in a manner identical to that of the Oddball task. Again, only a single stimulus pass was permitted.

Following the stimulus, the subject was asked to respond whether or not the pair of samples were the same, or different. Correct responses of "same" or "different" were noted as "hits" and "correct rejections," and incorrect responses were noted as "misses" and "false alarms (FA)." Table 2.2 provides a matrix of possible response-pair combinations and their associated notations.

Table 2.2. Evaluated response identifiers for labeling ERP events for the Matching task.

		Response	
		Same	**Different**
Stimulus Pair	**Same**	0 - Hit	1 – Miss
	Different	2 - FA	3 – CR

For this task, a total of 96 trials were performed: 12 identical target-stimulus pairs per sample (48 total), and 12 different target-stimulus pairs per sample (4 repetitions of each target sample with the other stimuli, 48 total). In a manner similar to the Oddball task, incorrect responses were disregarded.

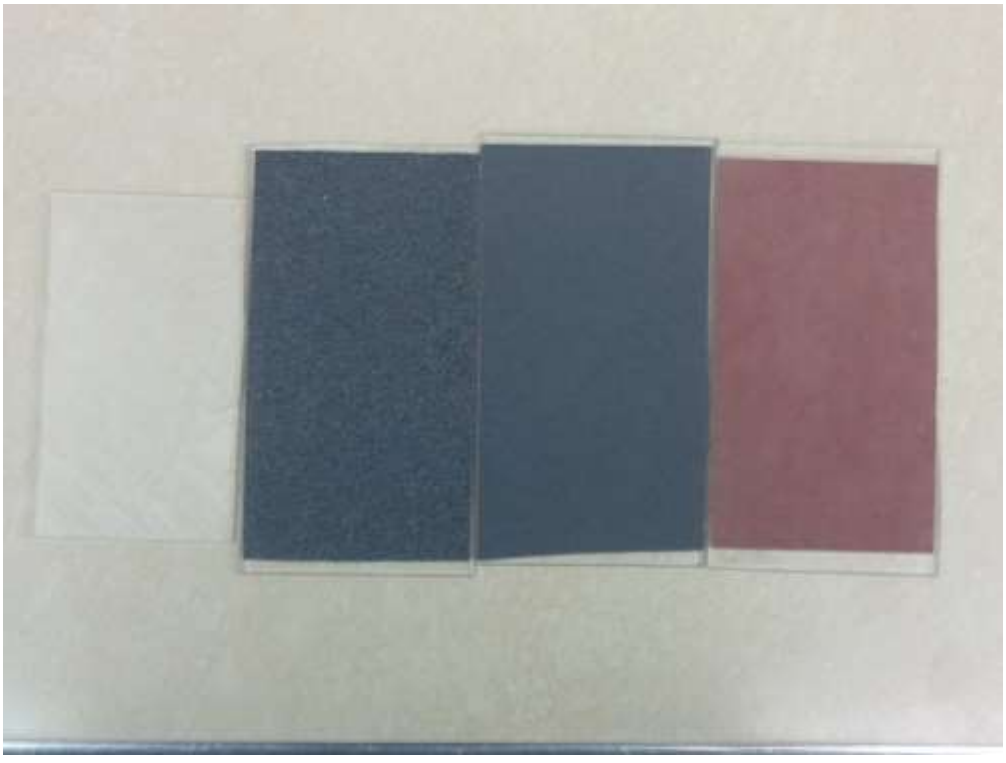

Figure 2.4. The target stimuli samples presented to the subjects during the first step of the matching task. From left to right: Control, Coarse, Medium, and Fine.

2.3 Results and Discussion

2.3.1 Skin-friction analysis for tactile stimuli

Coefficient of friction testing was performed on the four selected samples in order to quantify their skin-surface uniqueness. Normal and tangential load were simultaneously measured during fingertip sliding, and a mean COF was calculated for each swipe. Figure 2.5 presents an example of the loading components as well as COF data acquired from a single friction trial for the Fine texture. Each trial consisted of multiple swipes, and means from three swipes were taken from each trial. Coefficient of friction means were calculated by averaging the COF data across the entirety of each swipe's plateau, and these means were collected for Analysis of Variance (ANOVA) and Tukey statistical tests.

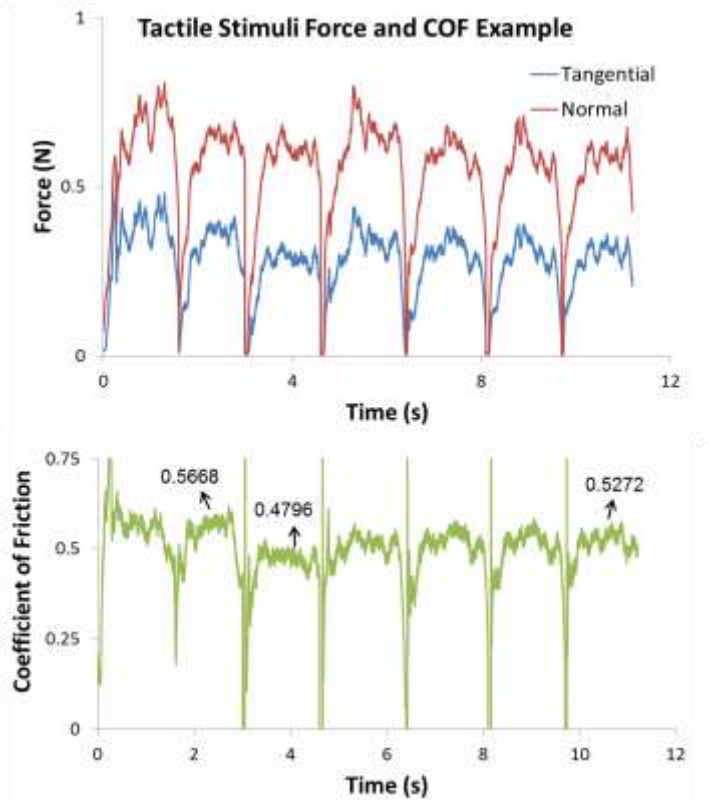

Figure 2.5. The force (top) and COF (bottom) data acquired from a single friction measurement trial for the Fine texture.

Statistical analysis indicated that all four samples, the three textured sandpapers and the non-textured acrylic, exhibited coefficients of friction that were significantly different from one another when slid in contact with a human fingerpad under low loading conditions. As expected, the smooth, non-texture acrylic sample had the lowest coefficient of friction value. Of the three textures, the Fine texture's coefficient of friction was much less than of the Medium and Coarse, and it more closely resembled that of the acrylic. The means of the Medium and Coarse textures were the closest to each other out of all sample comparisons, but as seen in the Tukey analysis grouping, each COF mean was statistically different from the rest (Figures 2.6 and 2.7).

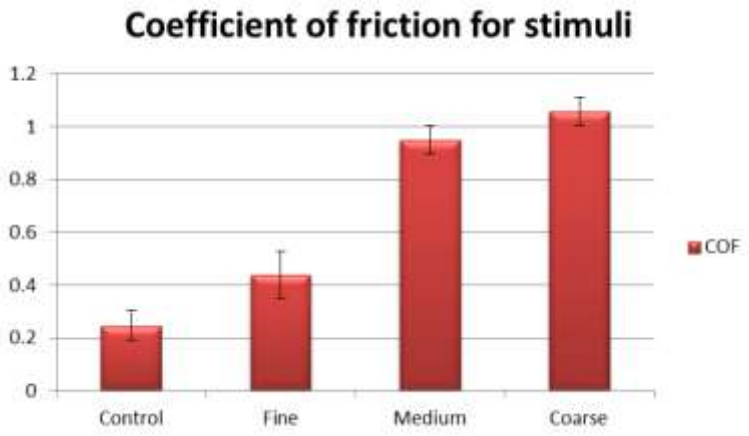

Figure 2.6. The coefficient of friction for the four stimuli was compared to one another, and the error bars represent the standard deviations from the averaged means.

COF

Tukey HSD[a]

Stimulus	N	Subset for alpha = 0.05			
		1	2	3	4
Control	9	.24653			
Fine	9		.43768		
Medium	9			.94739	
Course	9				1.05631
Sig.		1.000	1.000	1.000	1.000

Means for groups in homogeneous subsets are displayed.

a. Uses Harmonic Mean Sample Size = 9.000.

Figure 2.7. A statistical Tukey test separated the coefficients of friction for the stimuli into groups of statistical uniqueness.

2.3.2 Electrophysiological response to tactile stimuli during discrimination-based tasks

Based on the coefficient of friction study, the four stimuli were found to have quantitatively unique skin-surface tribological behaviors. Given this and the fact that the stimuli elicited qualitatively different tactual traits, the authors hypothesized that the electrophysiological response to each stimulus's tactile experience would be quantitatively unique as well. The electrode cap worn during the EEG-ERP study recorded electrical activity across the entire surface of the subject's scalp for the duration of the session. Events were signaled by the touch-sensitive trigger on the tactile wands, and during post-processing analysis, were identified by their respective stimulus ID and subject's response, in accordance with the randomized testing order.

Once all events were properly marked and identified for all subjects, events with like event IDs were averaged across all subjects and consolidated in an averaged data map depicting a top-down view of the electrodes' locations across a scalp (Figure 2.8). Data map averages were conducted for the epoch, or temporal window, surrounding the event because ERP analysis observes neural activity both before and after the stimulus has been experienced. An epoch of -200 ms to 1200 ms was used, where time zero referred to the stimulus trigger. During the 200 ms prior to the trigger, the subjects' fingers experienced finger sliding against the preliminary baseline control sample, followed by contact with the stimulus for 1.2 s.

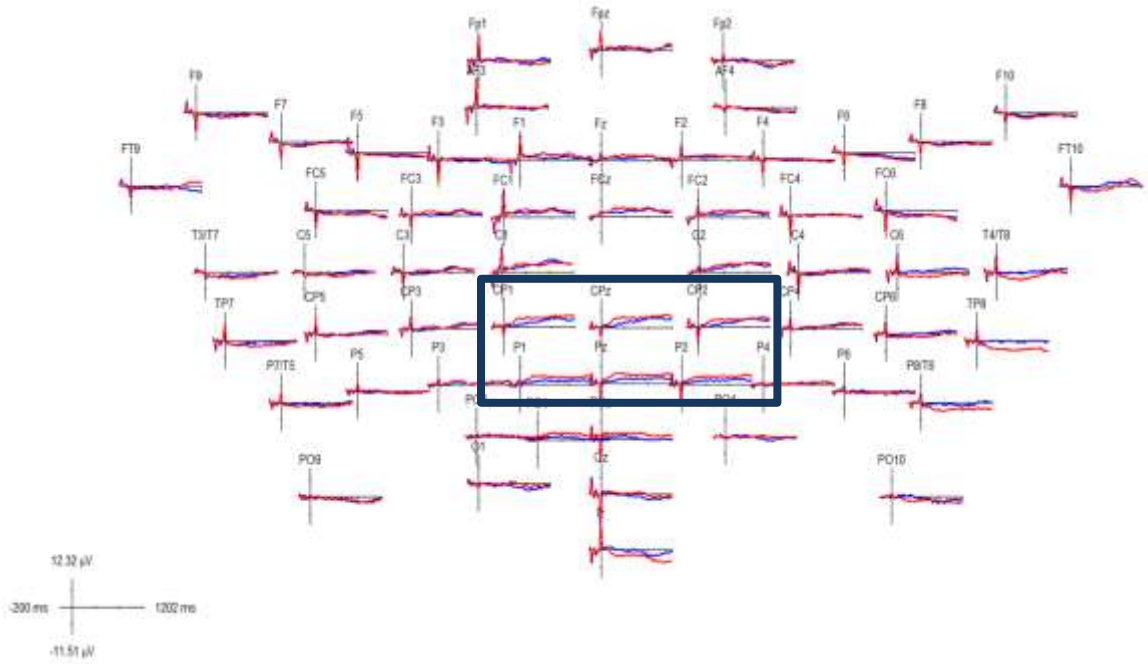

Figure 2.8. The data map generated from the Oddball task, displaying the "texture" response (red) in comparison to the "non-texture" response in an event window, or epoch, from -200 ms to 1200 ms for all channels recorded in the EEG-ERP sessions. The central-parietal and parietal lobes are located toward the rear of the scalp and are marked in the box.

While the data map provided the electrophysiological response across the entirety of the scalp, data analysis focused only on regions of the brain known to exhibit greater positivity to tactile stimuli: the parietal and central-parietal lobes of the brain, located near the top-rear section of the skull. For reference, the top of the data map represented the front of the subjects' skull, with odd numbered electrodes on the left side of the skill, and even numbered electrodes on the right. Electrodes marked with a "Z" were located in the skull's horizontal center.

2.3.2.1 Task 1: Oddball paradigm

The goal of the oddball paradigm was to condition the subjects to expect a predictable stimulus (non-textured control) in order to more easily detect the electrophysiological response to an unexpected stimulus (textured sandpapers). During this task, the subjects were not asked to discriminate between the textured samples but only to identify the presence of a texture. It was

hypothesized that the tactile experience caused by textured samples would elicit a greater electrophysiological response in either the central-parietal or parietal regions of the brain. Initial principal component analysis (PCA) was performed by the psychology specialists, and they indicated that the EEG-ERP techniques might have successfully detected unique physiological responses to the tactile stimuli, but that further analysis was required. One weakness in the experimental design was that the available subject sample size was quite low when compared to typical ERP-based experiments.

Unfortunately, paradigm differences between the collaborating parties yielded a challenging partnership and limited the authors' ability to perform independent analyses and draw effective conclusions that met the standards set by the psychology community. Additionally, implementing event-related potential to investigate the tactile domain has been largely unexplored, further reducing the amount of reference information and data to use for thorough analysis. As a result, conventional statistical techniques were implemented in order to analyze the data sets and verify the claims originally made by the collaborators. Once the raw data was obtained, an algorithm was written that compiled all the channels' data by event type and performed a statistical significance test ($\alpha = 0.05$) over the duration of the epoch for both the parietal and central-parietal electrodes. Initially, significance between the non-textured control response and the overall textured response (all textures combined) was investigated in order to validate the claims that the EEG-ERP technique could detect the brain's ability to recognize a tactile stimulus.

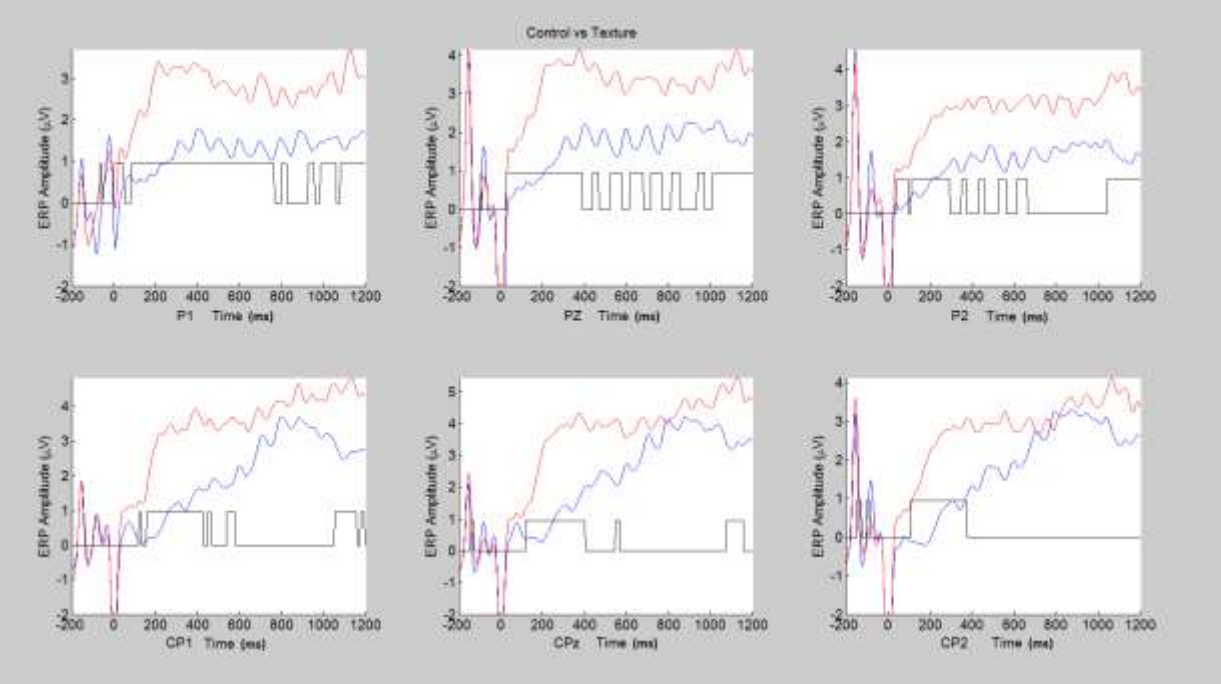

Figure 2.9. The statistical comparison of the non-textured (blue) response with that of the textured response (red) across the parietal (top row) and central-parietal (bottom row) channels, where the statistical significance over time was marked by the black plot.

Figure 2.9 illustrates the statistical analysis performed comparing the non-textured control vs textured responses. As the subject was conditioned to expect the control stimulus, the brain's response to a non-texture (blue) was discovered to be less in magnitude than when presented with an unexpected texture (red), as originally hypothesized. The difference in magnitudes was readily apparent, and the black curve in the figure annotates a statistically significant difference in means, where a value of zero represents insignificance, and a value of 1 represents significance at that instance in time. Based on this analysis, all observed electrodes detected significant deviation between the non-textured and textured signals from the onset of the stimulus event, and electrode P1, situated on the parietal lobe on the left side of the skull, displayed the most degree of significance for the longest duration. Given that the subjects were right-hand dominant, this result was consistent with literature stating that motor skills and sensation are dominated by lateralization of the brain, where the one side of the body is primarily governed by the opposite hemisphere [18].

Due to the promise from the Control vs Texture findings, pairwise comparisons of the non-textured control with respect to specific textured stimuli were compared to determine whether or not the subjects' brains more accurately discriminated between the samples (Figure 2.10). The authors anticipated that when comparing the control to each texture, their neural responses would be analogous to the coefficient of friction rankings, where the non-texture is most similar to the fine, followed by the medium and coarse textures. The data overwhelmingly supported this claim, in that the prominence and duration of statistical significance increased across all electrodes as the textures increased in abrasive coarseness. Like before, all three parietal electrodes more effectively detected statistically unique signals for each of the stimulus comparisons. When observing the Control vs Fine behavior, the parietal electrodes were able to detect differences in stimuli, but the central-parietal electrodes did not effectively discriminate between the two. The central-parietal area more effectively discriminated texture differences during the Control vs Medium and Control vs Coarse tests, possibly implying that this region of the brain is involved in more fine-tuned decision-making perception tasks. Conversely, the parietal region appeared to diminish in its ability to maintain stimulus discrimination as coarseness increased, suggesting its involvement in broader, more sweeping perception tasks like Control vs Texture. These differences are likely attributed to the fact that each region may serve different cognitive functions when evaluating somatosensory perception. As seen in previous ERP findings, specific electrophysiological responses may also be dependent on the specific prompt the subjects were given. When prompted with the question "is the stimulus a texture?", the subjects' goal was to detect the presence of a texture or lack of, not identify which texture was present. A more robust experimental design would be required to explore the decision-making aspects of tactile perception.

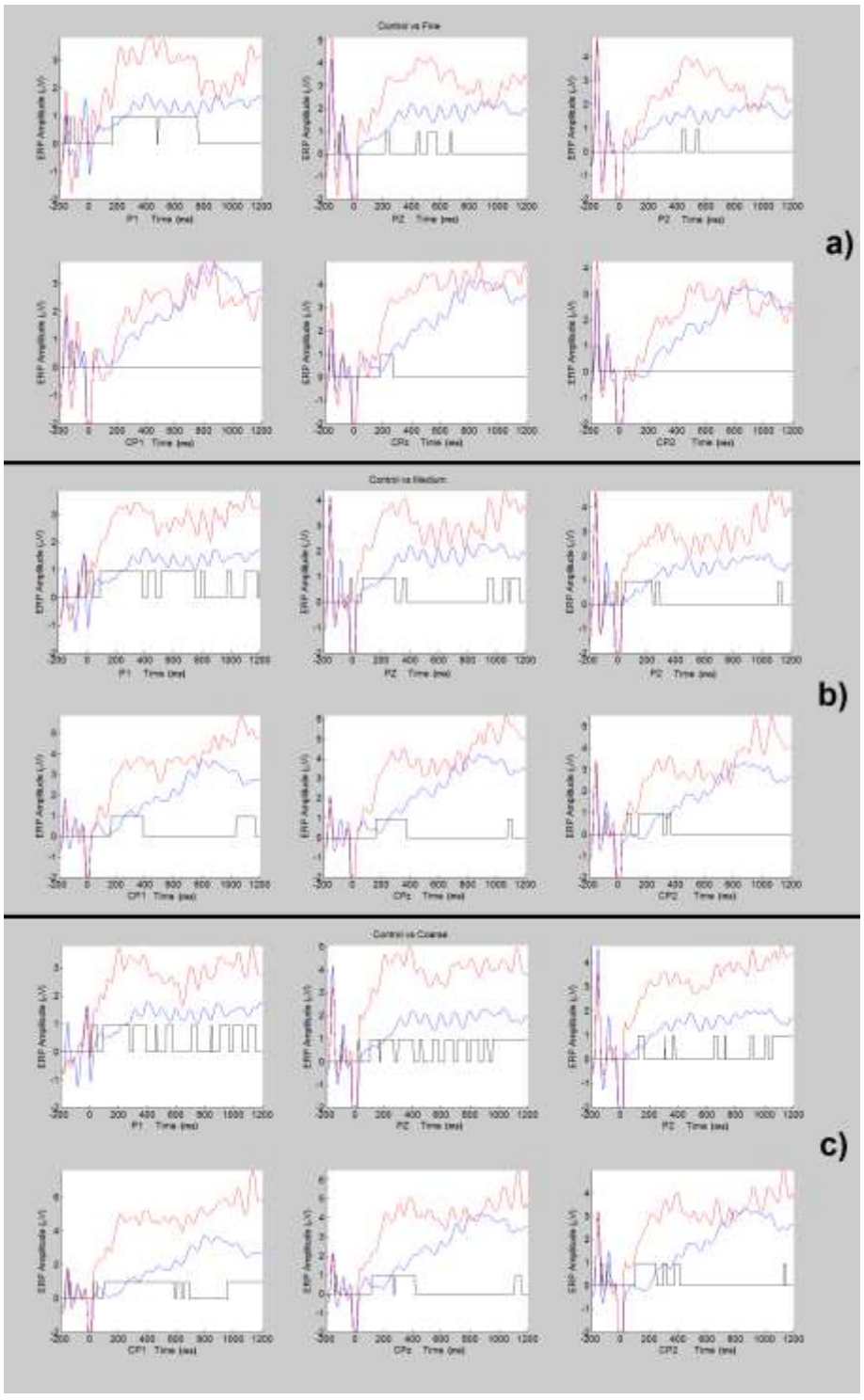

Figure 2.10. Pairwise tests comparing the statistical uniqueness of the non-textured control stimulus (blue) vs each of the textures (red): a) Control vs Fine, b) Control vs Medium, and c) Control vs Coarse.

The final data analysis performed for the oddball task investigated whether or not the subjects were able to discriminate between the textured stimuli, even though they were not prompted to do so. As expected, there was virtually no difference in electrophysiological response when the subjects experienced each of the textures, barring electrode CP1 identifying some brief perceptive differences between the Fine and Coarse stimuli, the two samples that exhibited the most different skin-surface coefficients of friction. This could suggest that the difference in Fine vs Coarse texture perception is related to the difference in sample coefficient of friction, but that assumption is unsubstantiated until further testing is performed. Visually, the Fine vs Medium and Medium vs Coarse comparisons are nearly overlaid on one another, implying the brain equated each of those tactile experiences. None of the investigated electrodes detected any significant difference in response between the other stimuli, and this is likely due to the oddball paradigm's original prompt.

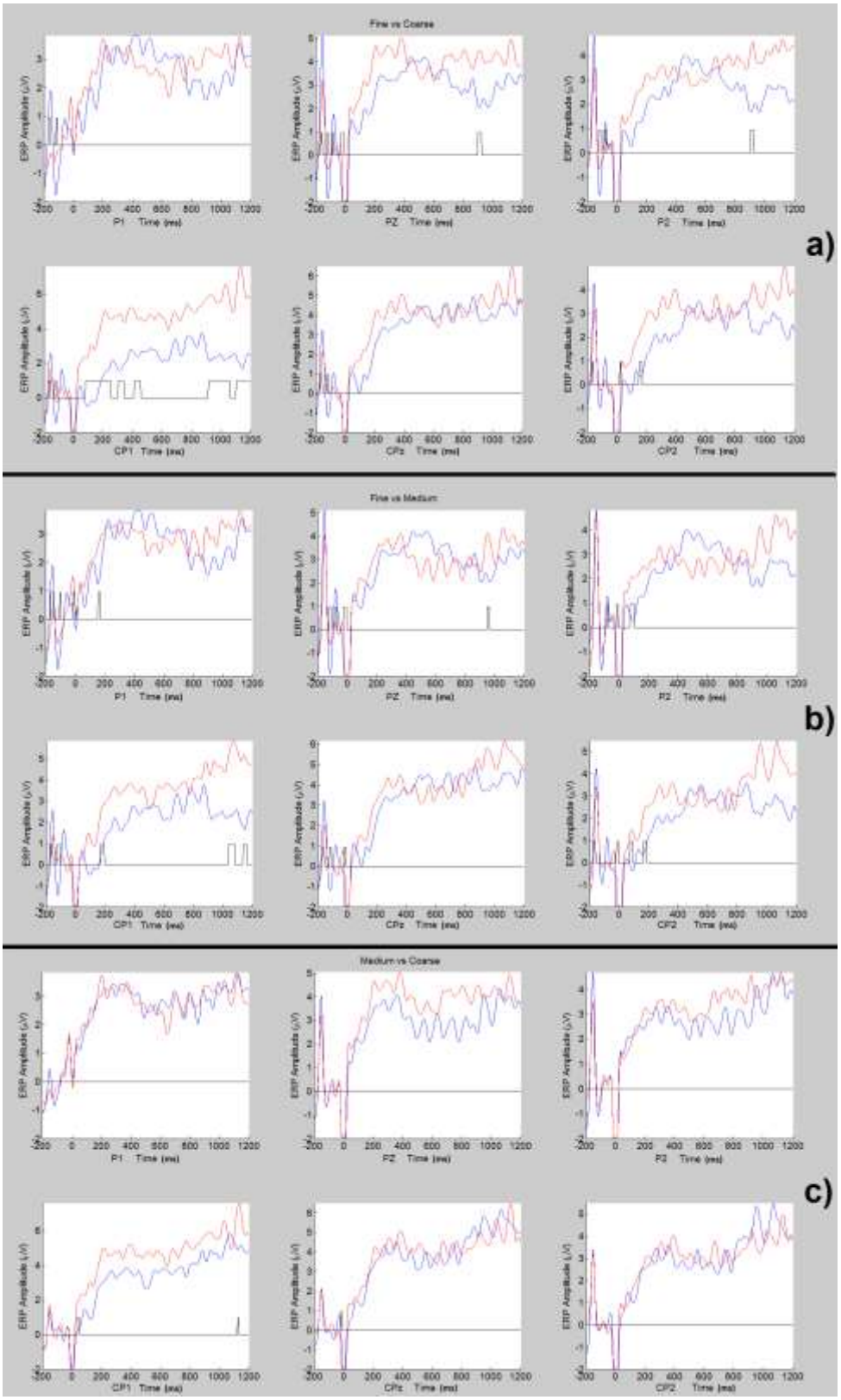

Figure 2.11. Pairwise tests comparing the statistical uniqueness between each of the textures: a) Fine (blue) vs Coarse (red), b) Fine (blue) vs Medium (red), and c) Medium (blue) vs Coarse (red).

2.3.2.2 Task 2: Matching task

The second matching task was much more complex in nature, in that it was essentially a memory-recall task that incorporated tactile discrimination response. Attempts at analyzing the recorded data proved that the experimental and analytical techniques implemented in the previous approach were not nearly robust enough for this task. Prompting the subject with the question "Are the stimuli the same or different?" was too dependent on a decision-making task without isolating the fundamental tactile experience. Memory and logical tasks have been shown to occur in other regions of the brain such as the pre-frontal and frontal lobes [19], but paradigms have not been effectively laid out to directly relate the logic-based signals from one region of the brain to somatosensory-based signals from another. Without this a priori knowledge, any specific inferences drawn from the performed test would be conjecture at best. To break ground in this area, experiments must first be designed to fundamentally identify the specific components of electrophysiological signals responding to tactile stimuli in the same manner that signals from the visual and auditory domain have been characterized. For reference, the data map generated from the performed matching task can is found in Figure 2.12.

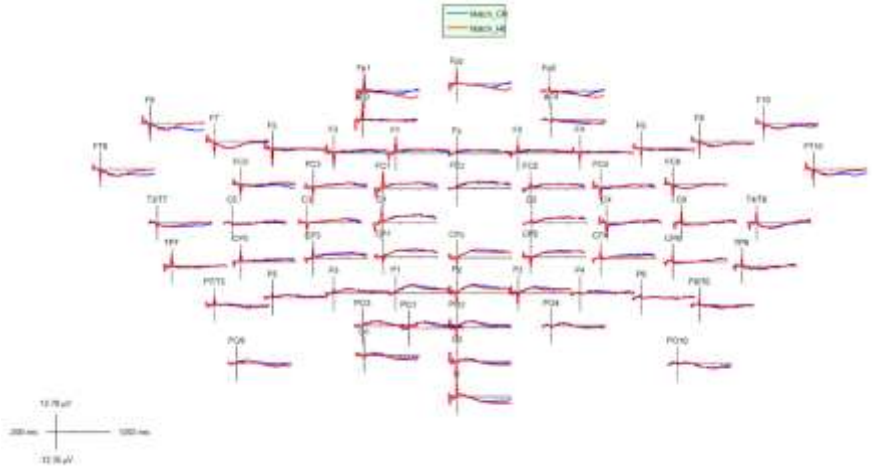

Figure 2.12. Data map generated from the data recorded from the performed matching task, comparing the amplitudes of the Correct Rejection (blue) responses to that of the Hit (red) responses.

2.4 Conclusions

Event-related potential (ERP) via electroencephalography (EEG) was used to investigate the viability of implementing electrophysiological measurement techniques (which are commonly used in the visual or auditory domain) into the tactile domain. Based on the findings, the following conclusions can be drawn:

- EEG-ERP shows enormous promise in granting tribologists the ability to biologically quantify skin-surface interactions and their elicited tactile attributes by observing the brain's parietal and central-parietal region.
- Through a revised experimental setup and a larger sample size, EEG-ERP allows for the opportunity to investigate specific temporal events in tactile perception – such as the time lapsed for detection or discrimination;
- Questions/tasks must be stated with specific intent in order to correlate applied stimuli with their respective neural response
- Tasks that involve a combination of memory-recall (pre-frontal and frontal lobe) and tactile discrimination (parietal and central-parietal lobe) require a priori knowledge of signal behavior to appropriately analyze and interpret the results

2.5 References

[1] Kenshalo, D.R., T. Decker, and A. Hamilton, Spatial summation on the forehead, forearm, and back produced by radiant and conducted heat. Journal of Comparative and Physiological Psychology, 1967. 63(3): p. 510-515.

[2] Kenins, P., Influence of Fiber Type and Moisture on Measured Fabric-to-Skin Friction. Textile Research Journal. 64(12): p. 722-728.

[3] Sivamani, R.K., et al., Coefficient of friction: tribological studies in man – an overview. Skin Research and Technology. 9(3): p. 227-234.

[4] Gwosdow, A.R., et al., Skin Friction and Fabric Sensations in Neutral and Warm Environments. Textile Research Journal. 56(9): p. 574-580.

[5] Gitis, N. and R. Sivamani, Tribometrology of Skin. Tribology Transactions. 47(4): p. 461-469.

[6] Derler, S., U. Schrade, and L.C. Gerhardt, Tribology of human skin and mechanical skin equivalents in contact with textiles. Wear, 2007. 263(7–12): p. 1112-1116.

[7] Skedung, L., et al., Finger Friction Measurements on Coated and Uncoated Printing Papers. Tribol Lett. 37(2): p. 389-399.

[8] Skedung, L., et al., Tactile perception: Finger friction, surface roughness and perceived coarseness. Tribology International, 2011. 44(5): p. 505-512.

[9] Bobjer, O., S.-E. Johansson, and S. Piguet, Friction between hand and handle. Effects of oil and lard on textured and non-textured surfaces; perception of discomfort. Applied Ergonomics, 1993. 24(3): p. 190-202.

[10] Smith, A., et al., Role of friction and tangential force variation in the subjective scaling of tactile roughness. Exp Brain Res. 144(2): p. 211-223.

[11] Stone, H., et al., Sensory Evaluation by Quantitative Descriptive Analysis, in Descriptive Sensory Analysis in Practice. 2004, Food & Nutrition Press, Inc. p. 23-34.

[12] Darden, M.A. and C.J. Schwartz, Investigation of skin tribology and its effects on the tactile attributes of polymer fabrics. Wear, 2009. 267(5): p. 1289-1294.

[13] Bertaux, E., et al., Textile, physiological, and sensorial parameters in sock comfort.(Report). Textile Research Journal. 80(17): p. 1803-1810.

[14] Smith, K., fMRI 2.0: functional magnetic resonance imaging is growing from showy adolescence into a workhorse of brain imaging.(NEWS FEATURE). Nature. 484(7392): p. 24.

[15] Granov, A., L. Tiutin, and T. Schwarz, Positron Emission Tomography, ed. L. Tiutin and T. Schwarz. 2011, Dordrecht: Dordrecht Springer.

[16] Norihiro, S., et al., Activation of the primary visual cortex by Braille reading in blind subjects. Nature. 380(6574): p. 526.

[17] Langley, M.M., An event-related potential investigation of the neural representations that support familiarity-based picture recognition. 2010, Digital Repository @ Iowa State University.

[18] Penfield, W. and L. Roberts, Speech and brain mechanisms. 2014: Princeton University Press.

[19] Von Hofsten, C., From Action to Cognition. Progress in Brain Research, ed. K. Rosander. 2007, Burlington: Burlington : Elsevier Science.

CHAPTER 3: SKIN TRIBOLOGY PHENOMENA ASSOCIATED WITH READING BRAILLE PRINT: THE INFLUENCE OF CELL PATTERNS AND SKIN BEHAVIOR ON COEFFICIENT OF FRICTION

A paper published in WEAR

M.A. Darden and C.J. Schwartz

Abstract

Efficient transmission of tactile information is vital for individuals who rely on their sense of touch to interact with and navigate their surroundings, including visually impaired persons. Somatosensory phenomena have been investigated with respect to surface topologies and neuron sensitivities in the skin, but there is little knowledge of the specific skin tribology when reading tactual-coded information such as braille. Braille is a tactual code that employs raised dome-shaped dots in six-position cells (2 columns by 3 rows per cell), with various dot patterns representing individual text characters, punctuation or mathematical operators. Due to the hypothesized significance of friction on tactile sensitivity, the authors investigated the effect of basic braille dot configurations on friction coefficient in fingertip sliding. Initial studies investigated the effect of multiple dot-row configurations and media type on friction coefficient, but the tribological effect of individual features and associated skin interactions were ill-defined. Subsequently, the frictional effect of an individual dot of varying radius was investigated and modeled against a multi-term frictional model implementing Hertzian contact, the Greenwood-Tabor hysteresis component of a spherical indenter against a soft surface, as well as Wolfram's traditional adhesion model. The results of the study show that macro-scale deformation of the fingerpad during fingertip-on-dot sliding is the primary friction mechanism. With this

understanding of the tribological interaction of skin against single dots, it remains vital to understand how feature spacing affects fingertip sliding and associated coefficients of friction. The ability to do so will provide a means to understand how much of a role friction plays in braille character recognition, as well as suggest potential friction-based methods to enhance the information density of braille codes.

3.1 Introduction

The sense of touch is one of the most fundamental ways an individual can interact with the surrounding environment. Touch and perception play a key role in handling and manipulating objects, evaluating products, or even obtaining tactual information. When it comes to investigating tactility, researchers have had great difficulty understanding and modeling the extreme complexity of the somatosensory system. Whereas most individuals rely on multiple senses in order to obtain information and navigate surroundings, instances exist where individuals rely almost entirely on their sense of touch to decode their environment; such is the case for blind or visually impaired persons (BVI). Where sighted individuals receive written language through visual text, BVI individuals read through their means of touch, via the tactile language, braille. It is understood that BVI persons use their hands and fingers to perceive and decode braille, but there have been and continue to be research studies that investigate what exactly is occurring in the somatosensory system of individuals with BVI.

Phillips et al. first discovered that certain afferent neurons located throughout the hand (SA1 mechanoreceptors and Merkel-cell end organs) are the main contributors in one's ability to distinguish spatial form, and they investigated the use of braille cells to prove this. These receptors permit the fingertips to perceive the number and orientation of the dots involved, and the brain can then discriminate between individual braille patterns and interpret them into the intended meaning

[1]. As previously mentioned, individuals who experience early onset blindness have been shown to adapt and eventually exhibit greater tactile acuity in these receptors [2]. Conversely, individuals who experience late onset blindness do not have such acuity and are at a disadvantage due to their lower tactile resolution. Tactile confusion plagues braille readers with decreased tactile acuity, but the specific source of this confusion is unknown. Other tactile studies have investigated perceptive thresholds and tactile resolutions through texture, feature, or grating densities [2-8], but they fail to ultimately define what lies at the heart of tactility. At its core, tactility is driven by skin tribology, the fundamental interaction of skin and a counter-surface under contact and sliding.

Friction is believed to be a significant player during braille reading, as the soft fingertip slides over and interacts with complex arrangements of braille dots, but little to no research has been performed to characterize the tribological interactions of skin on braille dots. More specifically, the frictional mechanisms that govern these interactions have not been studied extensively. To understand frictional behavior during braille reading, it is essential to first understand its fundamental mechanisms.

As one surface passes over another surface asperities interact with one another and produce resistive forces that are manifested as a bulk coefficient of friction. Given an applied normal load, these resistive forces will vary depending on the two surfaces in contact. The area of contact governs the adhesion between two surfaces, where secondary bonding and Van der Waals forces are generated at each contact and repeatedly form and break under sliding. Originally, Greenwood and Williamson implemented Hertzian contact theory towards investigating the sliding of two nominally flat, rigid surfaces [9], but Wolfram and Adams further developed the model to apply to the coefficient of friction between a rigid body against a soft, viscoelastic material [10, 11]. This latter model has wide applicability to any viscoelastic material and smooth surface and can be used

in the investigation of friction of human skin sliding against a rigid substrate. Given such, numerous studies have examined different regions of skin (fingerpad, palmar hand, and forearm) sliding against smooth surfaces such as paper, glass or plastics in both dry and lubricated settings [12-14].

This model provides an estimate of the surface adhesion contribution during skin sliding. On the other hand, it does not directly address sliding against macroscopic features, such as braille dots, where it may be hypothesized that deformation has a strong impact on overall friction. Greenwood et al. investigated this very issue by developing a macro-friction model to describe the hysteresis, or deformation component of friction caused by hard, spherical sliders against a bulk elastomeric surface [15]. Studies have been performed investigating skin on macro-textured surfaces such as ridge and groove patterns [13, 16], but these geometries are somewhat too complex to be directly addressed using existing hysteresis models such as Tabor's. A fundamental understanding of skin sliding against a simple geometry, such as a braille dot, must first be understood in order to understand frictional behavior in more complex situations such as full braille text.

The purpose of this investigation was to determine the underlying friction mechanisms that occur during braille reading. The first aspect of the study was to observe the frictional behavior of skin sliding across a single dot feature in order to determine the relative magnitudes of the adhesion and deformation components of the frictional contribution solely due to a dot feature inclusion. Understanding these mechanisms then allowed for further investigation into more complex braille configurations, studying the effect of directional dot spacing on the coefficient of friction of a fingertip sliding across multiple dot features.

3.2 Materials and Methods

3.2.1 Fundamental friction mechanisms involving individual dots

The emphasis of the initial phase of the investigation was to determine fundamental tribological mechanisms involved in fingertip sliding against braille-dot feature types. The focus was on determining the relative impacts of both adhesion and deformation on friction during braille reading. This was accomplished by investigating the effect of dot size and normal load on the coefficient of friction as the human fingertip slides across said feature. In order to apply Tabor's model of a bulk soft material passing over a rigid sphere, it was necessary to ensure that the fingerpad completely surrounded a single feature during sliding. While Tabor's model assumes a spherical cross-section, standard braille dots have ellipsoidal cross-sections. As defined by the Braille Authority of North America, a standard dot has a height of 0.48mm and base diameter of 1.44mm (projected circle with radius of 0.72mm). With this in mind, three dot radii (dot heights) were selected: 0.48mm (standard braille dot), 0.75mm, and 1.0mm.

Each sample consisted of a single row of four dots, spaced sufficiently far apart so that only a single feature would be encountered at any instance during sliding. For the sample media, 100lb. cardstock printing paper was selected due to its likeness to that of braille textbooks and reading material for the blind and visually impaired. The standard-sized braille dots were embossed using an American Printing House braille slate and stylus. The larger dots were created using an acrylic stencil and the embossing stylus. As the media lay across circular holes in the stencil, features were embossed using the braille stylus as the paper deformed under light pressure. Like that of the standard-sized braille dot, the features had ellipsoidal cross-sections. These topographies were consistent for all three sizes, where the ratio of each ellipsoid's cross-sectional height and width was maintained. These dimensions were verified through the use of a Dino-Lite

digital microscope and calipers. To ensure the structural integrity of the larger features, a hardening agent was used to reinforce the underside of each dot. Once all samples were constructed, they were affixed to a rigid substrate to be mounted for friction testing as shown in Figure 3.1.

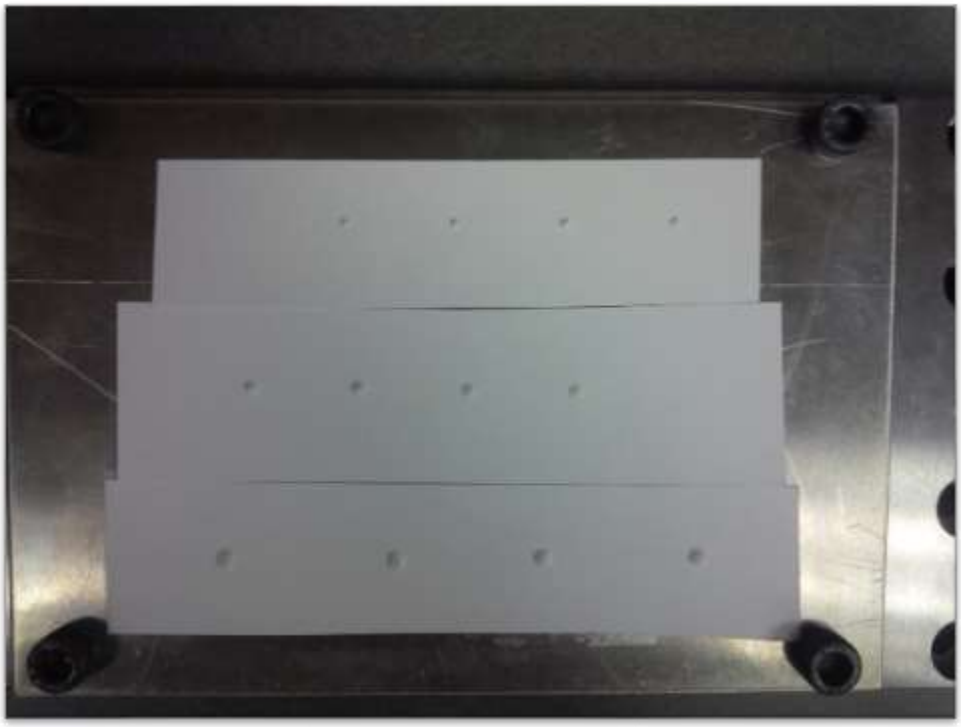

Figure 3.1. Embossed paper samples showing dot features of varying heights: 0.48mm, 0.75mm, and 1.0mm, respectively.

The coefficient of friction of a fingertip sliding against a sample was determined by recording the normal and shear forces produced during a fingertip swipe. These forces were measured with a piezoelectric three-force dynamometer and amplifier (Kistler 9254), and the data was exported to a data acquisition system. Data were taken at a sampling rate of 1,000 Hz and written to files for subsequent processing and analysis. To maintain that all finger swipes were performed consistently, the testing facility was maintained at 23°C and 50% humidity. The tester's left index finger was also cleaned with hand soap and water and thoroughly air dried every 5 trials to reduce tribological effects from oils and dirt.

Data were collected for all samples in a random testing order, where each parameter was repeated three separate times. A swipe's coefficient of friction was calculated by taking the instantaneous ratio of the tangential and normal loading. The beginning of a dot encounter was clearly observed in the data due to the transitional sliding between the featureless surface of the medium (paper) – referred to hereafter as the 'background' – and instances of each dot feature. Frictional effects due to each dot can be visualized in the COF data shown in Figure 3.2. The circled region indicates the coefficient of friction of the finger sliding across the background; and the abrupt transition is caused by the fingertip encounter with a dot feature.

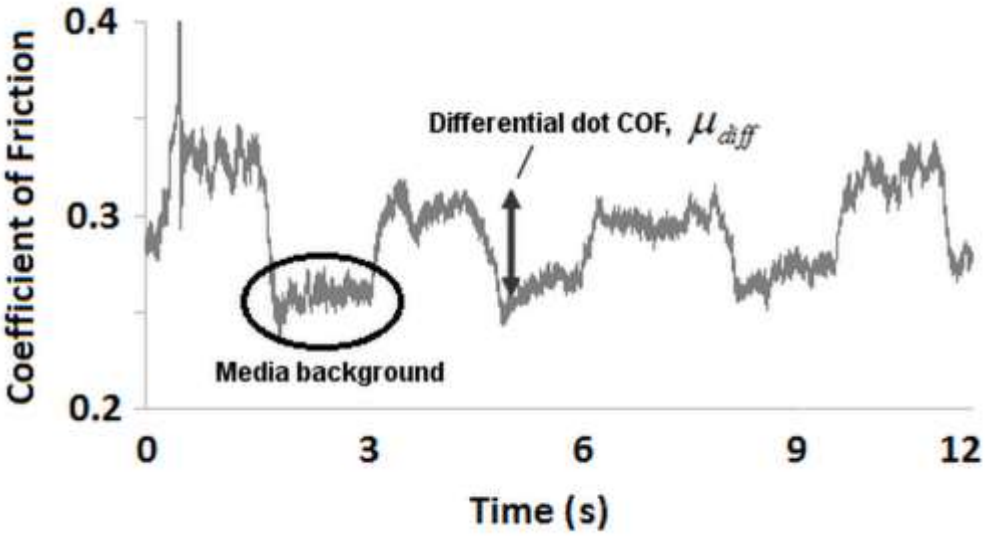

Figure 3.2. Sample coefficient of friction data, displaying the frictional transition while sliding across a smooth surface with consecutive dot features. The increase in COF due to a dot feature is calculated by comparing to the 'background' value.

The effect of normal load on the coefficient of friction was also investigated. For this study, the applied forces ranged from 0.5–2.5N in order to simulate extremely light to vigorous braille reading. The maximum load of 2.5N was selected in order to avoid damage to the features in the paper. The applied forces were categorized into the following ranges: 'light' (0.5-0.8N), 'medium' (1.0-1.5), and 'heavy' (1.75-2.5N), and each sample were tested three times for each loading range. At the start of each test, the normal load was applied with the left index fingerpad, where the

entirety of the pad came into contact with the paper. Prior to the onset of sliding, loading was observed and modified according to the assigned range, and once normalized, the finger was moved in a left-to-right motion across all four features. It was ensured that during each pass, every feature came into contact with the fingerpad's vertical midpoint, where the skin is most compliant. Each test run consisted of three passes, where three dot COF were extracted from each pass, yielding 9 values per run.

As opposed to focusing on the absolute COF value for a given dot size (i.e. 0.30 for the highlighted feature in Figure 3.2), the differential dot COF was considered for analysis. For each dot encounter, the data points before the dot were averaged to represent the background COF; and the average of the data on the plateau represented the dot's COF. To calculate the differential dot COF, the featureless background COF (0.25) was subtracted from the dot COF (0.30), and this value exclusively represented the friction contribution of a dot (0.05). This approach eliminated the effect of the sample media and allows for investigating effects strictly due to the dot features.

The final component to this investigation involved a rudimentary implementation of Hertz' spherical contact model toward skin deformation under normal loading on a flat plane. This test was performed in order to validate the assumption that apparent fingerpad contact due to bulk deformation behaves according to Hertzian contact (Equation 1). To do such, a transparent, acrylic plate was mounted to the dynamometer, extending a short portion of the plate beyond the dynamometer's edge. The fingerpad was placed on the cantilever, and normal loads from 0-3.0 N were applied in increments of 0.5 N. The skin deformations under each loading condition were observed and captured using a Dino-Lite digital microscope. Image analysis with ImageJ was then performed to approximate the apparent contact area dimensions. For the sake of the model, the

fingerpad was assumed to be circular in shape, and the short side of the elliptical fingerprint was used as the apparent contact area dimension, a_F.

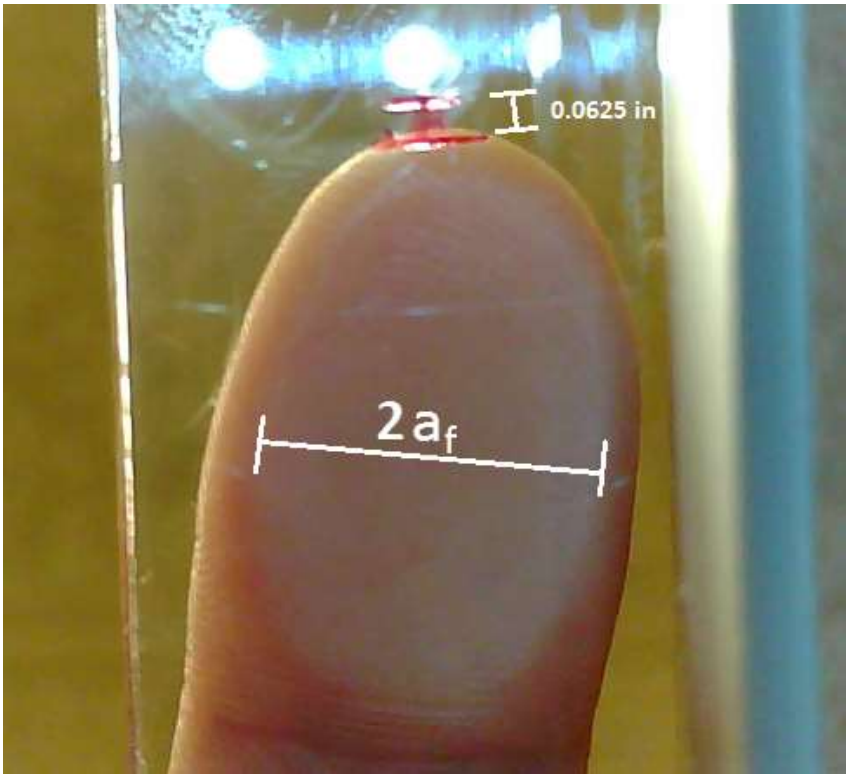

Figure 3.3. Apparent contact area dimension of a fingerpad under 5.0 N load, with the scale bar representing 1.6 mm.

$$a_F = \left(\frac{3 \cdot W \cdot r_F}{4 \cdot E'} \right)^{1/3} \tag{1}$$

The contact data were curve fit to a model based on (1), where r_f is the radius of a 'spherical' fingerpad, *E'* is the reduced Young's modulus of a fingerpad, and *W* is the applied normal load. For the contact area fit analysis, finger radius and modulus were held constant in the form of a regression coefficient versus variable input load, *W*. Using Microsoft Excel and sum of squares analysis, the COF data were then fit to a regression curve analogous to a multi-term friction model based on the components discussed in Greenwood-Tabor [15, 17], Wolfram [10], and Adams [11], thus allowing the investigators to observe and estimate the magnitudes of both the adhesive and deformation components of dot friction.

3.2.2 Friction behavior in multiple-dot configurations

The second phase of the investigation examined the effect of braille dot spacing on the coefficient of friction under fingertip sliding. In this study, only standard sized braille dots (0.48mm) were printed for investigation. Linear rows of dots were printed with either 'horizontal' (left-to-right) or 'vertical' (top-to-bottom) alignment. This produced two distinct scenarios: 1) dot alignment parallel to the fingertip sliding direction (H), and 2) alignment perpendicular to sliding direction (V). Figure 3.5 shows a schematic representative of two adjacent braille cells, where a single cell comprises six dot positions. In standard print, the distance between dots in an individual cell is approximately 2.5mm.

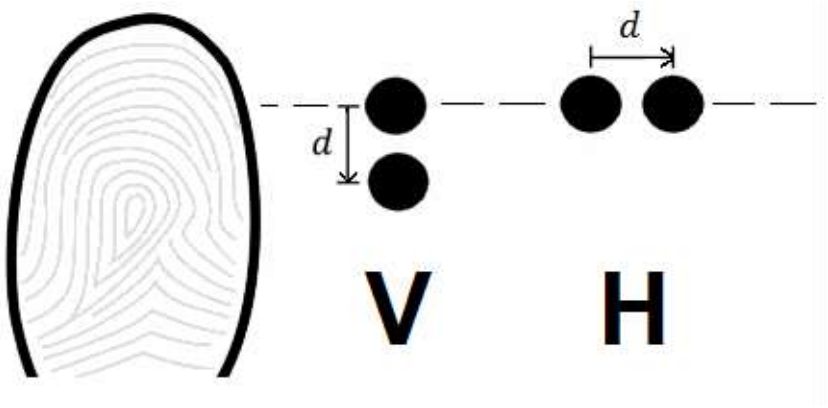

Figure 3.4. The index fingerpad's position was maintained with respect to a positional reference defined by the top row of dot features in both directional spacing configurations.

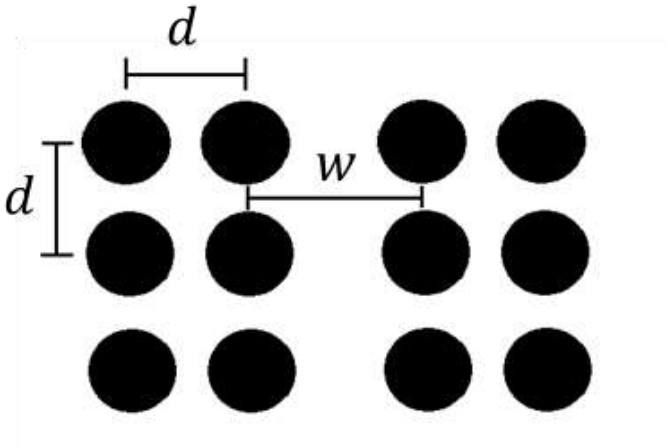

Figure 3.5. Standard layout of braille cells, where d = 2.34mm and w = 3.86mm.

For horizontal spacing, samples with varying dot-to-dot distances were created in increments of 2.0mm, up to a maximum distance of 16mm, to determine the horizontal spacing threshold where adjacent dots begin to exhibit interaction in terms of frictional behavior. For vertical spacing, samples were created in increments of 1.0mm, up to a maximum of 14mm for the same reason as stated above. Increased resolution of 1.0mm increments in the vertical direction was selected to account for an observed greater impact of testing variability in terms of fingerpad contact angle and position on vertically aligned dot patterns.

In this phase of the study, loading effects were eliminated by restricting the loading domain to 'light' loading of 0.5-0.75N. Additionally, the fingerpad's angular position was controlled to emulate that of braille reading and was maintained at an approximate 30 degree angle, with the top half of the index finger being the focal contact point. Figure 3.4 also illustrates the finger placement used for both the horizontal and vertical configurations. The dotted line represents the reference position of the finger with respect to the top row of dots. In the case of the vertical samples, the top dot contacted the fingerpad at the same point for each pass, but as spacing increased, the lower dot gradually moved downward, away from the finger's reference contact with the top row.

Each sample consisted of a pair of dots with chosen alignment, and one coefficient of friction value was collected per pass. Each spacing configuration was tested over three trials, where each trial consisted of 10 passes, yielding 30 friction data points per sample. Like that of the single-feature study, differential dot COF was investigated for all data collected. For samples that exhibited several stages of transitional friction behavior, the maximum differential was used to determine the largest possible friction effect achieved, independent of stage duration.

3.3 Results and Discussion

3.3.1 Fundamental friction mechanisms involving individual dots

This investigation was performed to determine whether the skin-on-braille dot interaction can be modeled by a multi-term friction model, where the driving mechanisms are bulk deformation and interfacial adhesion. In order to evaluate this hypothesis, these mechanisms were assumed to occur on both a microscopic 'multi-asperity' level as well as on the macroscopic 'single dot' scale. Referring to Figure 3.2, it is evident that there are two distinct stages of frictional behavior. The circled portion illustrates the coefficient of friction of skin sliding across the background surface. The plateaus represent the total coefficient of friction of a dot interaction where the fingerpad passes over and entirely surrounds a dot feature. This interaction is illustrated in Figure 3.6. In such an instance, the finger interacts with both the surrounding background surface, as well as the individual dot feature, with the total interacting area consisting of a combination of background contact and feature contact.

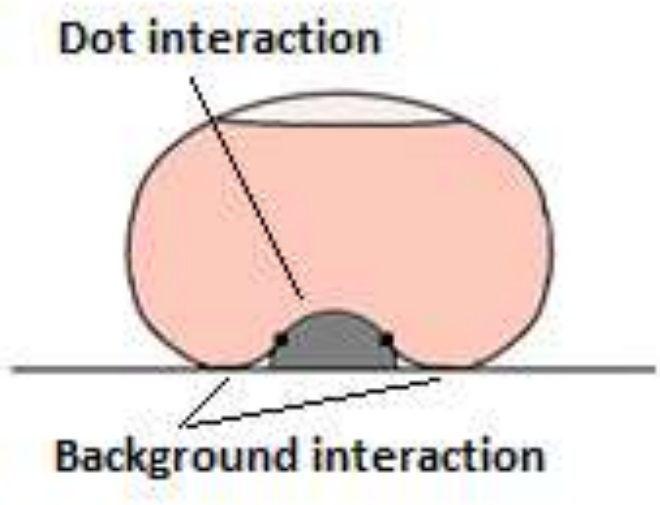

Figure 3.6. Illustration of the encounter with a dot feature. Deformation of the fingertip results in contact with both the dot feature and the background media.

Given that the same paper media was used for all dot sizes in this study, the frictional contribution generated exclusively by a dot feature can be isolated from the total interaction COF. The differential dot COF (the contribution solely due to dot geometry) can be written as:

$$\mu_{diff} = \mu_{dot\ event} - \mu_{media} \tag{2}$$

where $\mu_{dot\ event}$ represents the total COF realized at the dot encounter, and μ_{media} is the COF of skin sliding against the featureless background surface before the dot is encountered. The magnitude of the differential friction is indicated by the arrow in Figure 3.2. When the sliding finger encounters and traverses a dot, the total COF includes contributions from the skin *on* as well as *around* the dot. Considering these dual components during dot traversal (contact with both dot and background around the dot), (2) can be expressed as:

$$\mu_{diff} = \gamma \cdot \mu_{media} + \delta \cdot \mu_{dot} - \mu_{media} \tag{3}$$

where γ is the fraction of finger contact on the background surface around the dot versus the total finger contact area, and δ is the area fraction of finger contact on the dot, and thus the sum of the two area fractions is equal to unity. More accurately, the proportion terms γ and δ represent the force distribution across the feature set, but area fractions are assumed to be a valid approximation due to the dot's negligible size in comparison to the fingerpad. As the finger traverses the dot, the finger encounters both the micro-scale multi-asperity contact of the media on the *surface* of the dot, in addition to the macro-scale geometry of the dot itself. As indicated in Figure 3.6, the skin does not completely encompass the dot during traversal, but rather has a separation region around the base of the feature due to the elastic behavior of the fingertip. The resulting surface area in contact is a spherical sector with a base radius that is less than the full radius of the dot feature, *R*. The micro-scale multi-asperity adhesion between the skin and the dot surface is thus a function of this contact area. A reasonable assumption can be made that the surface area of the sector in contact

is approximately equal to the projected circular area of the full dot against the planar background surface. With this assumption, the surface component of total dot friction becomes equal to the friction of the background media of a flat disk of radius *R*. Therefore, a two-term model of total dot friction can be simplified to isolate only the effects of the dot feature's macro-scale geometry from that of the micro-scale multi-asperity surface, as shown below:

$$\mu_{dot} = \mu_{media} + \mu_{dot\ geometry} \tag{4}$$

Combining (3) and (4) and simplifying the result eliminates all terms involving the COF of the media and produces a relation that ties the differential friction coefficient directly to the macro-scale geometry of a single dot. The contributions of macro-scale adhesion and deformation can then be studied independently of the micro-scale friction mechanisms of the multi-asperity media.

$$\mu_{diff} = \delta \cdot \mu_{dot\ geometry} = \delta \cdot \left(\mu_{def} + \mu_{adh,} \right) \tag{5}$$

In order to identify the magnitude of the adhesive and deformation components of friction, it is essential that each component be exclusively defined by controllable parameters: material properties, geometric features, and normal loading. The deformation-based spherical indenter model of Tabor et al appears to be directly applicable to a single-dot traversal, as it predicts the deformation loss component of the coefficient of friction of a rigid sphere sliding across a bulk elastomer [17]. Here, the fingerpad takes the role of the soft elastomeric bulk, and the dot represents the spherical indenter. Tabor's model can be shown as:

$$\mu_{def} = \beta \left(\frac{9}{128 \cdot R} \right)^{2/3} \left(\frac{1}{E'} \right)^{1/3} W^{1/3} \tag{6}$$

Where β is the viscoelastic hysteresis loss fraction, *E'* is the reduced modulus of elasticity, *R* is the radius of the indenter, and *W* is normal loading. With media type and fingertip mechanical

properties assumed constant in this study, deformation-based friction is thus directly dependent on dot radius and normal load.

Turning to the adhesive component of single-asperity friction, Wolfram and, later, Adams developed a model also incorporating radius and normal load [10, 11]:

$$\mu_{adh} = \pi\tau_o \left(\frac{3 \cdot R}{4 \cdot E'} \right)^{2/3} W^{-1/3} \tag{7}$$

where τ_o is the intrinsic shear stress between the two surfaces, *E'* is the reduced modulus of elasticity, *R* is indenter radius, and *W* is normal loading. Note that this formulation, in line with Wolfram's treatment, assumes an incompressible material with no interfacial shear stress dependence on contact pressure. Again, *R* and *W* are independent inputs in (7), and the rest of the terms are constant for a single background media. It should be noted that in adhesion-dominated sliding, the frictional force is inversely related to normal loading, and this decaying behavior is commonly observed in sliding of soft materials, such as skin [18, 19]. It was surmised that the topology of the paper media would account for most of the true contact area because of the numerous micro-scale contacts, and thus very little additional contact area would be realized with the addition of the macro-scale dot feature. This suggests that the differential COF caused solely by dot adhesion would be very low.

The dot area fraction, δ, is defined as the ratio of projected dot area versus the apparent finger contact area from (1). Figure 3.7 illustrates the fingerpad's observed contact in comparison to predicted Hertzian contact. This observed behavior is reasonably in line with the Hertzian model for the given loading range, while also exhibiting long-term linear behavior. Relation (8) expresses dot area fraction with respect to skin mechanical properties and dot geometry:

$$\delta = \frac{\pi \cdot R^2}{A_F} = \frac{R^2}{\left(\left(\frac{3 \cdot W \cdot r_F}{4 \cdot E'}\right)^{1/3}\right)^2} \tag{8}$$

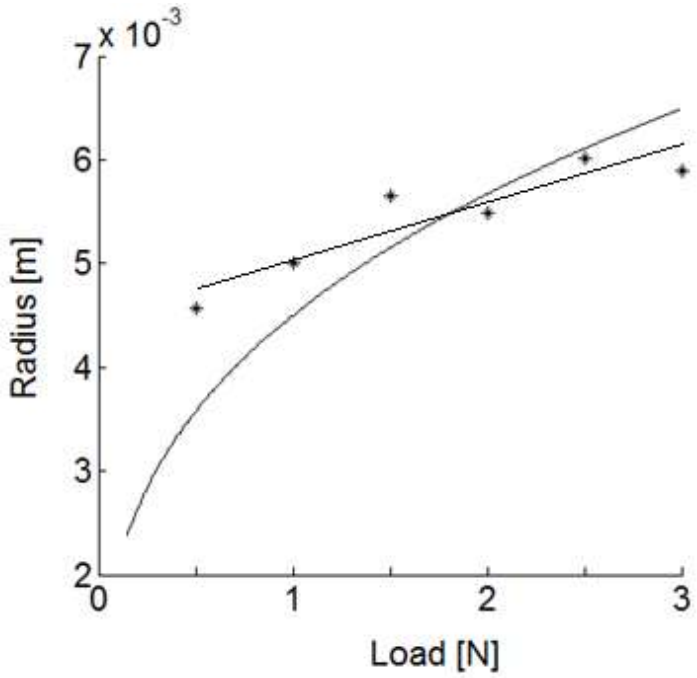

Figure 3.7. Measured effective radius of contact of a fingerpad against a nominally flat surface at varying applied load. The curve represents the Hertzian model fit to the data as well as a linear approximation.

Given the expressions for both the adhesion and deformation of sphere on skin contact, (5) through (8) can then be combined into the following form:

$$m_{diff} = \pi t_o r_F^{-2/3} R^{8/3} W^{-1} + r_F^{-2/3} b \left(\frac{3}{32}\right)^{2/3} \left(\frac{1}{E'}\right)^{-1/3} R^{4/3} W^{-1/3} \tag{9}$$

Where the two additive terms respectively represent the adhesion and deformation differential dot COF contributions. Excluding dot radius and normal loading, all remaining terms are based on material and interfacial properties. With the dot radii used in this study, and the assumption that fingertip radius is one order of magnitude larger than the dot radius, then the adhesion term in (9) becomes negligible as previously hypothesized. Based on this, the differential COF data were fit

to the model – after the adhesion term was removed – using a multi-variable least sum of squares regression for all tested values of dot radius and loading. This yielded a model coefficient of:

$$r_F^{-2/3}\beta\left(\frac{3}{32}\right)^{2/3}\left(\frac{1}{E'}\right)^{-1/3} = 565.3N^{1/3}m^{-4/3} \tag{10}$$

The differential COF data are plotted with respect to normal load in Figure 3.8, which also shows the fitted model. The squared correlation coefficient for this model was calculated to be 0.227, which is reasonable for an exponential relationship such as this.

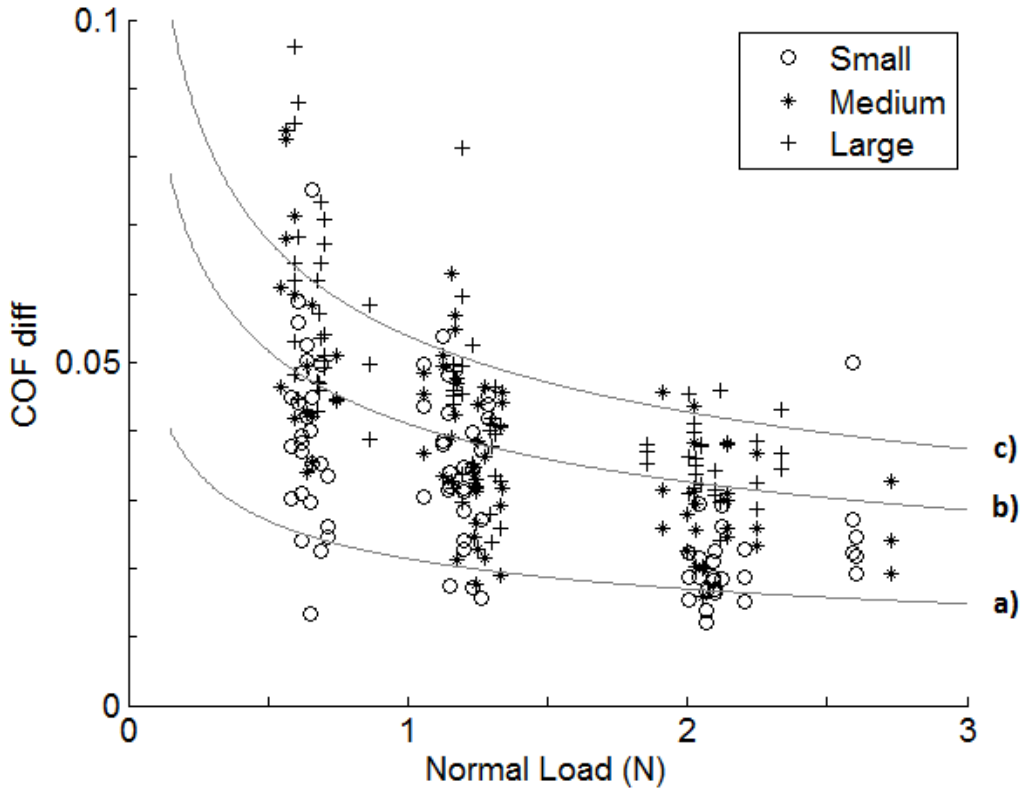

Figure 3.8. Predicted COF versus normal loading for small (a), medium (b), and large (c) dot radii against measured COF data.

Upon visual inspection of the data, it is clear that the differential friction exhibits a shallow decay at higher normal loads, as predicted by the deformation-dominated model. It is also noted

that differential COF has a positive exponential relationship to feature radius, and this behavior is reflected in Figure 3.8. Given these observations, hysteretic deformation due to macroscopic geometries appears to be the predominant contributor to the dot coefficient of friction, across all dot sizes and normal loads used in this study. This analysis suggests that additional adhesion friction due to the macro-scale geometry of the dot feature is negligible. This fundamental understanding of friction mechanisms of skin on a single feature can now be incorporated with respect to more complex configurations involving multiple-feature interactions.

3.3.2 Friction behavior in multiple-dot configurations

The purpose of the multi-feature study was to investigate how dot spacing and feature-to-feature orientation affects the coefficient of friction for skin in multi-dot configurations. The results of the previous phase of the study showed that deformation hysteresis is the primary frictional mechanism in the differential coefficient of friction produced when sliding over a dot feature. For this investigation phase, the maximum differential dot coefficient of friction was recorded and analyzed in order to strictly focus on the effects of neighboring dot features on COF differential, and to determine threshold feature spacing when multi-feature effects must be considered.

In order to better understand the results of multi-dot experiments, the instant of feature interaction must be considered. For single-feature sliding, this event is defined by the instant in time when the fingerpad entirely covered the dot feature. In the case of vertical multi-dot orientations (referred to as the ‘V’ orientation in Figure 3.4), the instant of dot interaction was identical to that of single-feature sliding, regardless of the position of the secondary dot. This is because both dots were at the same distance from the fingerpad at any point in the test. Results from a representative test of the vertical orientation of two dots is illustrated in Figure 3.9, where

the fingerpad pass over a 6.0-mm vertical spacing is detected as a single coefficient of friction plateau, which stays relatively constant for approximately 1 second of sliding.

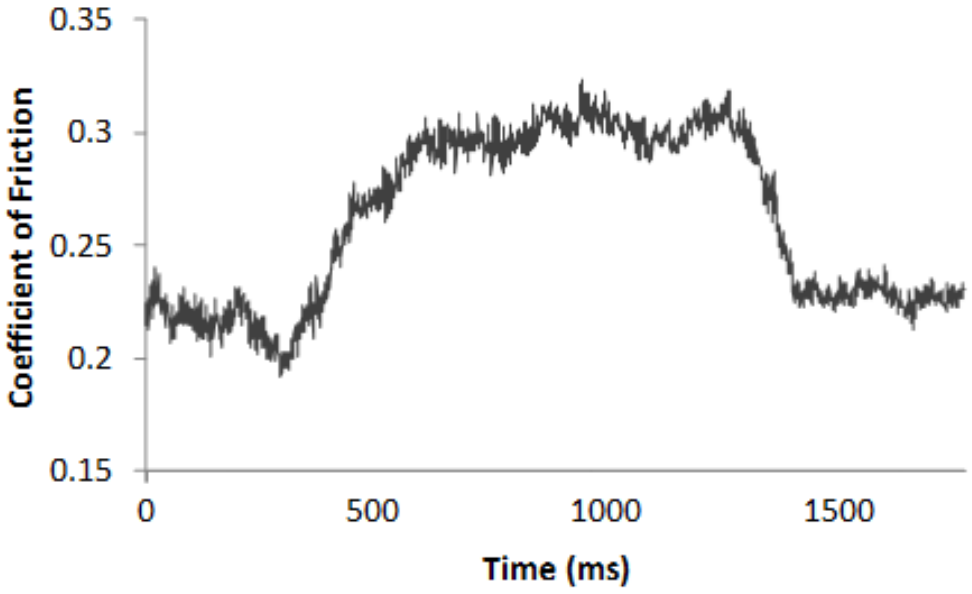

Figure 3.9. Single COF peak for a vertical spacing instance of d = 6.0 mm.

Contrast the vertical orientation with the timeline of events for a horizontal dot orientation ('H' in Figure 3.4). Samples with horizontally-oriented feature spacing experienced friction events in a significantly different manner. In these cases, the dots were positioned such that fingerpad encounter occurred sequentially in time, such that two distinct frictional plateaus could be observed in the data. However for sufficiently small spacing, two dot features could be encountered at the same time, thus exhibiting a somewhat complex frictional response. This is hypothesized to have occurred because the viscoelastic fingerpad did not have sufficient opportunity to fully penetrate the space between the two adjacent dots and reestablish contact with the background surface before the second dot was encountered. Additionally, the transition from background to feature contribution is slightly slower than that of the vertical spacing because the total contact distance is larger and not instantaneous. This resulted in an inability to resolve the frictional behavior into two separate features, as shown in Figure 3.10. One noteworthy

observation is that the differential COF produced during interaction with closely-spaced dots was not significantly higher than a single dot. What this suggests in practical terms, is that from a friction standpoint, there appears to be a spacing threshold below which two adjacent dots are experienced as a single feature.

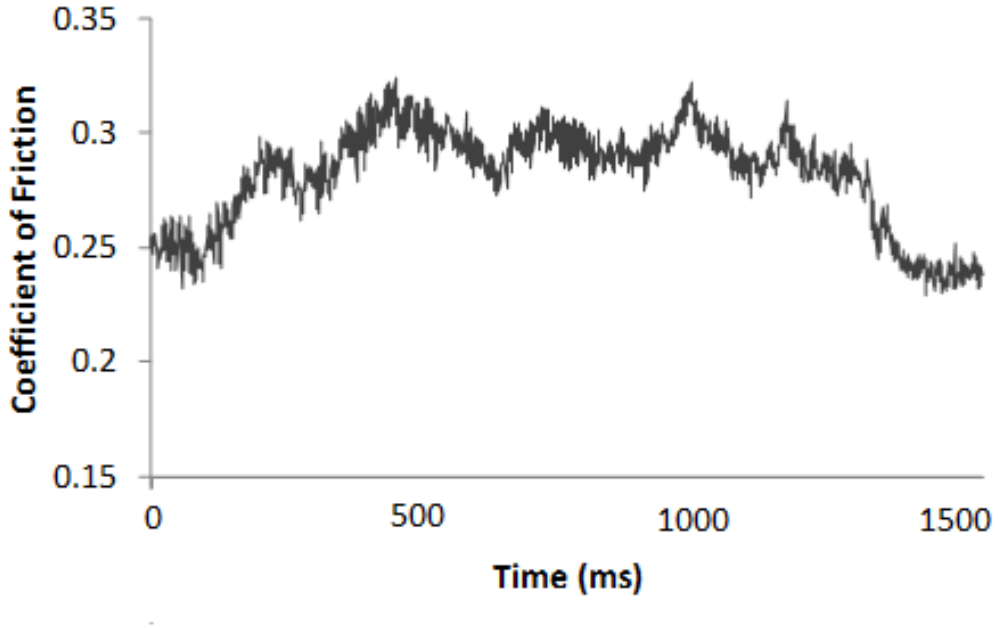

Figure 3.10. A horizontally-oriented sample (d = 2.5 mm) illustrating that for sufficiently small feature spacing, the frictional behavior resembles that of an extended single feature.

With somewhat greater horizontal distance between dot features, the coefficient of friction exhibited five distinct stages as shown in Figure 3.11. The first stage involved the expected interaction with the background medium (paper), as is seen in all tests. The second stage plateaued at a COF similar to that of a single dot. However, the third stage revealed an additional increase in friction for a short period of time. This is hypothesized to be due to the dots having enough spacing to allow sufficient finger penetration to produce significant hysteretic friction against both features simultaneously, effectively doubling the differential COF predicted by the single dot model above. The fourth stage showed a reduction in friction, similar to the level experienced at stage two.

Finally the fifth state indicated that the fingerpad was again in complete contact with the featureless background surface.

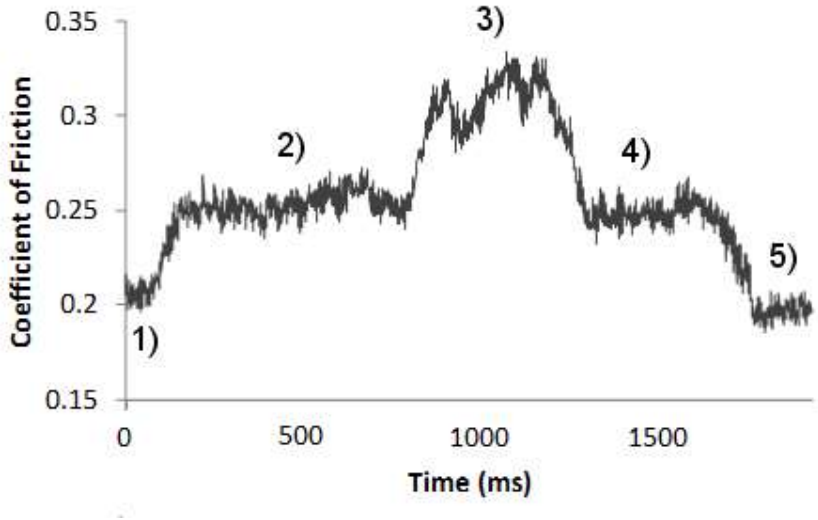

Figure 3.11. A horizontal sample (d = 6.0 mm) that illustrates the progressive behavior of coefficient of friction as the finger passes over sufficiently spaced dots, where the five stages of interaction are 1) background, 2) single dot, 3) multi-dot, 4) single dot, and 5) background interactions .

As would be expected, as horizontal feature spacing was further increased, the compounded interaction became less pronounced until two distance friction plateaus separated. This confirms that for sufficiently large feature spacing the fingerpad is able to fully penetrate between each of the dots and encounter them independently.

When investigating the differential coefficient of friction for multi-feature arrangements in both orientation directions, the average of the peak differential COF (stage 3, Figure 3.11) recorded during a test run was used for analysis. Figure 3.12 shows the maximum differential COF for various dot spacing with both orientations. As expected, sufficiently large spacing in either the horizontal or vertical directions yielded the lowest values of differential dot COF at 0.05 to 0.06, approximately equal to single dot results. This threshold spacing appeared to be approximately 12 mm for horizontal spacing, and 14 mm for vertical spacing, respectively. At these distances, the fingerpad only encountered one individual dot at any point during sliding. As distance decreased

below these threshold values, the differential dot COF was higher due to interaction effects of adjacent dots on the fingerpad.

At the smallest dot spacing in both orientations, differential COF is somewhat higher than for a single dot feature, with the vertical direction being slightly higher than the horizontal. This may be explained by the fact that with vertical spacing, there are two features imposing hysteretic deformation on the fingerpad from the onset of sliding; however the effect is tempered by the lack full skin penetration into the space between the dots. As vertical dot spacing increased to 8 mm, differential COF increased nearly steadily, with the exception of an unexplained lower value at 6 mm. The differential COF for a vertical spacing of 8 mm was approximately double that of a single dot, as would be expected if two regions of the fingerpad underwent simultaneous independent deformation-driven friction caused by the two adjacent dots. Beyond 8 mm, differential friction of vertically spaced features began to decrease toward the eventual resumption of single-dot behavior as described above.

For horizontal dot spacing, similar maximum differential COF values were observed as in the vertical direction, but the onset and release of multi-feature interactions occurred at slightly different spacing than the vertical. The maximum differential friction occurred at a horizontal dot spacing of 4 mm, with a five-stage behavior similar to that shown for 6-mm spacing in Figure 3.11. From this spacing, differential COF steadily declines until 12 mm, when friction stabilizes at the single-dot value. The steep increase in friction between 2 and 4 mm suggests that the latter spacing is just sufficient to allow meaningful penetration of the skin into the space between the dots, so that the fingerpad experiences two distinct regions of hysteretic deformation. However, it is likely that the penetration is not fully extended to reach the featureless intra-dot surface, so that the full heights of the dots are not interacting with the fingerpad. This reasoning may also be applied to

the observation of the decline in friction after 4 mm, in that while the fingerpad appears to be interacting with two adjacent features, the horizontal spacing may be such that the skin is not fully encompassing both sides of each dot and thus the area of interaction may be slightly reduced compared to the 4-mm spacing. This phenomenon would be dependent primarily on fingertip size and apparent area of fingerpad contact.

One final aspect to note when comparing the friction of the vertical and horizontal multi-dot orientations is the fact that the spacing threshold for horizontal spacing (12 mm) is less than for the vertical spacing (14 mm). The simplest explanation for this difference is the natural shape of the fingertip and the fact that the contact between skin and surface is approximately elliptical with the major axis parallel to the vertical orientation. Thus, there is more length of contact in the vertical direction than in the horizontal, so the dots must have greater spacing in the vertical direction to avoid fingertip contact with adjacent dots. This elliptical shape of the contact plane is evident in Figure 3.3.

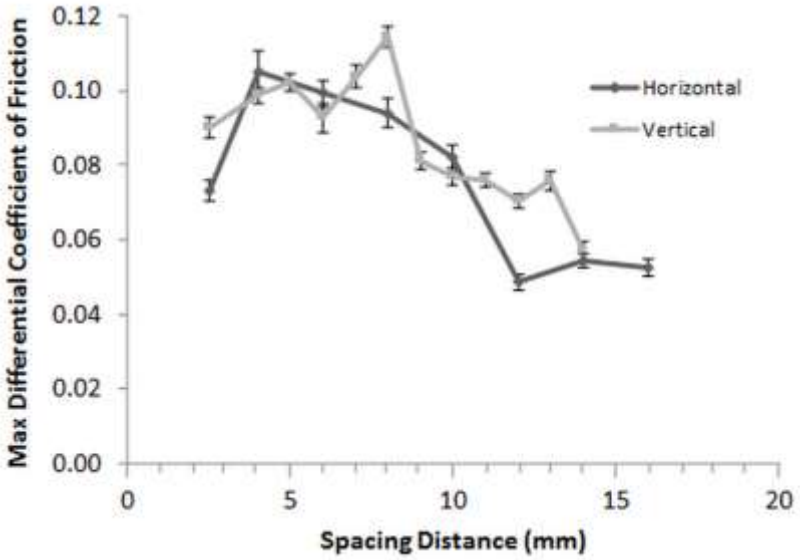

Figure 3.12. The differential coefficient of friction with respect to directional dot spacing, denoting the standard deviation for each spacing and direction.

The results indicate differential COF from skin-on-dot sliding is largely deformation driven and independent of adhesion, and in turn, medium; but one major limitation is that only one medium, braille embossing paper, was investigated. An investigation studying the frictional effects across multiple mediums with the same geometries would provide significant validation to the two-term model developed in this paper. Additionally, the results from the spacing investigation lead the authors to believe that certain spacings allow for increased and ideal penetration between the dot pair, but these claims have not been quantified. Empirical penetration or contact tests, or even computational modelling of skin-on-dot sliding would greatly benefit such claims.

3.4 Conclusions

The fundamental frictional mechanisms involved in fingertip-on-dot sliding (akin to braille reading) were investigated in both single-feature and multiple-feature configurations. Based on the observed results, the following conclusions can be drawn:

- These results for a common paper medium suggest that the differential increase in coefficient of friction due to the presence of dot features may be largely independent of the medium on which the features are embossed. This is due to the fact that the macro-scale topology of the features contributes little to the overall friction arising from adhesion mechanisms.
- Hysteretic deformation of the soft fingerpad around the dot feature during sliding was the dominant mechanism that governed overall friction. Its magnitude was directly related to dot feature radius and applied normal load.
- The spacing between adjacent dots in linear arrays with either horizontal or vertical orientations greatly affected the differential friction coefficient, due the sliding fingerpad ability to be in physical contact with two dots simultaneously. The spacing thresholds that

indicated the transition between single- and multiple-dot friction behaviors were 12 mm and 14 mm for the horizontal and vertical directions, respectively.

3.5 References

[1] J. R. Phillips, R. S. Johansson, K. O. Johnson, Representation of braille characters in human nerve fibres. Experimental brain research. Experimentelle Hirnforschung. Expérimentation cérébrale 81, (1990) 589.

[2] R. W. Van Boven, R. H. Hamilton, T. Kauffman, J. P. Keenan, A. Pascual–Leone, Tactile spatial resolution in blind Braille readers. Neurology 54, (2000) 2230-2236.

[3] R. W. Van Boven, K. O. Johnson, The limit of tactile spatial resolution in humans: grating orientation discrimination at the lip, tongue, and finger. Neurology 44, 2361.

[4] K. O. Johnson, S. S. Hsiao, Neural mechanisms of tactual form and texture perception. Annual review of neuroscience 15, (1992) 227.

[5] H. E. Wheat, A. W. Goodwin, A. S. Browning, Tactile resolution: peripheral neural mechanisms underlying the human capacity to determine positions of objects contacting the fingerpad. The Journal of neuroscience : the official journal of the Society for Neuroscience 15, (1995) 5582.

[6] K. O. Johnson, J. R. Phillips, Tactile spatial resolution. I. Two-point discrimination, gap detection, grating resolution, and letter recognition. Journal of neurophysiology 46, (1981) 1177.

[7] J. R. Phillips, K. O. Johnson, Tactile spatial resolution. II. Neural representation of Bars, edges, and gratings in monkey primary afferents. Journal of neurophysiology 46, (1981) 1192.

[8] J. R. Phillips, K. O. Johnson, Tactile spatial resolution. III. A continuum mechanics model of skin predicting mechanoreceptor responses to bars, edges, and gratings. Journal of neurophysiology 46, (1981) 1204.

[9] J. A. Greenwood, J. B. P. Williamson, Contact of Nominally Flat Surfaces. Proceedings of the Royal Society of London. Series A, Mathematical and Physical Sciences 295, 300-319.

[10] L. J. Wolfram, Friction of skin. Journal of the Society of Cosmetic Chemists 34, (1983) 465-476.

[11] M. Adams, B. Briscoe, S. Johnson, Friction and lubrication of human skin. Tribol Lett 26, (2007) 239-253.

[12] S. Derler, L. C. Gerhardt, A. Lenz, E. Bertaux, M. Hadad, Friction of human skin against smooth and rough glass as a function of the contact pressure. Tribology International 42, (2009) 1565-1574.

[13] O. Bobjer, S.-E. Johansson, S. Piguet, Friction between hand and handle. Effects of oil and lard on textured and non-textured surfaces; perception of discomfort. Applied Ergonomics 24, (1993) 190-202.

[14] L. Skedung et al., Tactile perception: Finger friction, surface roughness and perceived coarseness. Tribology International 44, (2011) 505-512.

[15] J. A. Greenwood, H. Minshall, D. Tabor, Hysteresis Losses in Rolling and Sliding Friction. Proceedings of the Royal Society of London. Series A, Mathematical and Physical Sciences 259, (1961) 480-507.

[16] M. A. Darden, C. J. Schwartz, Investigation of friction mechanisms during the sliding of elastomers against hard parallel-ridge textures. Tribology International 63, (2013) 2-7.

[17] J. A. Greenwood, D. Tabor, The Friction of Hard Sliders on Lubricated Rubber: The Importance of Deformation Losses. Rubber Chemistry and Technology 33, (1960) 129-141.

[18] S. Comaish, E. V. A. Bottoms, The skin and friction: deviations from Amonton's laws, and the effects of hydration and lubrication. British Journal of Dermatology 84, 37-43 (1971).

[19] A. F. El-Shimi, In vivo skin friction measurements. J. Soc. Cosmet. Chem 28, (1977) 37-52.

CHAPTER 4: CHARACTERIZING THE FUNDAMENTAL CONTACT LOADING AND FRICTION MECHANISMS THAT OCCUR DURING A LARGE SCALE REPRESENTATION OF FINGER ON BRAILLE SLIDING

A paper published in WEAR

M.A. Darden and C.J. Schwartz

Abstract

Beyond the sense of sight, the sense of touch is one of the primary ways that individuals experience their surrounding environment. Fundamentally understanding the relationship of skin-surface tribology and its elicited tactile attributes could provide a breakthrough in improving the ability to efficiently transmit tactile information to those who rely on the sense of touch to interact with their surroundings, such as the blind and visually impaired (BVI) community. The tactile language of braille has been adopted by the BVI community, employing configurations of raised dome-shape dots to convey what is ordinarily presented in text and image form. The coefficient of friction caused by skin sliding across a these dot features is hypothesized to affect the reader's tactile sensitivity, and skin-on-braille coefficient of friction has been investigated in previous work, where macro-scale deformation of the human fingerpad sliding over the dot contour was identified as the dominant friction mechanisms. This investigation succeeds that study by examining a simplified large-scale, two-dimensional representation of skin-on-braille sliding to characterize the underlying contact mechanisms in the loading behaviors that dictate the resulting coefficient of friction. This was accomplished by using a multi-axis tribometer to sliding a 25.4 mm radius cylindrical polyurethane (representing a human fingerpad) rod over a lubricated 3.17 mm aluminum half rod (representing a braille dot) under displacement-displacement-controlled

conditions. The results from the tribometer study indicate that the presence of the dot feature drastically affects the vertical and lateral loading behavior by vertically displacing the body's elastic bulk, generating rubber-like Poisson effect contributions. Most importantly, the Poisson effect rapidly increases the lateral load when the body contacts the dot's leading edge, and rapidly decreases when the body rests largely in contact with the dot's trailing edge. This rapid decrease is caused by a "propulsion" effect, where vertical compression expands the material laterally, and when situated on the trailing edge of the dot, propels it into the direction of sliding, virtually negating adhesive surface friction. Computational modeling validated these findings and also discovered that while normal contact pressures dominated the fluctuations seen in the vertical loading, effects due to both normal contact pressures and frictional shears nearly equally drove the lateral loading behavior.

4.1 Introduction

Touch is one of the fundamental sensory mechanisms that allow individuals to physically interact with and learn about their surrounding environment. Tactile exploration is generally not the primary method that individuals use to acquire information, for this designation would be given to the sense of sight. Unfortunately, not all individuals possess the ability to employ vision as their principal means of learning; and as a result, the blind and visually impaired (BVI) community relies on touch and tactile perception. Varying types of tactile language were developed in order to provide non-sighted with the tools to learn with and function in the same way that sighted individuals can, and the braille writing system was adopted as the standardized tactile language for the BVI community.

Perceiving and decoding the braille language requires an individual to tactually scan the text or images with the fingerpad, and this form of tactile perception is governed by the tribological

skin-surface sliding interaction experienced during the exploration of the dot configurations. It is believed that during this sliding interaction, the resulting changes in coefficient of friction (COF) aid the reader in translating the code, in the same way that coefficient of friction has been believed to influence perceived tactile attributes in other surfaces such as paper media [1, 2], or textile fabrics [3-8], or ridged textured metals and polymers [9, 10]. In the case of skin sliding over featureless paper media, Skedung et al. found that coefficient of friction was positively correlated to both perceived coarseness as well as the media's surface roughness. Conversely, friction correlations to tactile perception have not been as prominent for skin interactions with textiles or ridged surfaces. Highly specific attributes such as abrasiveness or softness were not found to be related to skin friction [6], but perceived comfort and friction have been positively correlated for both wearable textiles as well as rigid textures, primarily influenced by the degree of moisture at the skin-surface interface [3, 4, 7]. Complementary to this finding, variations in surface topographies with macroscopic features have been found to produce skin deformations and surface vibrations that in turn affect friction and perception [8, 9]. While not explicitly dictating tactile perception, skin friction and its interaction with topographical surfaces still affect the tactile experience to some degree, and understanding these sliding interactions would prove valuable for a multitude of applications.

Understanding the fundamental friction and contact mechanics of the skin on braille dot tribology would allow for a deeper understanding in friction's impact on the quality of learning and perception for the BVI community. The tribological interaction of a human fingerpad sliding over a braille dot is analogous to Wolfram and Adams' model of a small rigid sphere being dragged across an elastic half-plane [11, 12] (based on Greenwood and Tabor's [13, 14]), and this model was key in discovering the major impact that the friction mechanism of deformation has on

coefficient of friction behavior during skin-dot sliding [15]. During this investigation, the trends exhibited in the coefficient of friction behavior were investigated, but the specific contact mechanisms driving the loading behavior, which in turn dictated the COF, were not analyzed.

The purpose of this investigation was to determine the underlying contact mechanisms that drive loading behavior during braille reading, and this was executed in two phases. The first aspect of the study was to observe the vertical and lateral loading behavior of a large-scale, two-dimensional representation of a simulated braille reading. The second aspect of the study entailed validating the data and claims drawn from the initial phase by performing computational modeling and decomposing the loading components and coefficient of friction behavior.

4.2 Materials and Methods

Previous work has determined that the friction mechanism of deformation plays a major role of sliding interactions during braille reading, where a soft fingertip slides against a rigid braille dot feature. The motivation for this study was to gain a better understanding of the exact contact mechanics that occur during this tribological interaction. This paper investigates the force interactions and presents two phases that were performed concurrently in order to complement and validate the other's data and analyses.

4.2.1 Empirical study of a soft cylindrical body sliding over a rigid half-cylindrical feature

The first phase of this investigation explored the contact mechanics of braille reading by recreating the tribology of braille reading in a large-scale, yet simple manner. While braille reading involves forces and deformations in three directions, this design simplified the problem by reducing the finger's and dot's spherical geometries to cylindrical bodies. Here, sufficiently long cylinders assume plane strain conditions, where strains and forces were restricted to only two

directions in order to be analyzed more easily. The testing during this phase employed a multi-axis tribometer (Rtec Instruments) for all sliding interactions and force measurements.

The projected contact area of the human fingerpad is ellipsoidal in shape, but as observed in previous work [15], it can be assumed to be a homogeneous, elastic spherical (for this sake of this study, cylindrical) body. Typically, one measures approximately 20 mm across (10 mm radius), and the standard hemispherical braille dot is 0.48 mm high. This comparison yields roughly a 20:1 scale between fingerpad and dot feature radii. Due to the availability of commercial materials, the scale of the finger-to-dot ratio in this study was reduced to 8:1. A 50.8 mm (2 in.) diameter polyurethane rod was selected to simulate the finger's elastic behavior. The polyurethane rod had a durometer hardness rating of 40A, and according to Equation 1,

$$E = e^{[S_A \cdot 0.0235 - 0.6403]} \tag{1}$$

It had an equivalent modulus of elasticity of 1.35 MPa, where E is the modulus of elasticity in MPa and S_A is the ASTM D2240 type A hardness rating. The rod was cut to 30 mm in length so that the loads produced from the required displacements would not exceed the limitations of the tribometer's load cell. Polyurethane was selected to represent the human fingerpad as it, along with silicone, has been shown to successfully exhibit frictional and mechanical properties as mechanical skin equivalents [5]. While the skin fingerpad is a textured surface covered in ridged surface textures, this study ignored these textures in order to solely focus on observing bulk material deformations due to the introduction of a macroscopic topography, absent of surface interactions.

The rod's circular cross-section was squared off on three of the four sides so that it could be mounted into a stainless steel U-channel. This was performed in order to ensure that both the vertical and lateral displacements were uniformly applied, as well as to eliminate rotation due to sliding. This mounting treated the rod as a half cylinder where applied displacements and boundary

conditions could be maintained at the vertical center of the cylinder. A stainless steel shaft was welded to the top surface of the channel to mount to the tribometer's load cell.

The dot surface counterface consisted of a 6.35 mm (1/4 in.) diameter aluminum half cylinder affixed to 6.35 mm (1/4in.) thick 152.4 mm X 152.4 mm (6 in. X 6 in.) aluminum plate. The top surface of the counterface was manually polished with P2500 grit abrasive paper and subsequently cleaned. This counterface was then mounted to the tribometer's dual-axis, stage, and the final experimental setup can be seen in Figure 4.1.

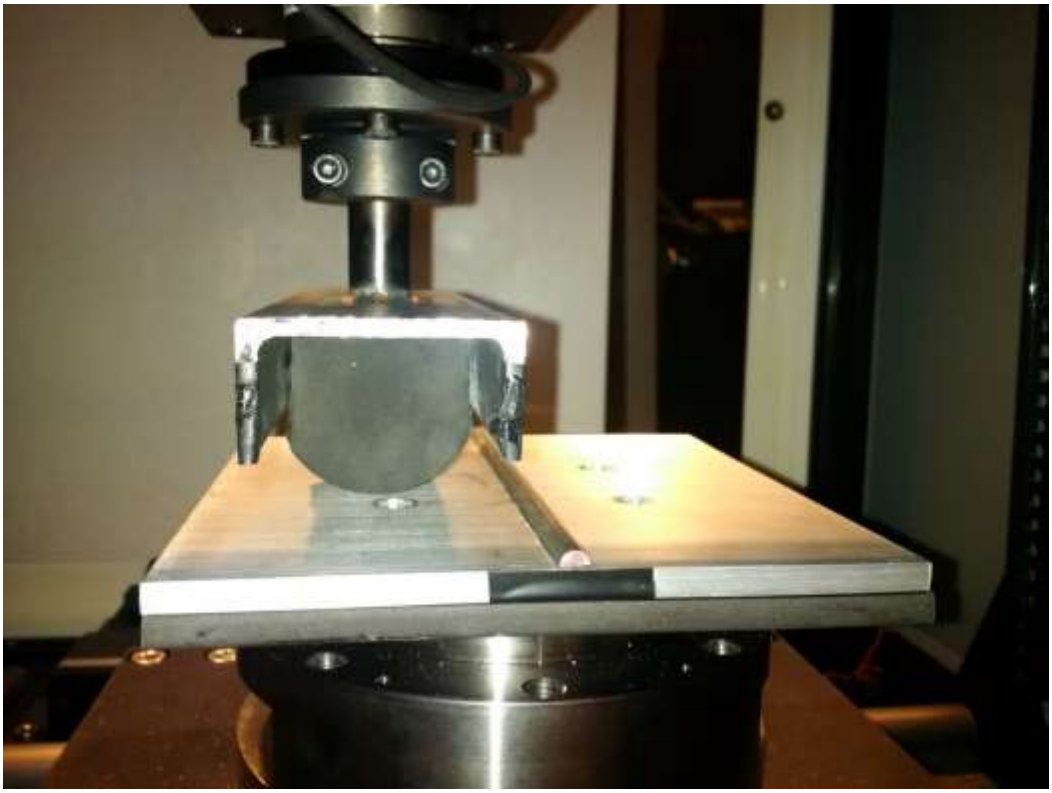

Figure 4.1. The polyurethane rod brought into contact with the counterface surface prior to a tribological test.

A 6D, 500 N limit load cell was used to record both the vertical and lateral forces at a sampling rate of 1,000 Hz during all sliding tests. Additionally, the tribological tests were performed under displacement-controlled conditions in an environment where temperature and humidity measured at 23.8 deg. C and 50% humidity, respectively. Vertical displacements were controlled by the Z-axis motor and load cell suspension, and lateral displacements were controlled

by the dual-axis stage (X-axis only). Additionally, a GoPro HD camera was mounted to the stage to record video of the rod sliding across the surface. This footage was then synchronized with the force data to visualize the sliding interaction with respect to the data's loading behavior.

Because this study sought to isolate and understand the sliding mechanics caused by a large scale feature (not due to small-scale surface interactions), the surfaces of both the polyurethane rod and counterface were coated with a thin film of food-grade mineral oil lubricant. Additionally, the lubrication reduced the polyurethane-aluminum COF to roughly 0.25, resembling the skin-paper interaction experienced during braille reading [15]. Each run was displacement-controlled, where the rod was brought into contact with the flat portion of the counterface on one side of the dot feature and then vertically displaced by 10 mm. This displacement was chosen during preliminary testing in order to guarantee that the soft material would fully surround the dot feature during sliding (like that of a fingertip during braille reading).

Once vertically displaced, the counterface stage was laterally translated for 60 mm at a velocity of 1 mm/s. This low sliding speed was used in order to reduce dynamic sliding effects and promote a quasi-static force analysis, complementary to the investigation's computational modeling phase. The vertical and lateral forces were recorded at all times during sliding, and ten independent trials were performed under identical conditions.

4.2.2 Computational simulation of a soft half-cylindrical body sliding over a rigid half-cylindrical feature

The second phase of this investigation employed computational modeling techniques to validate the loading behaviors observed in the large-scale tribometer study and aid in identifying the fundamental contact mechanics in the sliding interaction. All finite element analyses (FEA) and computational simulations were performed in the Abaqus FEA software suite.

The simulation's components and parameters were set up in parallel to that of the tribometer's experimental design, albeit in a more simplified manner. The model was created in 2-D planar space, where the mathematical models effectively assumed unit length depth, under plane strain conditions. It consisted of two independent parts: one representing the soft cylindrical body, and the other representing the dot-feature counterface. The soft body was simplified as a semicircle with a radius of 25.4 mm, and its material properties were defined as a homogeneous elastic body with a modulus of elasticity of 1.35 MPa and a Poisson's ratio of 0.48 (like that of the polyurethane and its rubber-like nature). The counterface was defined as an analytical rigid surface that consisted of two smooth 50 mm segments separated by a 3.17 mm radius semicircle representing the dot feature. The corners created by the dot's semicircle were smoothed with 1 mm fillets to avoid computational discontinuities. The parts' assembly can be seen in Figure 4. 2.

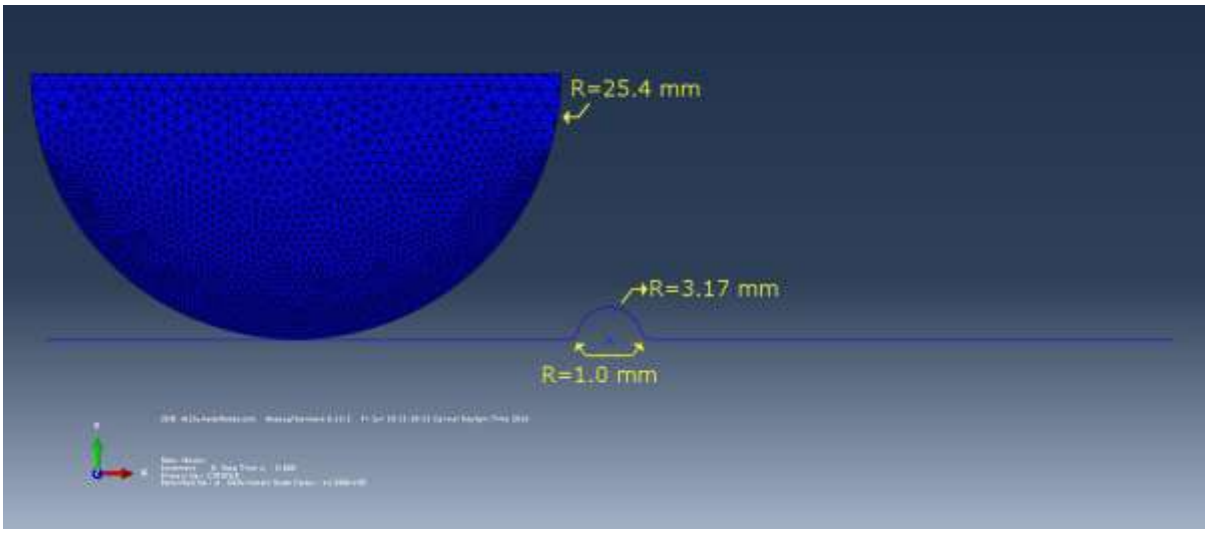

Figure 4.2. The soft semicircular body rests in contact with the rigid counterface prior to any applied displacements.

The frictional interaction (smooth surface-to-surface coefficient of friction) between the two surfaces (soft body and rigid counterface) was pre-defined as 0.25, similar to that of the lubricated rubber sliding on aluminum or a finger sliding on paper media as seen in literature [15].

For the model's applied displacements, the dot counterface was fixed in all directions of motion and rotation, and all displacements were applied to the soft body's top surface.

The simulation consisted of displacing the soft body's top surface downward by 5 mm then laterally for 60 mm. The vertical displacement was decreased from 10 mm to account for the soft body's difference in cross-section in comparison to the empirical sample as well as to achieve a similar degree of deformation surrounding the dot feature experienced during sliding. The force balance calculations were performed under quasi-static analysis, thus negating any inertial effects due to sliding speed. While displacing in both the vertical and lateral directions, the relative positions of the nodes across the top surface were held constant with each other. This constraint kept the top surface horizontal and prevented it from expanding under vertical displacement, like that of the tribometer's mounting device. Throughout sliding, the total interaction forces in both the lateral (1) and vertical (2) directions were recorded, and each was decomposed into contact mechanisms: a) due to "contact pressure" (CP) normal to the contoured surface, and b) due to "frictional stresses" (FS) tangent to the contoured surface. Forces were also recorded for each surface node on the body that came into contact with the counterface, and during post processing analysis, global nodal positions were attributed to the nodal loads to classify loads as being produced either due to contact with the counterface's flat, background region (Base) or raised dot region (Dot).

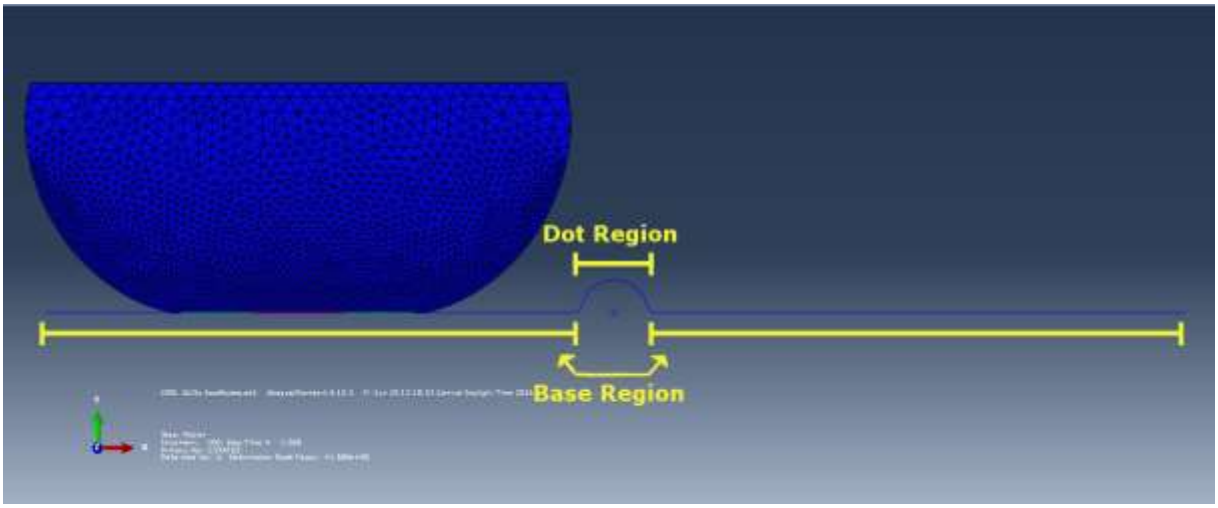

Figure 4.3. The soft body is displaced vertically by 10 mm, and stick-slip (red and blue, respectively) contact points are indicated at the interface. Additionally, Base and Dot contact regions are identified for determining loading sources.

4.3 Results and Discussion

4.3.1 Empirical study of a soft cylindrical body sliding over a rigid half-cylindrical feature

This phase of the investigation sought observed the frictional behavior of a human fingerpad sliding over a singular, embossed braille feature by mimicking this interaction in a highly controlled and simplified two-dimensional environment. This was accomplished by using a multi-axis Rtec Instruments tribometer to slide a homogeneous elastic polyurethane rod over a lubricated aluminum half rod while recording the vertical and lateral forces generated during the sliding process. In these displacement-controlled tests, all geometries, displacements, and sliding parameters were held constant across all trials. As seen in Figure 4.4, the sliding behavior for both loading directions, as well as in the coefficient of friction, was consistent for all behaviors and extremely repeatable among trials.

The pre-loading interaction is analogous to the Hertzian contact mechanics scenario in which two cylinders with parallel axes are normally compressed. In this scenario, the rigid, flat counterface can be represented by a cylinder with an infinitely long radius with an infinitely high

modulus of elasticity (relative to the polyurethane). Under these assumptions, the composite radius and effective modulus of elasticity were directly proportional to that of the polyurethane cylinder. The applied displacement produced a vertical baseline force of approximately 400 N, and under this load and the experiment's design parameters, the maximum contact pressure on the baseline surface was calculated to be 913 kPa (Equation 3). Throughout sliding, the maximum contact pressure reached as high as 1.0 MPa at the largest achievable vertical load of nearly 500 N (shortly after Instance C).

$$p_0 = \left(\frac{E \cdot F}{\pi (1-\upsilon)^2 L \cdot R} \right)^{1/2} \tag{2}$$

Where E is the modulus of elasticity, F is the vertical load, υ is Poisson's ratio, L is the cylinder length, and R is the rod's radius.

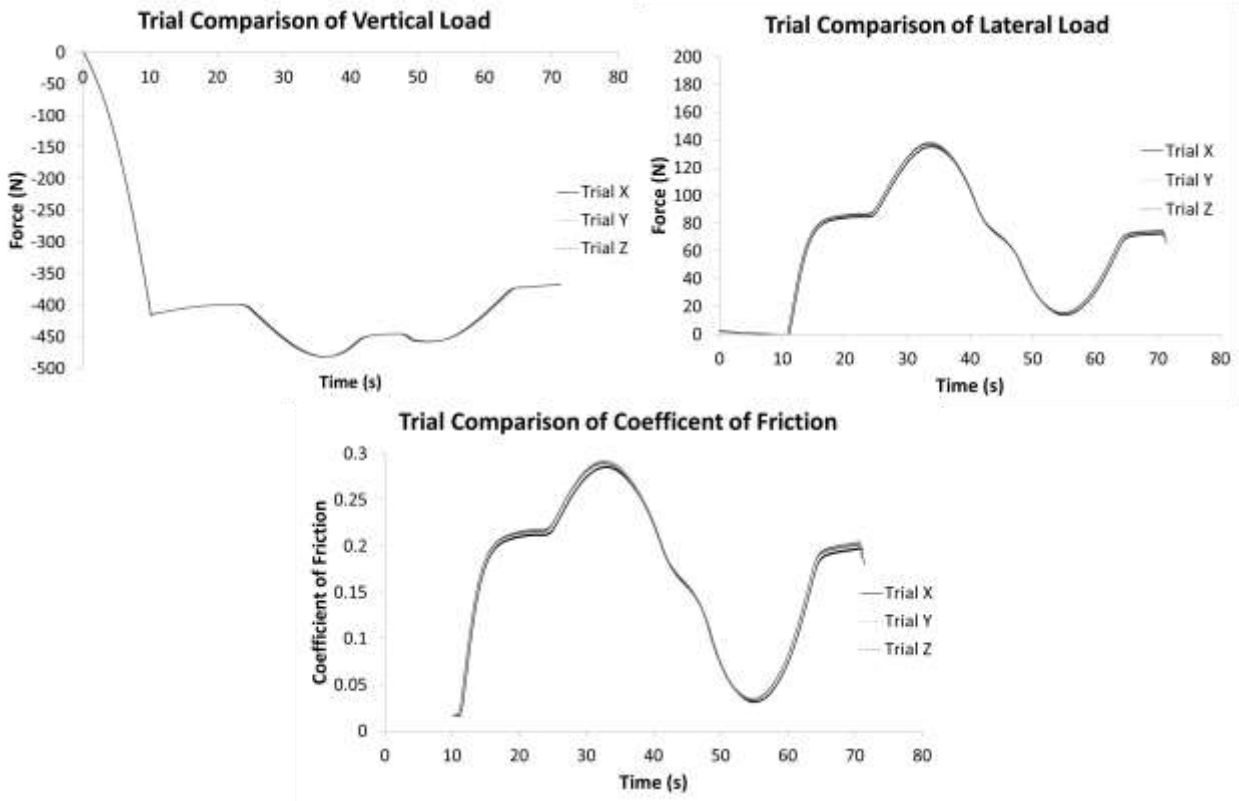

Figure 4.4. Vertical load (top left), lateral load (top right), and coefficient of friction (bottom) for three of the ten trials are presented to demonstrate the repeatability of the test and consistency of the sliding behavior.

Upon initial observation of the data, two interesting trends were immediately apparent: the unique, two-peak behavior in the vertical loading component and the rapid, extreme decrease beyond that of the baseline values in both the lateral loading component and COF. For all data sets, it was hypothesized that the each would begin to increase once the soft body came into contact with the dot, stabilize as it passed over the dot, and subsequently decrease as the trailing edge lost contact with the leading baseline surface. Instead, after the predicted initial increase, the vertical load unexpectedly decreased rather suddenly, only to stabilize temporarily before rising to and falling from peak smaller than the first. This resulted in two independent peaks separated by a brief stabilization. The lateral load and COF did not behave as originally hypothesized either, and while consistent with each other, their trends radically differed from that of the vertical load. After reaching a brief maximum, the lateral load and COF suddenly drop to values nearly 75% below their baseline values and 90% from their maximum values.

To better understand the specific contact and sliding mechanisms that produced these changes in behavior, the times at which the events took place were noted and used to construct a storyboard for visual analysis. Figures 4.5 and 4.6 identify seven points in time at which highly identifiable transitions take place for the loading components and COF data.

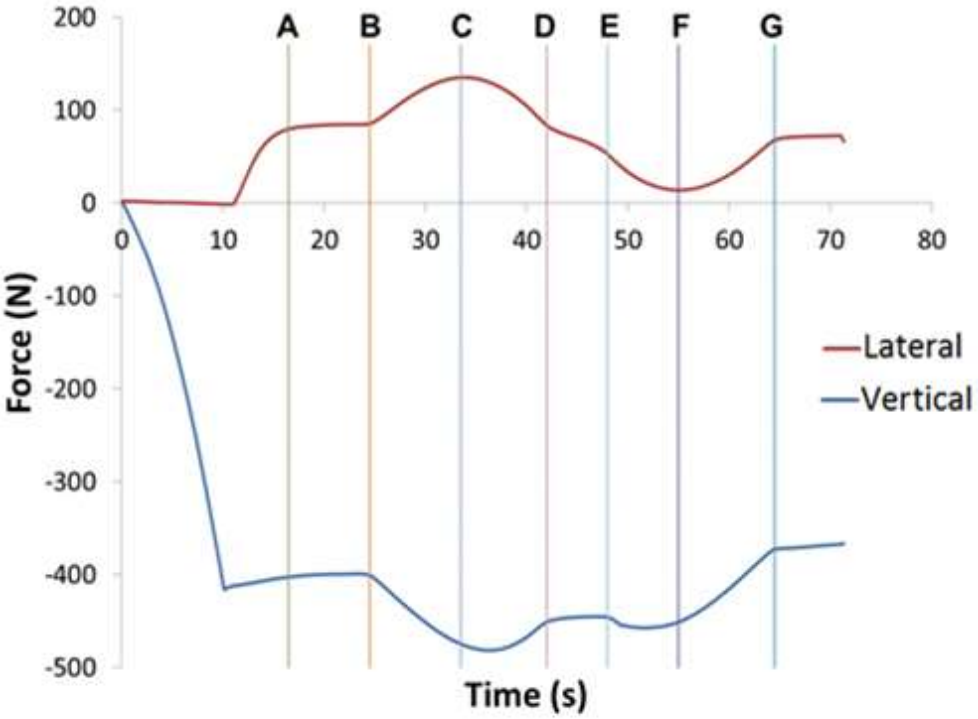

Figure 4.5. Times at which unique loading behavior occurs have been noted for the vertical and lateral loading trends: A) steady state sliding, B) onset contact with the dot, C) maximum lateral load and COF achieved, D) beginning of vertical load stability, E) end of vertical load stability, F) minimum lateral load and COF achieved, G) loads and COF stabilize.

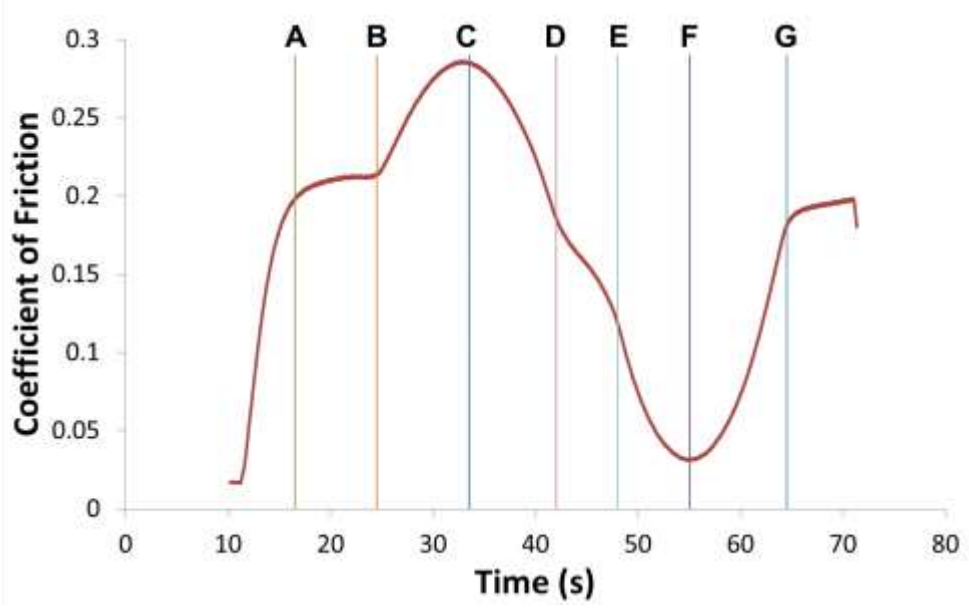

Figure 4.6. Times at which unique loading behavior occurs have been noted for the coefficient of friction trends: A) steady state sliding, B) onset contact with the dot, C) maximum lateral load and COF achieved, D) beginning of vertical load stability, E) end of vertical load stability, F) minimum lateral load and COF achieved, G) loads and COF stabilize.

The video footage was then synchronized with respect to the data, and after comparison to the video storyboard (Figure 4.7), the following seven events were identified and analyzed: A) steady state sliding, B) onset contact with the dot, C) maximum lateral load and COF achieved, D) beginning of vertical load stability, E) end of vertical load stability, F) minimum lateral load and COF achieved, G) loads and COF stabilize.

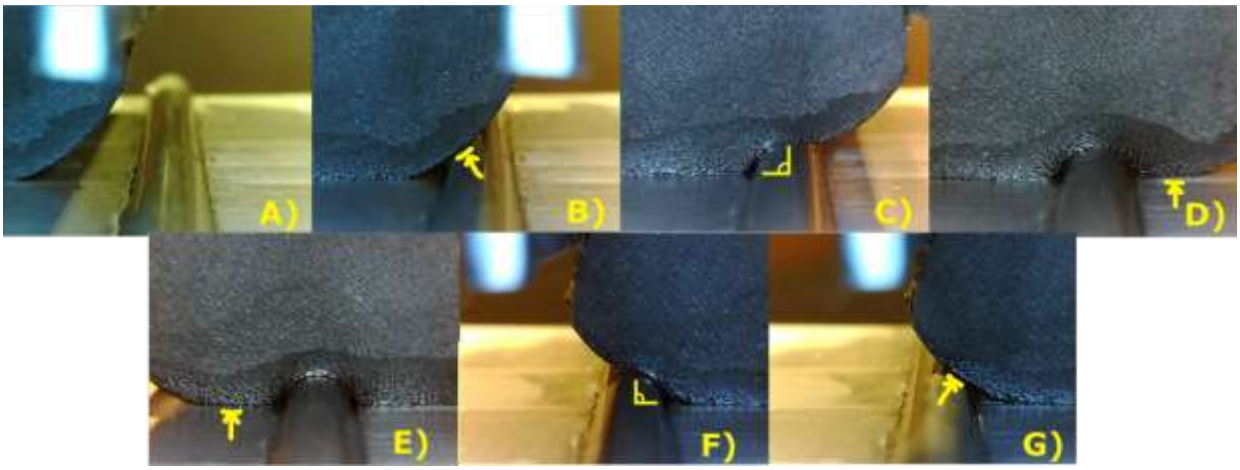

Figure 4.7. In conjunction with the timestamps noted in Figures 4.5 and 4.6, the storyboard shows the soft body's positions as it slides over the dot feature.

During the first 10 s, the polyurethane was vertically displaced, and once this pre-load was applied, sliding began. For the vertical loading, it can be seen that there is a minor decrease in load once sliding commences. As the rod was lowered onto the surface, it deformed symmetrically about the central point of contact. Once sliding began, stick-slip had to be overcome before the body could reach steady state sliding. As stick-slip was overcome, the bulk material shifted, and the rod's surface in contact with the counterface was dragged, creating an asymmetry in the polyurethane's cross-section. This asymmetry decreased the total volume beneath the tribometer's mounting, reducing the amount of material to push downward and create a vertical force.

Instance A indicates the point in time at which the vertical and lateral forces reached equilibrium. Instance B indicates the moment in time at which the soft body initiated contact with the dot feature. When the body came into contact with the dot feature, the contour resisted the

motion of the body in the lateral direction and vertically compressed the bulk material. As the body continued to slide forward, it deformed over the contour of the dot, and both the lateral and vertical forces began to increase. This resistance yielded a cumulative effect: 1) the lateral force increased due to sliding resistance, and 2) the vertical force increased as lateral compression caused the bulk to expand vertically via the Poisson effect as well as due to vertical compressive displacement (Figure 4.8).

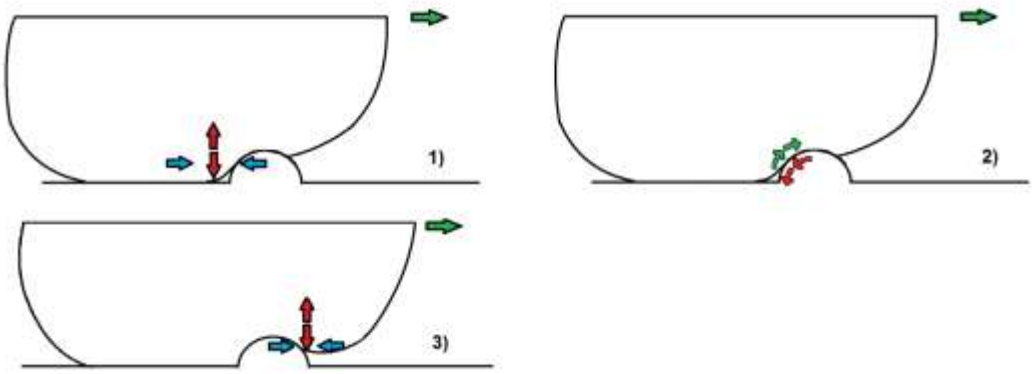

Figure 4.8. The Poisson (1 and 3) and frictional (2) effects caused by the soft body sliding over the dot contour.

Instance C represents the time at which the lateral force and COF achieved a maximum value, and as seen in Figure 4.7, the soft body in contact with respect to the dot surface was at approximately 90 degrees from horizontal, or the 12 o'clock position of the dot feature. In addition to the dot feature resisting bulk sliding through the Poisson effect, frictional forces around the contour of the dot resisted the body's sliding tangent to the dot's face. As the soft body climbed over the dot contour, tangential forces resist the clockwise sliding motion of the surface. The lateral force, and in turn the COF, reached a maximum as the body climbed to the 12 o'clock position on the dot because the entirety of the material in contact with dot surface rested on the left, or leading, side of the dot. It is believed that once the material surpassed the 12 o'clock position on the dot, the Poisson effect began to have an adverse effect on the total lateral load and COF. Figure 4.8 Part 3 illustrates that as the bulk slid past 12 o'clock, the material on the right side of the dot

expanded laterally (similar to Figure 4.8 Part 1), but in this case, the dot effectively propelled the material into the direction of sliding. This contribution rapidly decreased the lateral friction force until Instance F, where the lateral force and COF reached a minimum. The reason for the drastic decrease was likely due to the elastic body's dynamic inertial effects that caused it to spring forward and roll down the trailing edge of the dot in a downhill motion. At this point, as seen in the storyboard, the soft body has reached the 12 o'clock position, except the entirety of the material rested in contact with the trailing side of the dot. It was here where the Poisson effect was at a maximum in terms of propelling the bulk forward, promoting sliding. The contributing effect was so great that the lateral load and COF decreased to 75% less than that of baseline sliding, rendering adhesive frictional behavior as negligible in comparison to the deformation effects. This finding was extremely noteworthy, in that it demonstrates the significance of the friction mechanism of deformation and the impact macroscopic-scale geometries can have on frictional forces and sliding behavior.

In the case of significant events for the vertical loading behavior, Instances D and E appear to be notable and represent the start and endpoints that the vertical load appeared to stabilize after its initial climb and descent. Unlike the maximum lateral force, the maximum vertical force did not occur simultaneously with that of the coefficient of friction, and instead it reached a maximum shortly afterward. Even though the vertical maximum was not in phase, the COF behavior indicated that vertical loading is not the driving frictional component, but instead was driven by the lateral force. Interestingly, the storyboard shows that the vertical load stagnation first occurred when the leading edge of the soft body came into contact with the trailing baseline surface. The stagnation continued as the bulk material transitioned its surface contact from the leading baseline surface to the trailing baseline surface, and once contact was lost with the leading side, the second,

albeit smaller vertical loading peak began. This second peak occurred due to the Poisson effect on the trailing side of the dot, in the same manner as on the leading side. Additional vertical expansion resulted from the dot pushing the bulk forward, thereby increasing the vertical load compared to its stagnant, transitional contact behavior.

Instance G was consistent for both loading cases as well as the COF behavior. Here, the soft body lost contact with the trailing side of the dot feature, and equilibrium baseline sliding resumed. The lateral force and COF were nearly identical to the original steady-state values, but the vertical load decreased from its initial pre-load. This occurred due to the same reason the original displacement load decreased once sliding began. As the body climbed over the contour of the dot feature, it was pulled and dragged laterally, decreasing the volume directly beneath the displaced tribometer mount. The vertical load did not equalize with respect to its initial steady-state sliding because while the polyurethane is assumed to be perfectly elastic and homogeneous in composition, it is unable to completely recover until fully unloaded.

4.3.2 Computational simulation of a soft half-cylindrical body sliding over a rigid half-cylindrical feature

The second phase of the investigation employed finite element analysis to computationally validate and confirm the hypothesized mechanisms observed and reported during the empirical testing phase. All material and geometric constraints represented that of the empirical study, except the two-dimensional FEA completes all force balance calculations under the assumption that the soft body has a thickness of one base unit, or 1 mm. The magnitudes of the simulation can be compared to that of the empirical study by multiplying the computational loads by a factor of 30, where the polyurethane rod was 30 mm long. For the sake of computational time required to complete the analysis, a sliding speed of 5 mm/s was used, as opposed to 1 mm/s as seen with the

tribometer, but due to the fact that the simulation was performed using quasi-static analyses that disregarded all dynamic effects, sliding speed and inertial behavior did not influence the data in any way. Additionally, modifying the modulus of elasticity only affected the scale of the loading magnitudes and not the loading behavior, due to the relationship of Hooke's Law:

$$\sigma = E \cdot \varepsilon \tag{3}$$

Where σ represents the resulting contact stress in MPa, ε is the surface strain, and *E* is the modulus of elasticity of the material being strained. All subsequent data sets begin at 2.0 s, the onset of steady state sliding, due to the position-based algorithm used to calculate the loading based on surface contact region.

The Abaqus model proved to be a reasonable predictor when comparing the loading and COF trends to that of the tribometer testing data, and Figure 4.9 displays the same storyboard events discussed in the previous section, with the exception of Instance C.

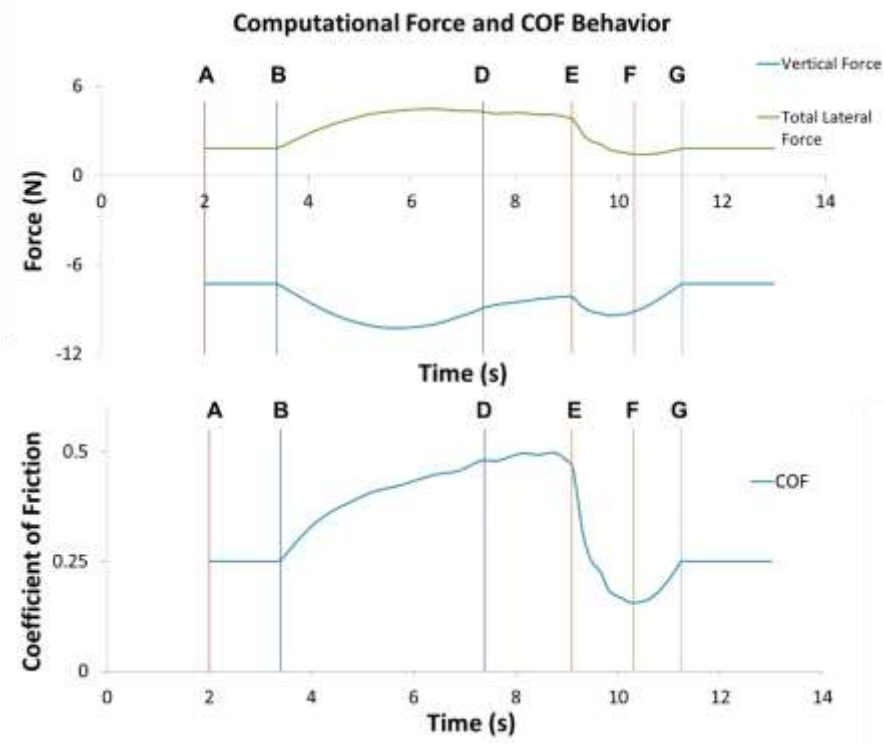

Figure 4.9. Aside from Instance C, the modeled loading (top) and COF (bottom) predictions for Instances A-G were quite agreeable with the empirical tribometer data.

Instance C was not included due to the significant departure from the empirical data in both the lateral loading and coefficient of friction behavior between Instances B and D. Here, as opposed to a sharp climb followed by rapid decline, the lateral load stabilized until the trailing edge of the soft body released contact from the leading baseline surface. It was hypothesized that the sharp decline was possibly due to dynamic effects from the rebounding material, and the model's load stabilization and quasi-static analysis reinforce that idea. Future work needs to be performed to model the loading behavior with dynamic effects. It is essential to note that the dot's negative effects on lateral load and frictional were evident in the predicted model as well, validating the previous claim that the dot feature promoted sliding and decreased the total lateral loads and COF. The computational model's storyboard and its similarities to that of the empirical data are found in Figure 4.10.

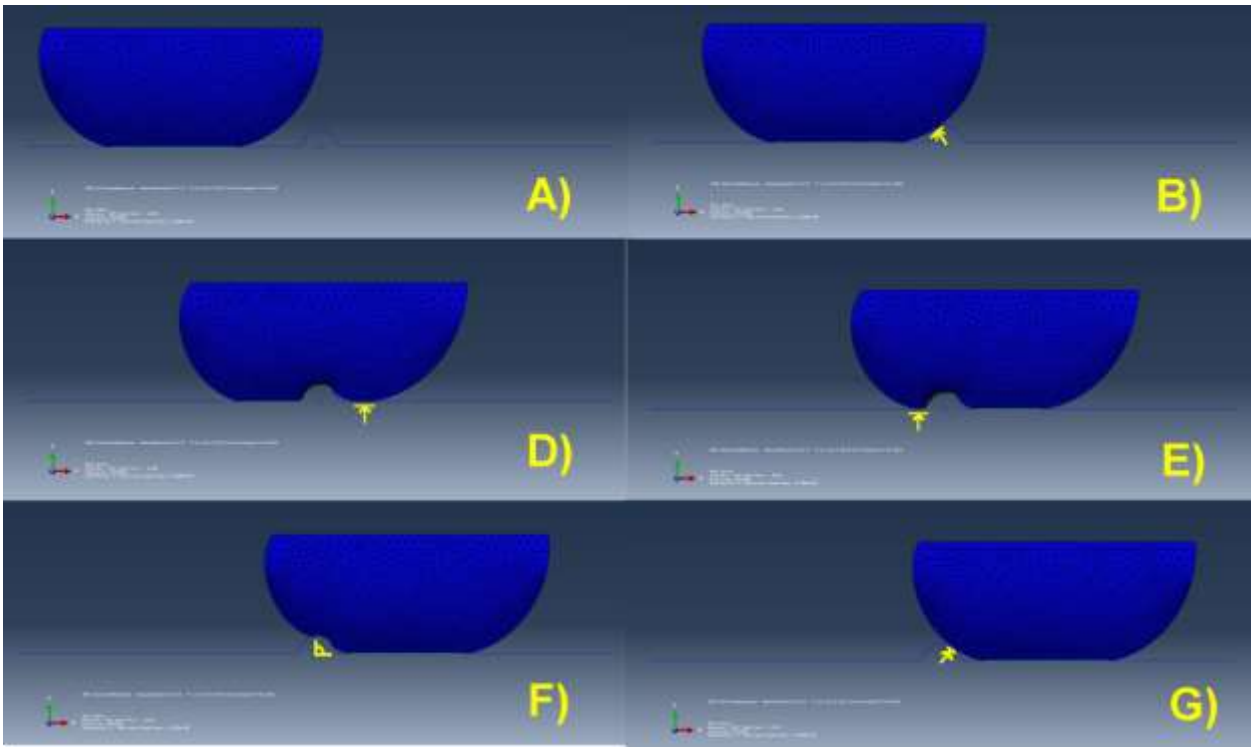

Figure 4.10. The storyboard from the predictive computational model is nearly identical to that of the empirical study, barring Instance C due to the dynamic effects that were not taken into consideration in the simulation.

Further loading analysis was performed to better understand how the counterface's two contact regions (baseline or dot region, Figure 4.3), explicitly affected loading behavior. Total loading due to each contact region was calculated by tracking the specific contact load at each surface node with respect to its vertical position, and nodes in contact with the surface at a vertical position greater than the baseline were defined as loading due to the dot region. Performing this analysis successfully explained the two-peak effect seen in the vertical loading behavior. As seen in Figure 4.11, classifying the loading contributions as either baseline or dot contact regions shows that the two peaks are produced as a cumulative effect of the loading from both regions. As originally hypothesized, the inclusion of the dot feature produced an increase in loading, but that hypothesis did not consider that loading due to the baseline surface would vary over time. As the soft body passed over the dot, the baseline forces decreased due to decreasing contact with the baseline region, and were at a minimum when the body was centered over the dot (when dot region forces are at a maximum).

Loading contributions were then further classified by specific loading mechanism: due to contact pressure normal to the surface (CP), or due to frictional stresses tangent to the surface (FS). As expected, contact pressure was the primary mechanism driving the vertical loading. As the soft body traversed the dot region, the surface elements were vertically displaced, producing a contributory vertical spring load. It can also be seen that vertical loading over the baseline zone was positively affected when the body first contacted the dot. As the bulk was laterally deformed starting at Instance B, the Poisson effect caused the material to expand vertically, briefly increasing the vertical load.

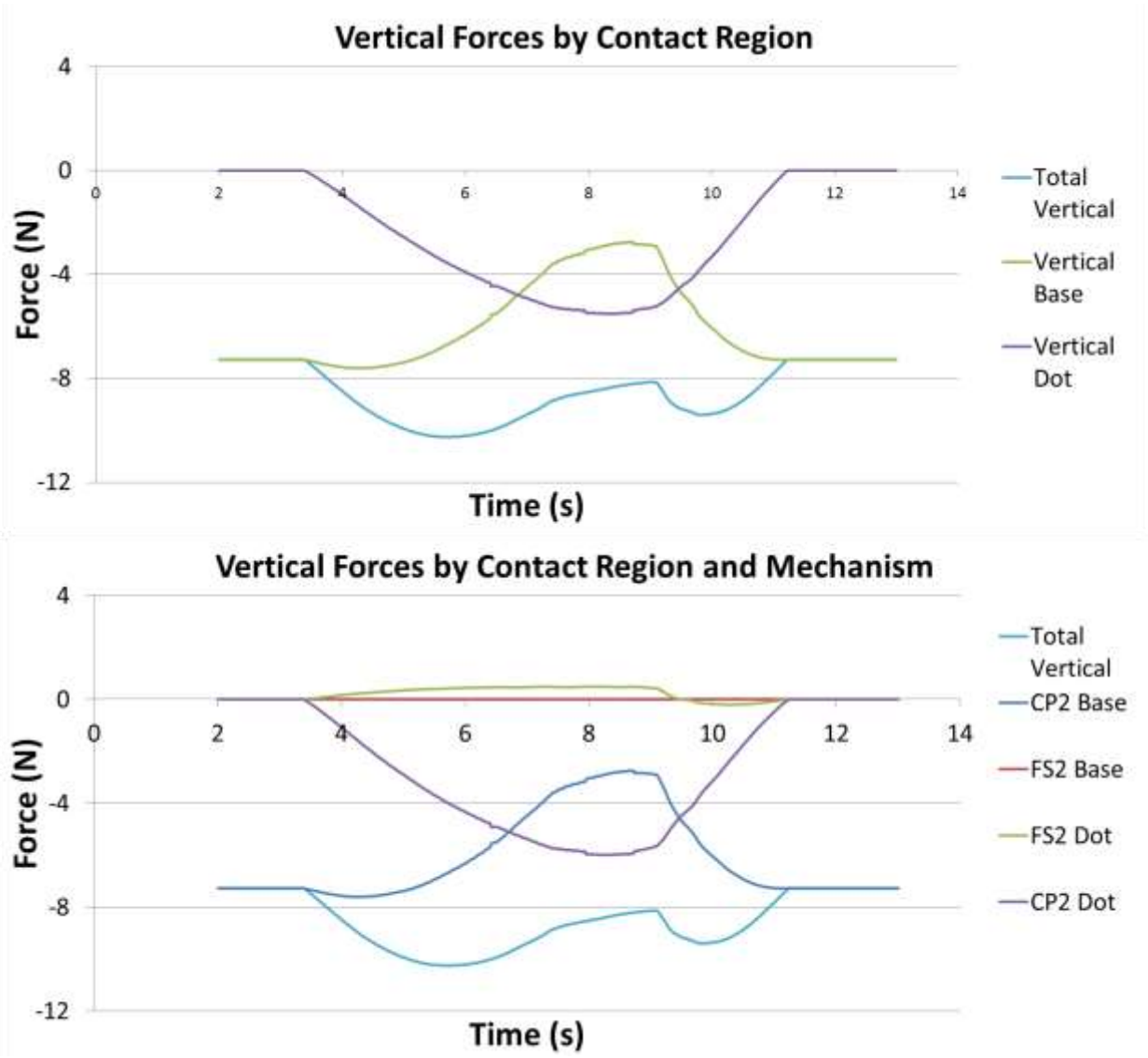

Figure 4.11. Vertical loading contributions classified according to counterface region (top), and further defined by specific loading mechanism (bottom).

An unexpected finding also came from this analysis. While minimal, frictional stresses around the contour of the dot both contributed to, as well as reduced the total vertical loading, depending on the position of the soft body. Prior to Instance E, the soft body resided mainly on the leading edge of the dot contour, flowing in the clockwise direction. This clockwise motion on the leading edge of the dot produced frictional shear with an upward force component, resisting the

downward loading due to contact pressure. Once the body lost contact with the leading baseline surface, the frictional shear component from dot contact produced a minor downward force component and promoted the clockwise sliding.

The primary contributors to lateral force behavior differed from those of the vertical force. Here, both loading mechanisms, contact pressure and frictional stresses due to the dot, influenced the loading behavior much more equally. As the soft body traversed the dot, forces due to contact pressure in the dot region were so great that they equaled the pre-defined frictional shear of the baseline and essentially doubled the total lateral force. This drastic increase resembled the trend seen in the tribometer testing, where the lateral force increased because the dot resisted bulk motion, resulting in resistive horizontal force components over the dot contour. The hypothesis on "propulsion" lateral forces from the tribometer testing was also validated based on the mechanism decomposition. The simulation clearly depicted that once the soft body lost contact with the leading baseline surface at Instance E and rapidly climbed the leading edge of the dot, the vertical compressive forces on the trailing side of the counterface caused the bulk to expand laterally, pushing the bulk into the direction of sliding. As a result, this Poisson effect generated negative lateral loads due to contact pressure.

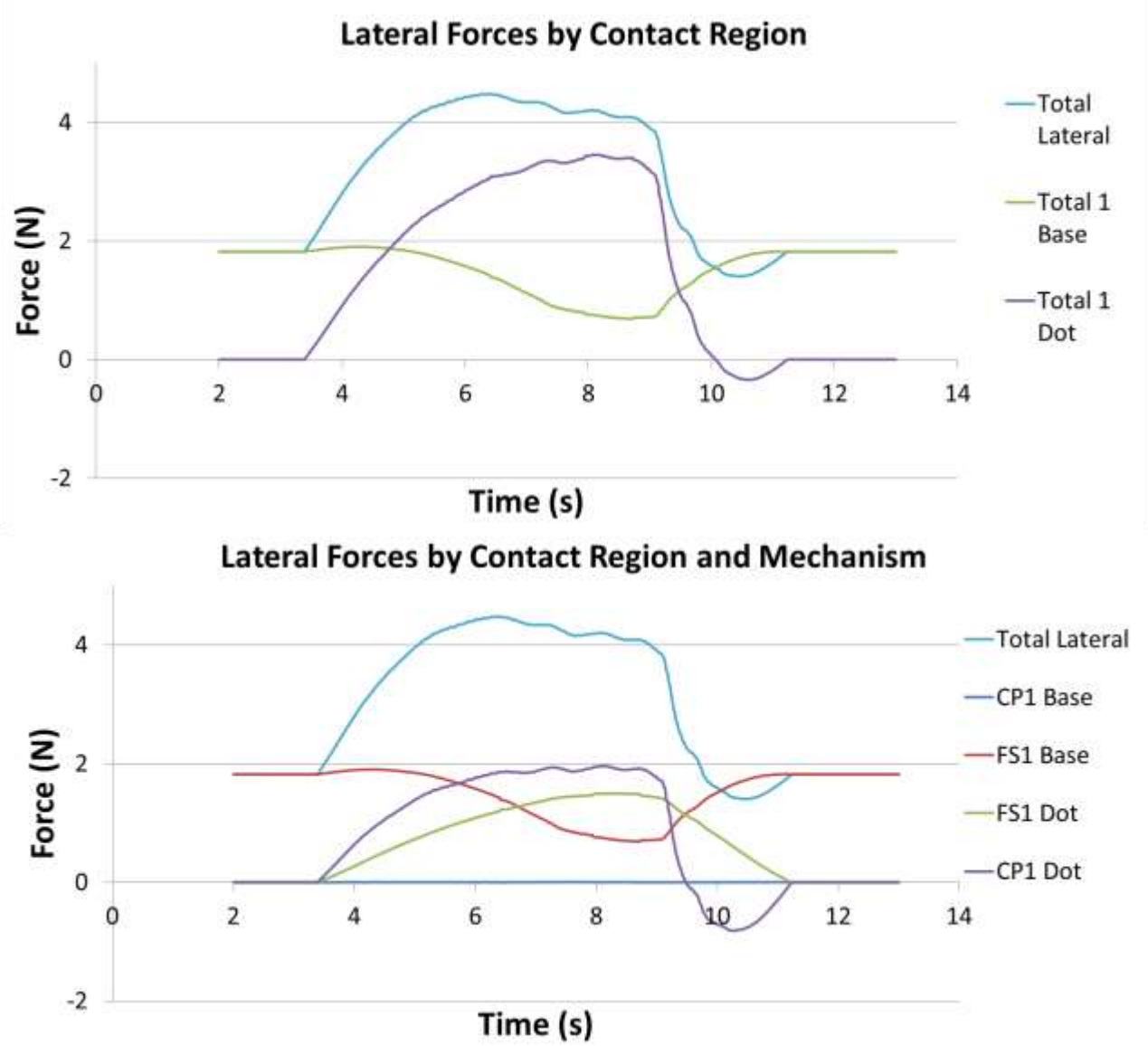

Figure 4.12. Lateral loading contributions classified according to counterface region (top), and further defined by specific loading mechanism (bottom).

4.4 Conclusions

The fundamental friction and contact mechanisms involved in a large scale simulation of braille reading were investigated in both an empirical testing as well as a predictive computational model. Based on the observed results, the following conclusions can be drawn:

- As the soft-bodied cylinder slides over the dot contour under controlled vertical displacement, the elastic surface in contact with the raised dot region significantly impacts the load behavior in both the vertical and lateral directions due to bulk material deformation.
- The vertical compressive forces are cumulatively driven by compression against the flat surface, the body's elastic deformation over the raised dot region, as well as from vertical expansion due to the Poisson effect from lateral displacement, where the elastic surface's vertical and lateral displacements are the primary loading mechanism.
- Due to the macroscopic geometry of the dot surface, frictional shearing effects in the vertical direction create both tensile and compressive loads on the leading and trailing sides of the dot, respectively.
- Contact pressure and macro-scale deformation contact are equally significant to lateral loading in comparison to frictional shear effects.
- Lateral loading due to contact pressure depends on the finger's location with respect to the dot, where sliding is resisted on the leading half and aided on the trailing half.

4.5 References

[1] Skedung, L., et al., Finger Friction Measurements on Coated and Uncoated Printing Papers. Tribol Lett. 37(2): p. 389-399.

[2] Skedung, L., et al., Tactile perception: Finger friction, surface roughness and perceived coarseness. Tribology International, 2011. 44(5): p. 505-512.

[3] Kenins, P., Influence of Fiber Type and Moisture on Measured Fabric-to-Skin Friction. Textile Research Journal. 64(12): p. 722-728.

[4] Gwosdow, A.R., et al., Skin Friction and Fabric Sensations in Neutral and Warm Environments. Textile Research Journal. 56(9): p. 574-580.

[5] Derler, S., U. Schrade, and L.C. Gerhardt, Tribology of human skin and mechanical skin equivalents in contact with textiles. Wear, 2007. 263(7–12): p. 1112-1116.

[6] Darden, M.A. and C.J. Schwartz, Investigation of skin tribology and its effects on the tactile attributes of polymer fabrics. Wear, 2009. 267(5): p. 1289-1294.

[7] Bertaux, E., et al., Textile, physiological, and sensorial parameters in sock comfort.(Report). Textile Research Journal. 80(17): p. 1803-1810.

[8] Fagiani, R., et al., Contact of a finger on rigid surfaces and textiles: friction coefficient and induced vibrations. Tribology Letters, 2012. 48(2): p. 145-158.

[9] Bobjer, O., S.-E. Johansson, and S. Piguet, Friction between hand and handle. Effects of oil and lard on textured and non-textured surfaces; perception of discomfort. Applied Ergonomics, 1993. 24(3): p. 190-202.

[10] Smith, A., et al., Role of friction and tangential force variation in the subjective scaling of tactile roughness. Exp Brain Res. 144(2): p. 211-223.

[11] Wolfram, L.J., Friction of skin. Journal of the Society of Cosmetic Chemists, 1983. 34(8): p. 465-476.

[12] Adams, M., B. Briscoe, and S. Johnson, Friction and lubrication of human skin. Tribol Lett, 2007. 26(3): p. 239-253.

[13] Greenwood, J.A. and D. Tabor, The Friction of Hard Sliders on Lubricated Rubber: The Importance of Deformation Losses. Rubber Chemistry and Technology, 1960. 33(1): p. 129-141.

[14] Greenwood, J.A., H. Minshall, and D. Tabor, Hysteresis Losses in Rolling and Sliding Friction. Proceedings of the Royal Society of London. Series A, Mathematical and Physical Sciences, 1961. 259(1299): p. 480-507.

[15] Darden, M.A. and C.J. Schwartz, Skin tribology phenomena associated with reading braille print: The influence of cell patterns and skin behavior on coefficient of friction. Wear, 2015.

CHAPTER 5: SKIN TRIBOLOGY PHENOMENA ASSOCIATED WITH READING BRAILLE PRINT: THE INFLUENCE OF COMPLEX TACTILE CONFIGURATIONS AND SKIN DEFORMATION ON COEFFICIENT OF FRICTION

Abstract

Beyond the sense of sight, the sense of touch is one of the fundamental ways that individuals experience their surrounding environment. The blind and visually impaired community (BVI) rely primarily on the sense of touch to receive information, and when transmitting information, efficiency is vital when communicating tactually. This requires a fundamental understanding of the skin tribology involved in reading the coded information, as well as the somatosensory phenomena during tactile perception. Researchers have begun investigating the friction mechanisms of skin sliding over surfaces tactually coded with the braille language. Braille employs raised dome-shaped dots in six-position cells, with various dot patterns representing individual text characters, punctuation, or mathematical operators. Previous work has investigated the frictional sliding mechanics involved during human skin (fingerpad) sliding over an individual Braille dot feature, and a deformation-focused model, as opposed to adhesion, was found to effectively predict the frictional behaviour, but little is known how the skin interacts with more complex braille dot geometries. This work investigated spacing effects of braille dot features as well as complex braille dot configurations representing very simplistic tactile graphics. Two-dimensional computational modelling, as well as large scale tribometer testing has been performed to better understand the relationship between a texture's perceived uniqueness and its tribological parameters. It was hypothesized that sliding attributes such as tactile vibration and oscillatory coefficient of friction played a role in distinguishing one tactile surface from another.

5.1 Introduction

At its core, the sense of touch is the fundamental mechanism that allows individuals to simultaneously interact with as well as acquire information from their surrounding environment. Tactile perception plays a key role in manipulating an object, navigating an environment, and evaluating a product. Oftentimes, touch is used complementary to other sense such as sight or sound, but instances exist where one may rely entirely on tactility to learn about and make sense of his/her environment; and this is the case for the blind and visually impaired (BVI) community. Because these individuals cannot receive written language or pictographic information through visual prompts, BVI individuals read text and perceive images through means of touch.

The tactile language, braille has been adopted to represent written language in tactual form, and tactile graphics are used to represent graphical or symbolic images in tactual form. The implementation of tactile symbols and graphics has become increasingly prominent in the teaching of grade-school students, particularly in the science, technology, engineering, and mathematics (STEM) fields. In these cases, as opposed to being presented linear information, such as a line of text, students are presented two-dimensional tactual information, and to effectively present efficient, yet valuable information to the students, the code must be easily identifiable as well as spatially dense in content. The Braille Authority of North America has outlined standards and guidelines recommend educators follow certain techniques when designing tactile graphics for their students [1], but these have been constructed from a pedagogical sense first, not considering the science behind tactile perception and resolutions. This due to the fact that researchers have yet to find a way to effectively and directly relate the intricacies of the somatosensory system with that of surface engineering and skin tribology.

When it comes to investigating tactility, friction is commonly believed to be a significant player in perception during skin-surface sliding interactions, but definite correlations have yet to be determined. In attempt to bridge the two, researchers have performed tactility studies with a multitude of surface materials and topographies in which they relate tactile attributes such as perceived roughness or abrasiveness with mechanical properties such as coefficient of friction or surface roughness. Some of these materials have included varying textile fabrics. [2-8], paper media [9, 10], glass surfaces [11], and ridged polymer surfaces [12, 13]. Based on these findings, there appears to be no single tactile attribute that directly relates to a surface's coefficient of friction, and attributes instead are functions of a variety of surface and material properties. What is unique to the tactual coding domain is that the perceptive traits of surface features, topographies, and media have been defined independent of the quantifiable tribological traits. If the skin-surface tribology of these standardizations can be thoroughly and fundamentally understood, tactual coding techniques and optimizations can then be made in order to facilitate more effective teaching tools for the BVI community.

The purpose of this investigation was to apply the experimental techniques and research findings from Chapters 3 and 4 toward understanding more complex tactile graphics configurations and braille patterns in a brief, three-aspect study. The first aspect of the study was to utilize the computational modeling techniques developed from Chapter 3 to validate the loading and frictional behavior of a finger sliding over a pair of dot features as seen empirically in Chapter 2. The second aspect of this study sought to understand the loading and friction behavior of a finger sliding over a simple tactile graphic by computationally modeling a soft, bulk material sliding over a series of evenly spaced standard-sized braille dots. The final aspect of the study was to

empirically quantify the frictional behavior of a finger sliding over simple tactile graphics grouped by tactual likeness according to the Braille Authority of North America (BANA).

5.2 Materials and Methods

5.2.1 Computational model for dot pair configuration

The emphasis of this initial phase of the investigation was to replicate the modeling techniques employed in Chapter 4 in order to determine if the horizontal spacing effects experimentally observed in Chapter 3 could be simulated in a repeatable and consistent manner. Once again, all finite element analysis (FEA) and computational simulations were performed in the Abaqus FEA software suite.

As was in Chapter 4, the model was created in 2-D planar space, where the mathematical models effectively assumed unit length depth, under plane strain conditions. The human fingertip was modeled as an elastic, homogeneous half-cylindrical body with a radius of 10.0 mm, assuming the average fingertip measures 20 mm across. While the human finger does not have a homogeneous cross-section and is instead a layered composite as modeled by Amaied et al. [14], a modulus of elasticity of 250 kPa was chosen as an effective modulus for a uniform representation that considers both the soft outer tissue as well as the rigid bone beneath. While the skin on a fingertip is not perfectly elastic in nature, the representative soft body was assumed to be rubber-like in nature with a Poisson's ratio of 0.48.

The dot surface counterface was defined as an analytical rigid surface that consisted of two smooth 30 mm segments separated by a pair of standard-sized braille dots with 0.48 mm radii separated by spacing distance, *s*. For this study, spacing distances of 1.5 mm and 2.5 mm were selected. In standard braille, the smallest permitted distance between dot features is 2.5 mm, and this is due to tactile resolutions in the human fingerpad, where features closer than this spacing

cannot be identified and discriminated as unique dots. This is believed to occur due to skin penetration between the features and the resulting friction effects due to deformation (Chapter 3). It was observed than for when modeling the sliding system with a dot spacing of 2.5, the soft body completely penetrated the dot gap and came into contact with the baseline surface between the features, leading to selecting a spacing of 1.5 mm as the lower limit. The assembly can be seen in Figure 5.1.

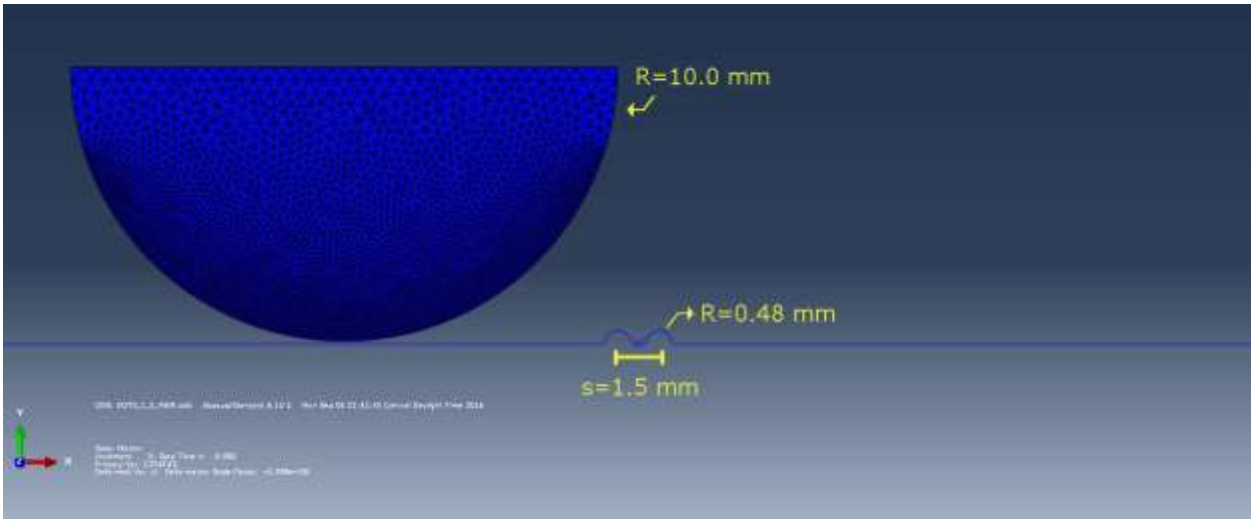

Figure 5.1. The soft half-cylindrical body rests in contact with the dot pair counterface prior to any applied displacements.

The frictional interaction (smooth surface-to-surface coefficient of friction) between the two surfaces (soft body and rigid counterface) was pre-defined as 0.25, similar to that of a finger sliding on cardstock paper media [15]. For the model's applied displacements, the dot counterface was fixed in all directions of motion and rotation, and all displacements were applied to the soft body's top surface.

The simulation consisted of displacing the soft body's top surface downward by 1.45 mm, producing a vertically displaced pre-load of 0.5 N. This displacement and pre-load were selected to simulate the low loading target range investigated in Chapter 3's spacing investigation. Additionally, the chosen displacement ensured that at the midpoint of sliding, the entirety of the

soft body completely surrounded both dot features, contacting the baseline on either side. Once vertically displaced, the top surface of the soft body was laterally displaced 20 mm at a velocity of 5 mm/s. While displacing in both the vertical and lateral directions, the relative positions of the nodes across the top surface were held constant with each other. This constraint kept the top surface horizontal and prevented it from expanding under vertical displacement. It should be noted that sliding speed and dynamic inertial effects do not impact the loading and frictional behavior in any way due to the simulation's quasi-static analyses. Throughout the simulation, the total interaction forces in both the lateral (1) and vertical (2) directions were recorded, and each was decomposed into contact mechanisms: a) due to "contact pressure" (CP) normal to the contoured surface, and b) due to "frictional stresses" (FS) tangent to the contoured surface. It was hypothesized that the loading and frictional effects due to horizontal spacing would reflect those seen in Chapter 3, where the introduction of a second dot produces interaction, or cumulative effects super imposed on finger on single dot sliding behavior.

5.2.2 Computational model for simple tactile graphic

The aim of the second phase of the study was to investigate the loading and frictional behavior of a simulated finger sliding over a series of evenly spaced dots (or 2-D ridges) likened to the most fundamental tactile graphic. For this study, all material parameters were identical to the initial phase, and the sole difference between phases was the dot counterface topography being considered. This counterface consisted of a series evenly spaced standard-sized braille dots (0.48 mm radii) with constant spacings of 1.5 mm and 2.5 mm. The length of the counterface was chosen such that the soft body reached steady state sliding over the features before contacting the trailing baseline surface. This allowed the vibratory response due to sliding over a periodic surface to be analyzed.

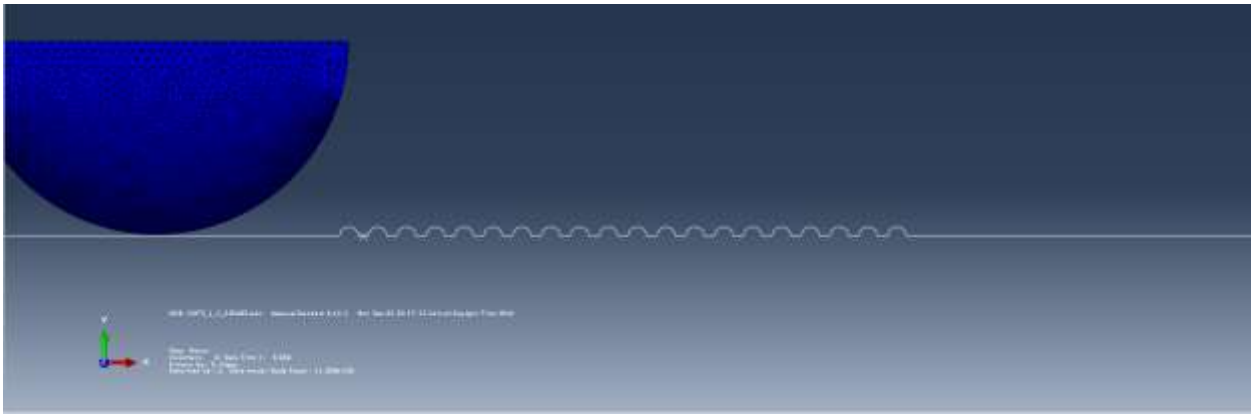

Figure 5.2 The soft half-cylindrical body rests in contact with the dot series counterface prior to any applied displacements.

The simulation consisted of vertically displacing the top surface of the soft body by 1.45 mm producing a similar 0.5 N pre-load. The top surface was then laterally displaced 60 mm across the entirety of the ridge pattern at 5 mm/s. It was hypothesized that sliding over a periodic surface would produce fluctuations in both loading and coefficient of friction, likened to that of vibratory response. With this data, averages and standard deviations were recorded for maximum peak, minimum peak, amplitude, and overall magnitude, and Fourier transforms were performed to identify the vibrational behavior in the simulations. The frequency response and change in amplitude during oscillation were believed be highly influential in one's ability to discriminate between tactile graphic surfaces.

5.2.3 Characterization of skin-surface tribology for tactile graphic samples organized by perceptive uniqueness

The final phase of the study examined the frictional behavior of a human fingerpad sliding across simple tactile graphic patterns by mimicking this interaction in a highly controlled tribometer setup. This was accomplished by employing a multi-axis Rtec Instruments tribometer for all sliding and interactions and force measurements. As seen in Chapter 3, the human fingerpad can be assumed to behave similar to a homogeneous, elastic and spherical body while exhibiting

Hertzian contact behavior at sufficiently low loads. Given such, a 25.4 mm (1 in.) diameter high-temperature silicone sphere was selected to simulate the fingerpad's elastic behavior for this investigation. The silicone had a durometer hardness rating of 60A, and according to Equation 1,

$$E = e^{[S_A \cdot 0.0235 - 0.6403]} \tag{1}$$

It had an equivalent modulus of elasticity of 2.16 MPa, where E is the modulus of elasticity in MPa and S_A is the ASTM D2240 type A hardness rating. The rubber sphere was cut in half and then affixed to a small rectangular 6.35 mm thick aluminum plate; and the rigid substrate was affixed to the same stainless steel U-channel mount used in Chapter 4. The substrate-mount combo allowed for displacements to be evenly distributed across the top surface in both the vertical and lateral directions, identical to the boundary conditions set on the soft body's top surface in the computational modeling.

The tactile graphics samples used in this study were inspired by work previously done by Darden et al., in which the coefficients of friction were investigated for uniform, parallel ridged textures [16]. The textures resemble some of the patterns and tactile groupings described by the Braille Authority of North America (BANA) in the standards and guidelines set for producing tactile graphics on microcapsule paper, a media commonly used for tactual images [1]. The tactile groups in Figure 5.3 are organized according to distinguishing feel, and as noted, samples within like groups are not permitted to be adjacent to one another due to perceptive likeness. These standards were developed with ensuring tactile uniqueness in mind, but they were not characterized according to any tribological properties, and it is the aim of this phase to identify such in order to better understand what surface and material properties affect perception.

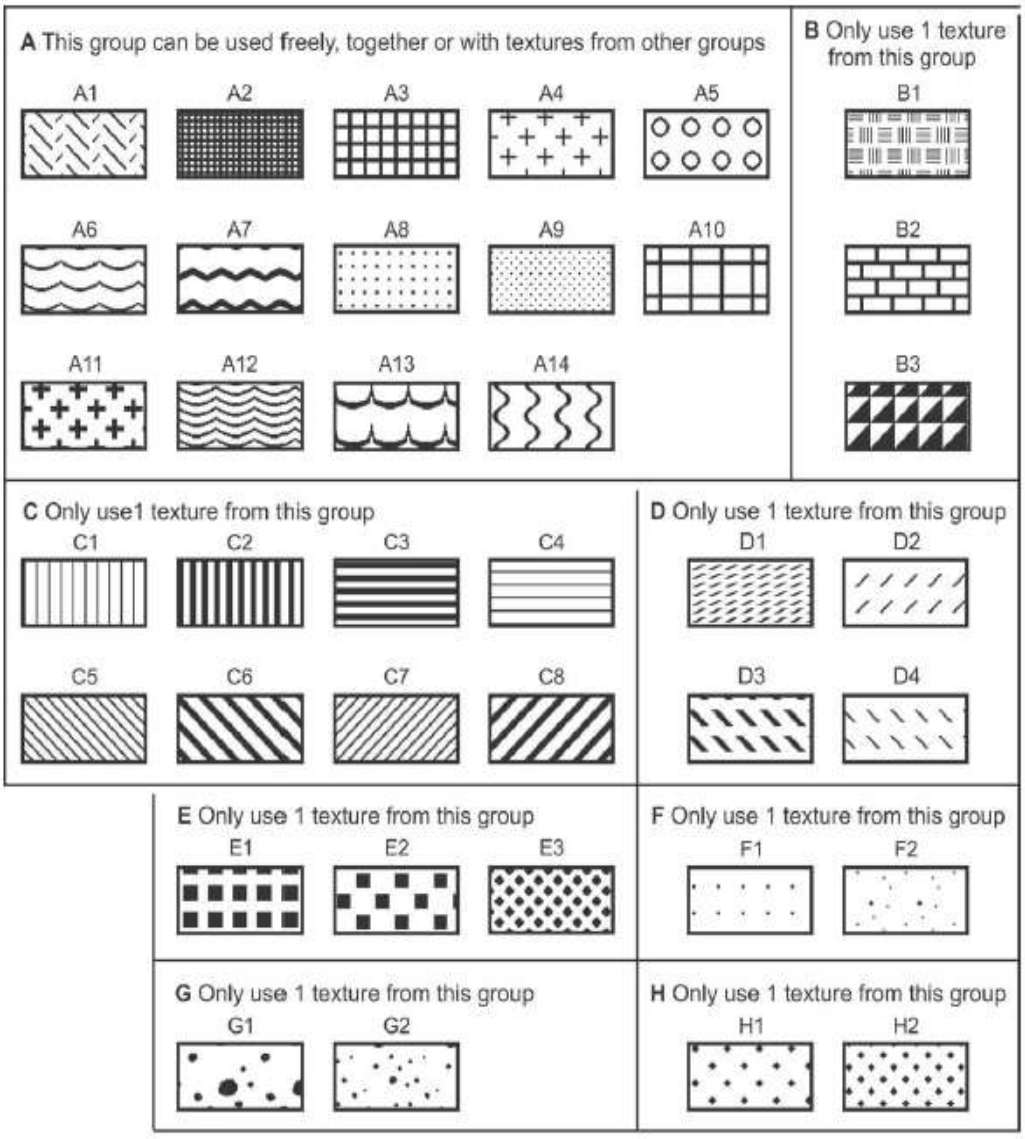

Figure 5.3. Tactile graphics standards and guidelines used when embossing graphics on microcapsule paper. [1]

Five injection molded polypropylene samples of unique texture patterns (courtesy of Japan Polypropylene Corporation) were used for this study, and samples were selected in topographically similar pairs in order to investigate Groups A and C from the BANA Guidelines for Tactile Graphics (Figure 5.3). The fifth sample was a smooth, control polypropylene sample to be used as a featureless reference. The samples chosen to represent Group A were two grid-like patterns of different mesh densities, like that of A2 and A3, and textures in this group were deemed perceptively unique enough to be adjacent to any of the listed textures from any of the groups. The

samples chosen to represent Group C were two parallel ridged textures of different ridge and groove widths, like that of C1 and C2. Samples within this group were deemed too perceptively similar and cannot be placed adjacent to one another. The patterns discussed in these guidelines were not represented with quantifiable topographies, but instead were only presented perceptively. As a result, a DinoCapture microscope camera and ImageJ analysis were used to quantify the topographical parameters: ridge, groove, and period widths for all samples.

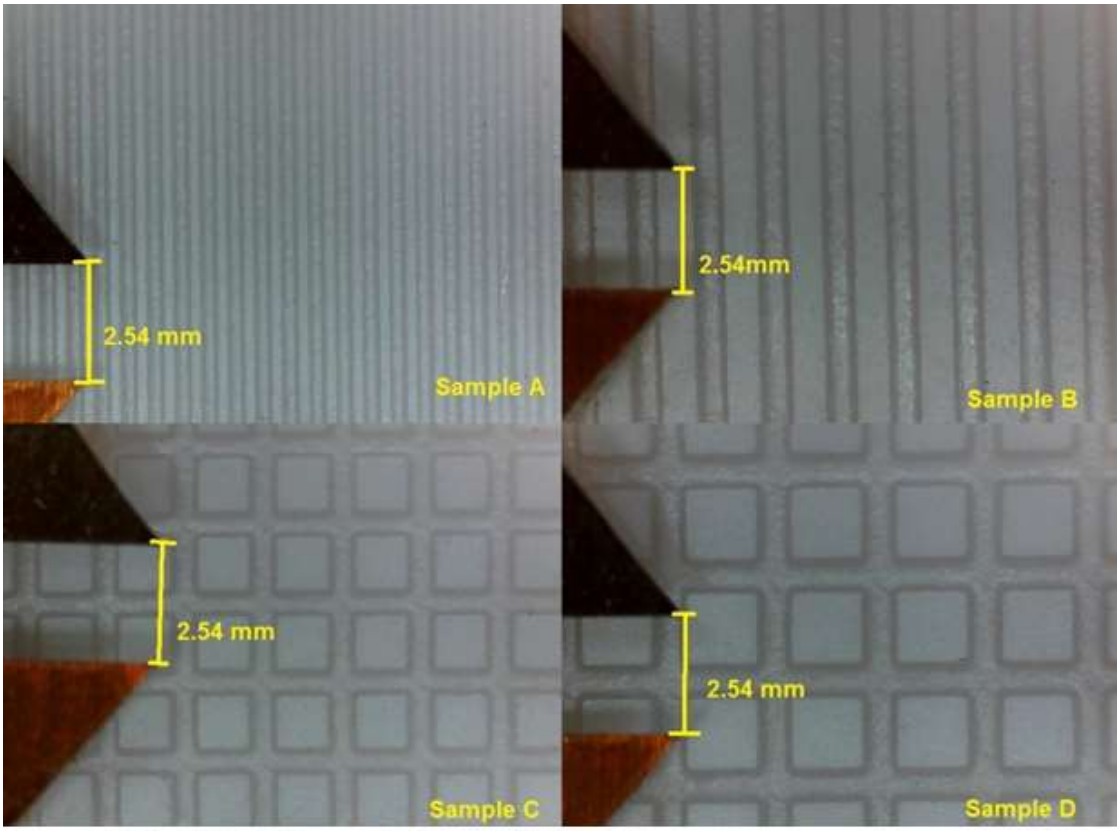

Sample	Ridge Width (mm)	Groove Width (mm)	Pitch (mm)
A	0.3	0.3	0.6
B	0.61	0.84	1.45
C	0.47	1.27	1.74
D	0.62	1.72	2.34
E	Non-textured with non-directional 0.15 µm Ra surface roughness		

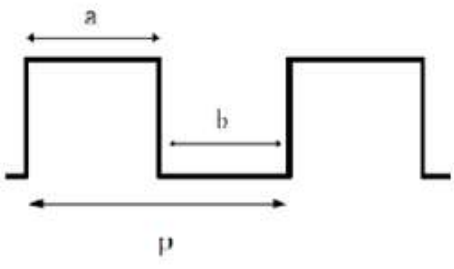

Figure 5.4. The tactile graphics samples selected to investigate the tribological properties of perceptively like and different patterns as defined by the BANA.

A 6D, 500 N limit load cell in conjunction with a multi-axis tribometer were used to record the vertical and lateral forces and COF at a sampling rate of 1,000 Hz for all silicone sliding tests. All tests were performed under identical environmental conditions: temperature was measured at 23.8 degrees Celsius and humidity was measured at 50%. In these displacement-controlled tests, the vertical, Z-axis motor and its load cell suspension controlled normal loading and vertical displacements, while the dual-axis stage controlled lateral displacements. In the case of this study, only the X-axis motor was used for sliding in one direction.

For each test, the samples were affixed to the stage using an adhesive, and the silicone sphere was brought into contact with the sample and pre-loaded. Forces exerted during braille reading typically range from 0.5-1.5 N, but due to the sensitivity of the load cell, a 3 N pre-load was applied for all sliding tests. Once pre-loaded, the stage was translated at 1 mm/s for 30 mm, and the load cell recorded the resulting vertical and lateral loads. Six repetitions were performed for each sample, and the sliding location across the sample was varied to ensure transfer films or debris did not accumulate across the surface.

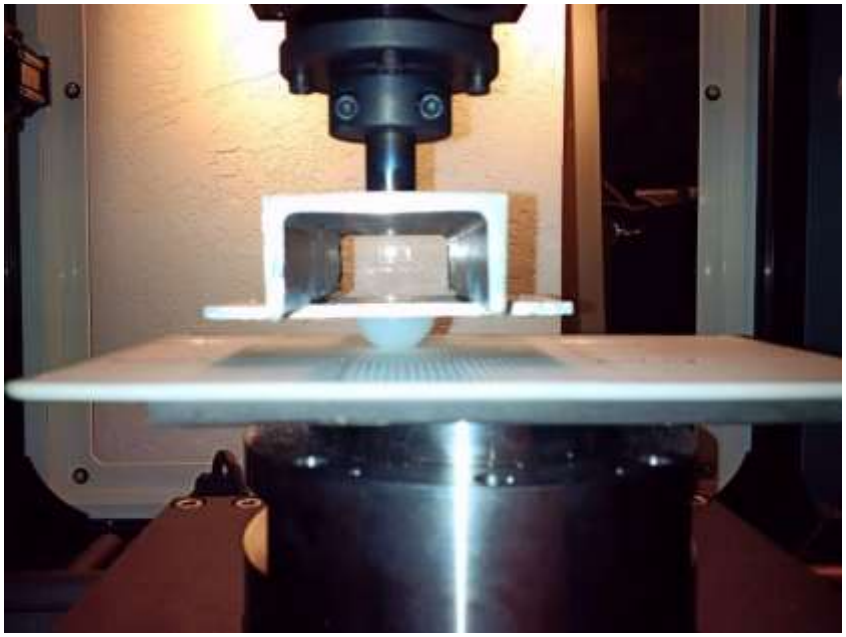

Figure 5.5. The tribometer test setup used to characterize the skin-texture tribology during tactile graphics scanning.

Once data were collected, it became apparent that system noise decreased the signal resolution rather significantly. Running averages were then taken for the loading and COF data in order to properly identify the frequency response and vibrational behaviors. With this data, averages and standard deviations were recorded for maximum peak, minimum peak, amplitude, and overall magnitude, and Fourier transforms were performed to identify the vibrational behavior in each of the sliding tests. It was hypothesized that samples in like groups exhibited loading and vibratory behavior so similar to one another that the mechanoreceptors in the skin were unable to distinguish between the two stimuli, and that COF and vibrational frequency were the driving factors in making these discriminations.

5.3 Results and Discussion

5.3.1 Computational model for dot pair configuration

The purpose of this phase was to determine if the loading and frictional trends and behaviors seen in the experimental braille dot spacing study in Chapter 3 could be recreated using the computational techniques developed for the large-scale single dot investigation from Chapter 4. Based on the findings, the computational spacing behavior is quite similar to the horizontal spacing trends experimentally determined in the skin on braille dot pair study. In the computational simulation, the soft body representing the fingerpad was able to deform and recover much quicker than that of the fingerpad, and this was due to the material's perfectly elastic nature and the quasi-static negation of inertial effects assumed in the simulation. During the fingerpad sliding in the 2.5 mm spacing sample in Chapter 3 (standard spacing during a braille cell), it was believed that the skin did not penetrate between the two dots, and the loading and coefficient of friction behavior large resembled that of a single dot, simply larger in relative magnitude due to the cumulative effect of the dots resisting the lateral deformation.

In the case of the computational modeling, dot spacing had to be reduced to 1.5 mm in order for the homogeneous, elastic dot to slide over both features without penetrating between them and touching the brief baseline surface in between. As the body slid over the pair, the coefficient of friction exhibited a step-like behavior as seen in the single dot simulations (Figure 5.6). And as seen in the previous modeling study, the coefficient of friction dropped below that of the pre-defined interactive surface friction (0.25) due to the back side of each dot propelling the body into the direction of sliding. The secondary effect of the additional dot can be seen in the in a brief dip during the propulsion.

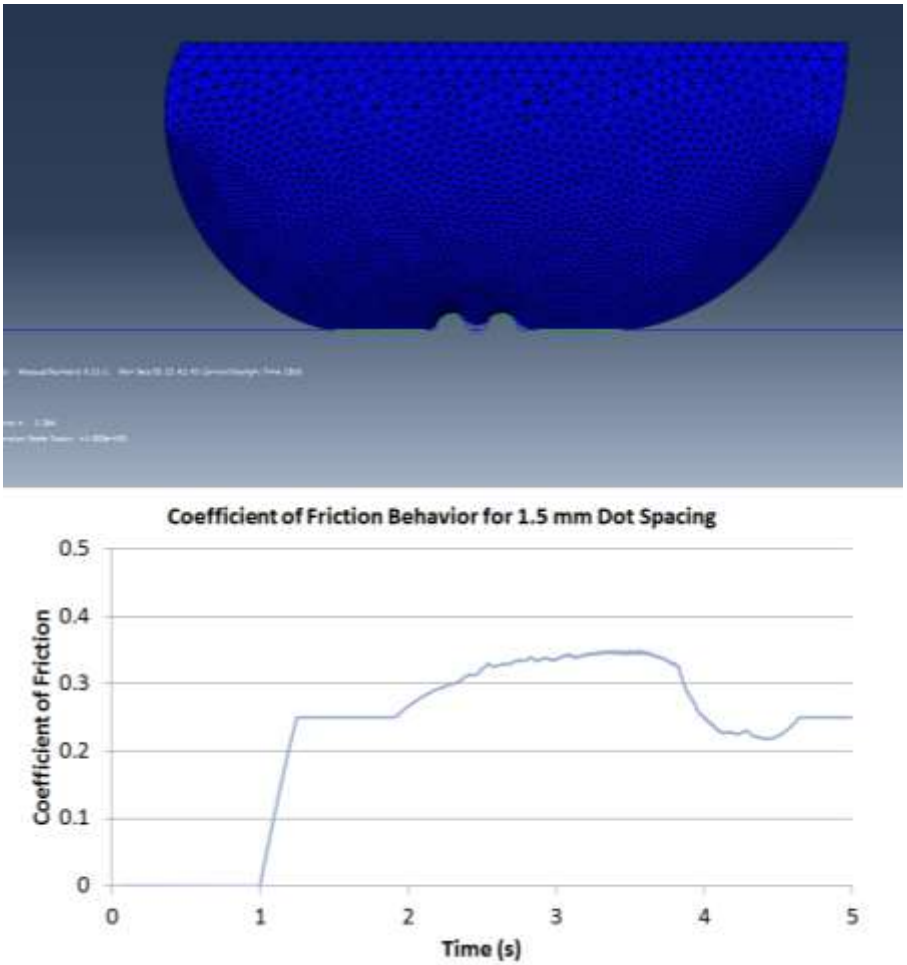

Figure 5.6. Maximum penetration achieved for the soft body sliding over a dot pair with 1.5 mm spacing (top). The coefficient of friction resembles that of a simulated fingerpad sliding over a single dot (bottom).

The unique difference in this model compared to that of the single dot was that the onset of the second dot and its initial cumulative contribution were apparent, where each peak in the vertical loading's two-peak behavior had two smaller peaks superimposed on each. It was believed that the mild penetration between the features produces more of an impact on the lateral loading than the vertical, where contact with the leading edge of the second dot contributed an additional instance of deformation resistance. The cumulative dot effect was most prominently observed in the lateral loading due to contact pressure as the body exited dot contact and transitioned to baseline sliding, where two distinct dips were produced.

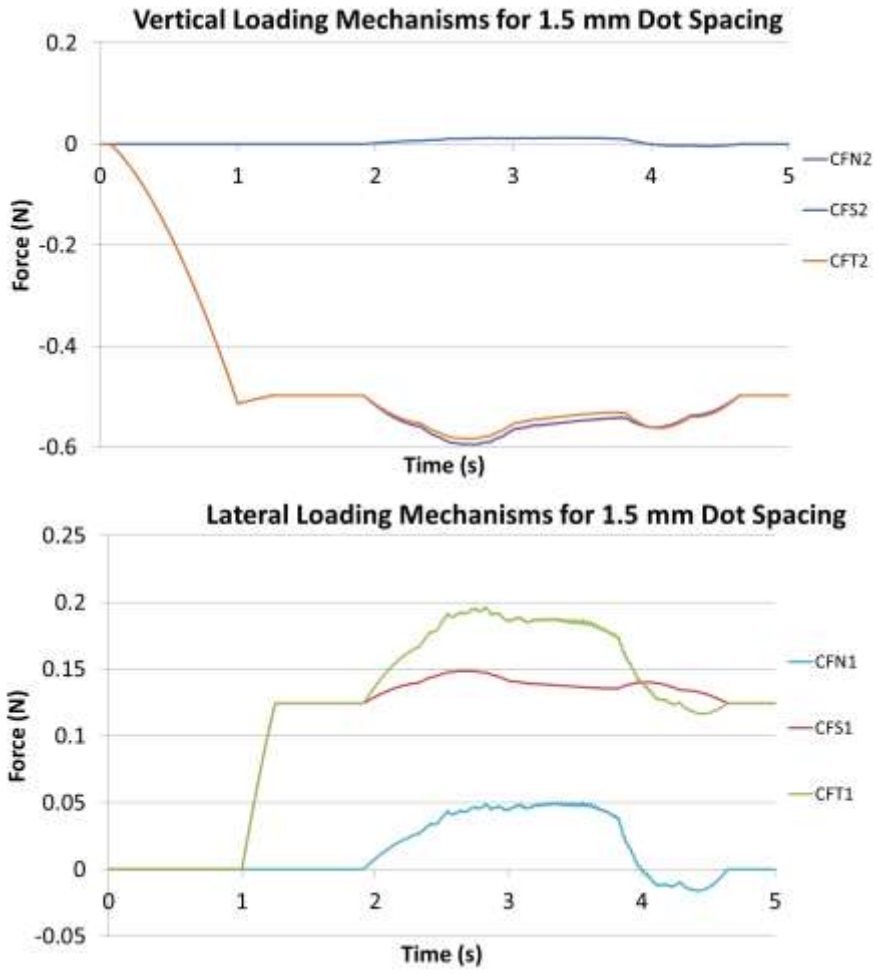

Figure 5.7. The vertical and lateral loading behaviors decomposed by loading mechanism for the 1.5 mm dot pair spacing.

At a spacing of 2.5 mm, the transitional behavior witnessed in the horizontal spacing study in Chapter 3 became much more apparent. Because the dots were sufficiently spaced apart, the soft body friction had an opportunity to briefly normalize after onset contact with the first dot, and once contact with the second dot occurred, the interacting compound effect took place. Additionally, complete penetration between the dots occurred, creating a second instance of dot contact that is superimposed onto the frictional behavior of a single dot.

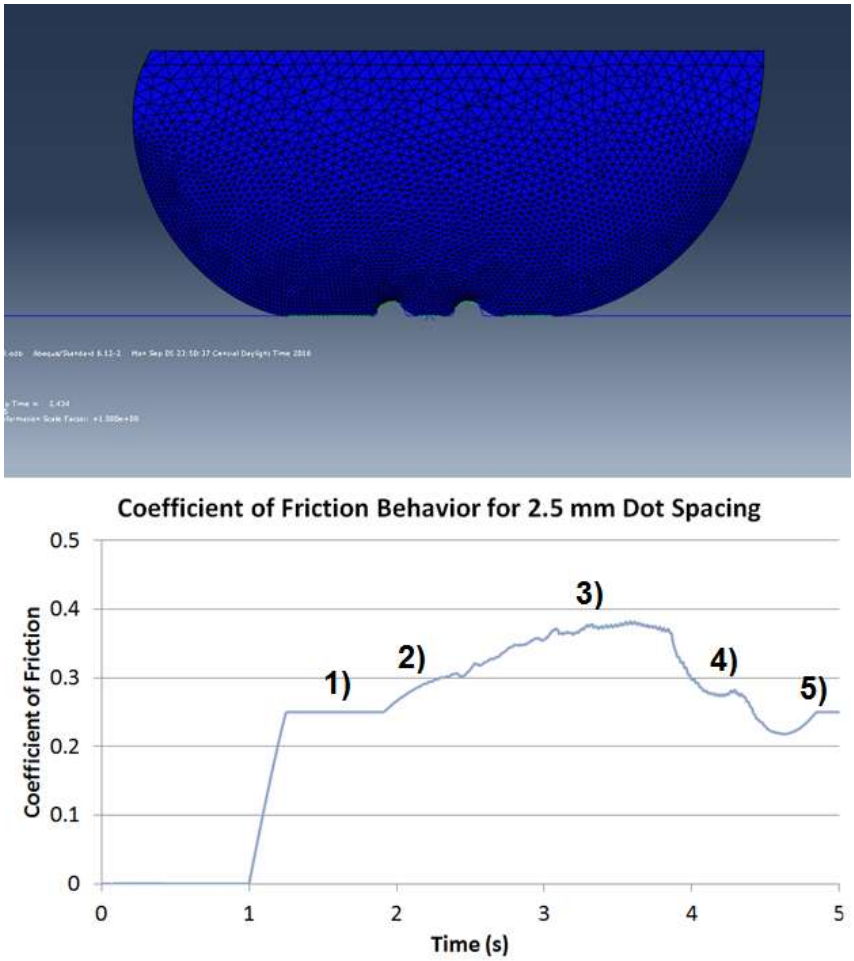

Figure 5.8. Maximum penetration achieved for the soft body sliding over a dot pair with 1.5 mm spacing (top). The transitional coefficient of friction behavior was clearly evident like that seen in the experimental fingertip on braille dot study (bottom).

Interestingly, the dot spacing does not appear to have any impact on the overall magnitude of the vertical load, which reached a maximum near -0.58 N in both spacing cases. The only noticeable change is the phase change of the two-peak behavior due to the timing of sliding during dot contact. The primary component that affected the coefficient of friction behavior was the lateral loading component. The loading due to frictional stress is largely unchanged due to its direct relationship to the vertical loading component. Here, it is clearly evident that the lateral loading due to contact pressure is the driving mechanism, and this is due to the predicted secondary instance of leading edge dot contact. It was hypothesized that as long as the soft body completely surrounds two dot features, the loading behavior would exhibit the cumulative sliding behavior of two independent dots superimposed on top of one another.

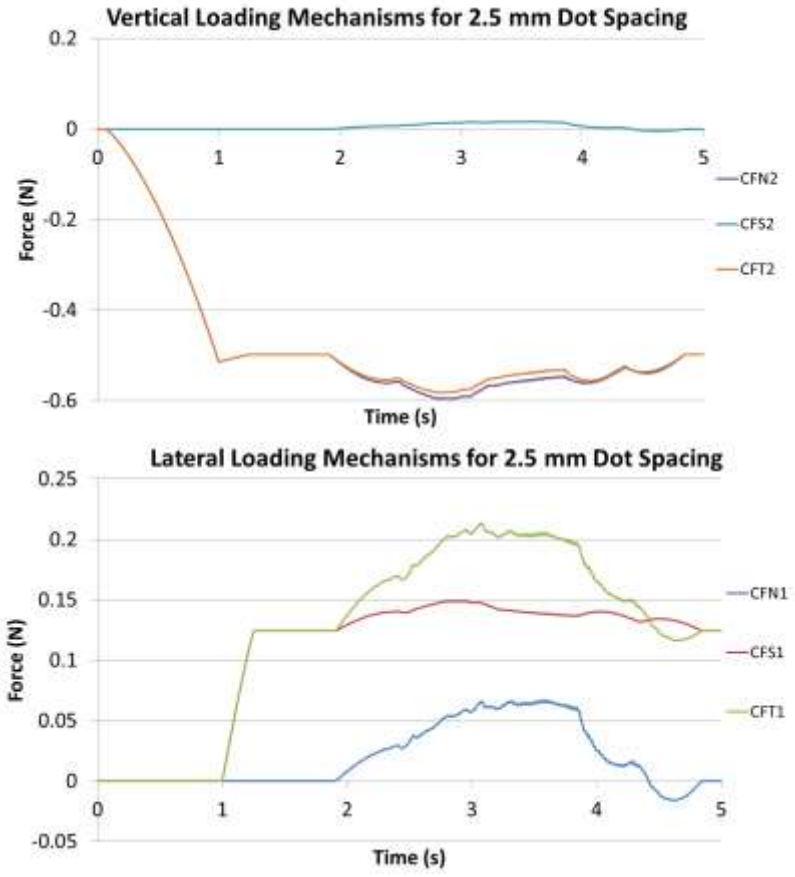

Figure 5.9. The vertical and lateral loading behaviors decomposed by loading mechanism for the 2.5 mm dot pair spacing.

5.3.2 Computational model for simple tactile graphic

Because the aforementioned modeling techniques have proven reliable predictors to observing dot pair behavior like that in a single braille cell, this phase of the study sought to investigate the sliding behavior of a simple tactile graphic that consisted of a series of evenly spaced standard-sized braille dots. Due to the plane strain assumption, this model is analogous to a finger sliding over a series of uniform parallel ridges.

It was hypothesized that the body sliding over the series of dots would produce vibratory loading tendencies, and the data validated that claim. As opposed to previous studies with a finite number of dot features, entering the dot series produced a nearly linear increase in coefficient of friction and lateral load until contact was lost with the leading baseline surface. As the body came into contact with new dots while still remaining in contact with the baseline, it produced increasing resistance forces due to contact with increasing leading edges of the dots. Once contact with the baseline was lost, the first dot no longer pushed against the remainder of the bulk material, and the body quickly reached a steady state of oscillating sliding with a coefficient of friction of mean 0.34.

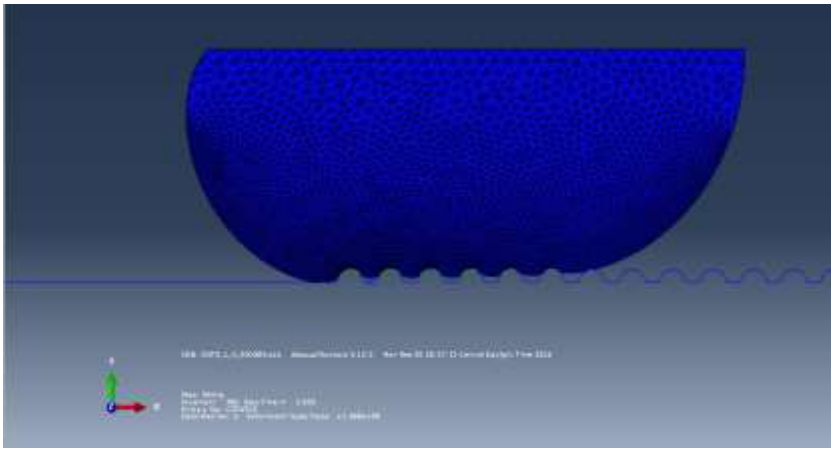

Figure 5.10. The instance of maximum achieved coefficient of friction.

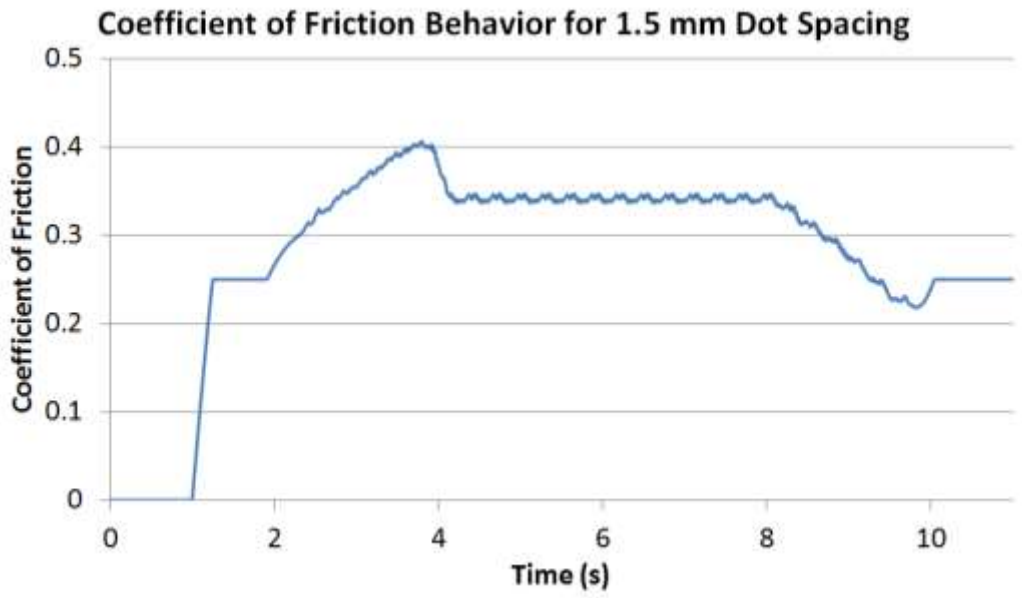

Figure 5.11. The COF behavior of a soft body sliding over a ridged surface of 1.5 mm spacing (bottom).

These oscillations were directly related to the period of the dot features and the sliding speed of the body. At a velocity of 5 mm/s and a dot spacing of 1.5 mm (for the first simulation), the finger came in and out of contact with the dot features at a frequency of 3.33 Hz. Fourier analysis was performed on the signal, and a frequency response of 2.55 Hz dominant. This was found to be an acceptable approximation for the ridge pattern's periodicity due to the asymmetry resulting from the pre-defined adhesive friction component of 0.25. It was believed that if the soft body remained symmetric while sliding over a frictionless surface, the frequency response would have been more representative of the pattern's period. The oscillating loads produce a mean coefficient of frequency of 0.34, with a mean peak to peak of merely 0.008, 2.4% of the mean steady state COF.

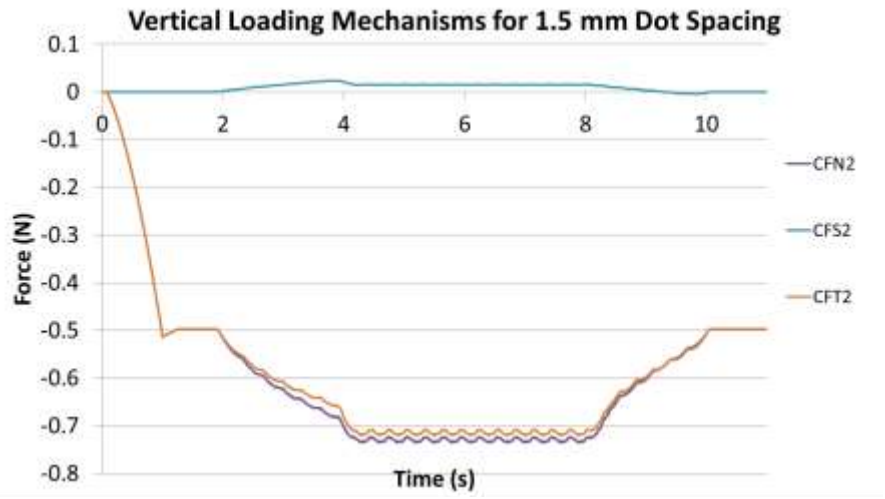

Figure 5.12. The vertical loading behavior decomposed by loading mechanism for the 1.5 mm ridged pattern.

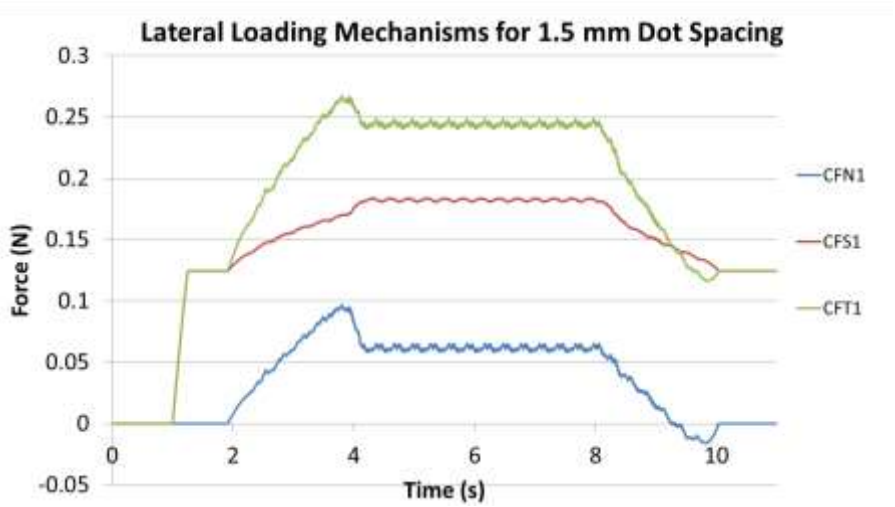

Figure 5.13. The lateral loading behavior decomposed by loading mechanism for the 1.5 mm ridged pattern.

Compared to the ridged pattern with 1.5 mm spacing, the 2.5 mm spacing pattern was much more consistent in coefficient of friction when entering the ridged region and transitioning into steady state vibratory sliding. Because the dots were spread sufficiently far apart from one another, the soft body was able to completely penetrate the gap between each dot, bottoming out and contacting the baseline surface. The complete simultaneous penetration between several dots compounded the cumulative friction to an even greater effect. Once the soft body released contact from the leading baseline surface and steady state sliding was reached, the decrease in coefficient

of friction from the maximum achieved to the steady state COF was significantly less than that seen in the 1.5 mm ridges pattern. For the 2.5 mm ridges, the degree of penetration between dot features was so great that the impact of losing the lateral resistance caused by the leading dot was minimal because each subsequent dot contributed nearly as much as the first.

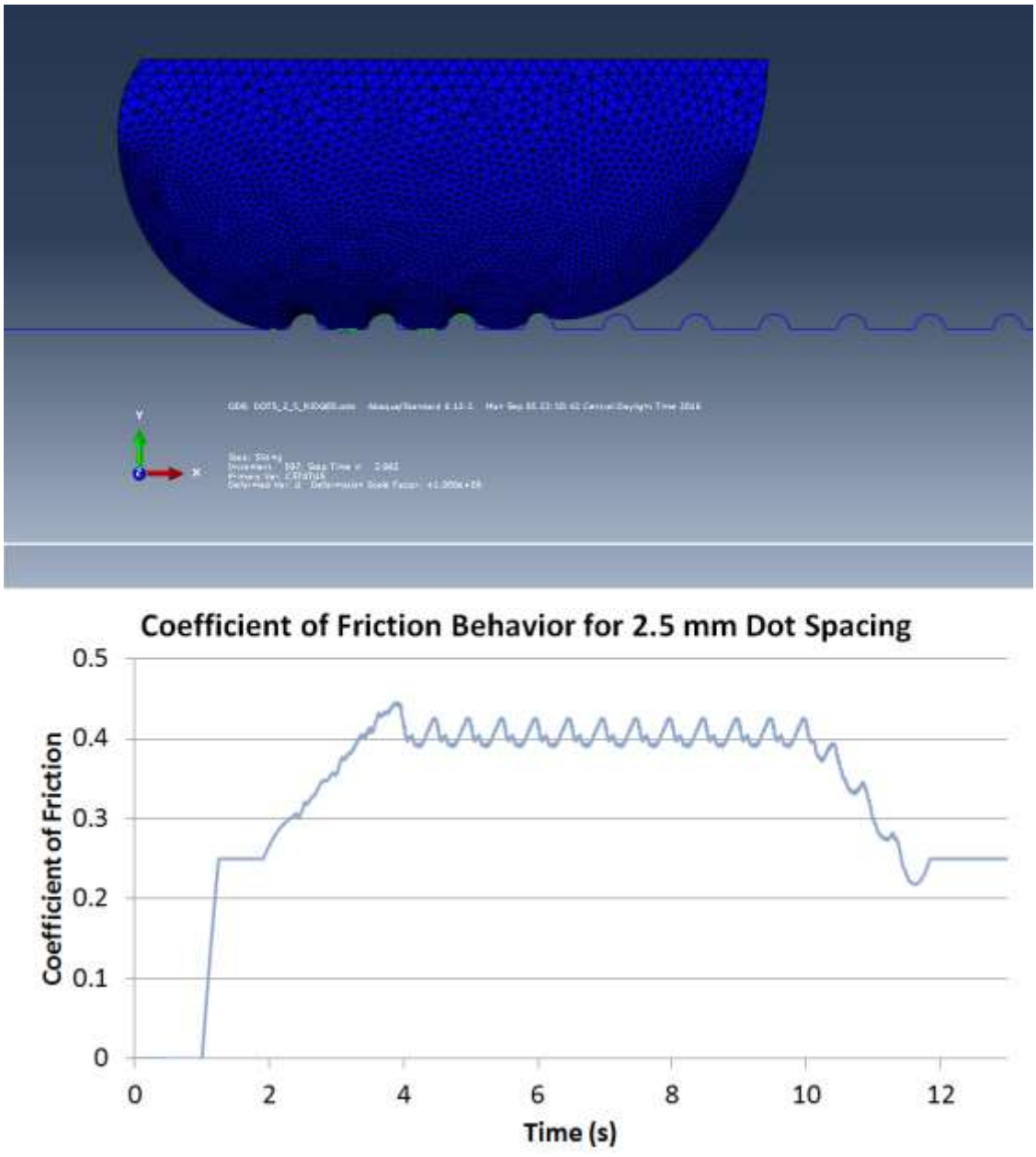

Figure 5.14. The maximum achieved coefficient of friction (top) along with the COF behavior of a soft body sliding over a ridged surface of 2.5 mm spacing (bottom).

Fourier analysis determined that the vibratory frequency exhibited by the oscillating surface was exactly as predicted: 2.0 Hz (5 mm/s sliding over a 2.5 mm period). It was believed that this frequency was much more accurate because the soft body experienced all of the periodic oscillation due to contact as opposed to during sliding over the 1.5 mm spacing pattern. Additionally, the mean coefficient of friction for the steady state oscillatory sliding was much greater at 0.40, with a peak-to-peak change in coefficient of friction was 0.024, triple that of the other case. It was hypothesized that significant differences in oscillatory change in COF contribute to perceptive differences seen in tactile graphics comparisons.

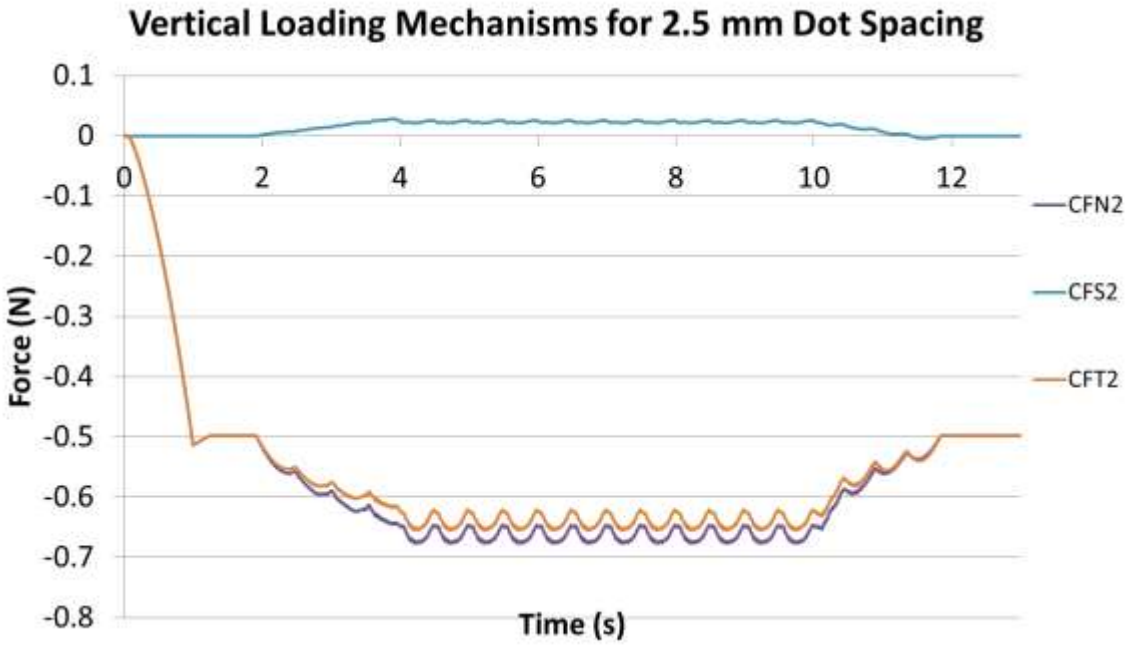

Figure 5.15. The vertical loading behavior decomposed by loading mechanism for the 2.5 mm ridged pattern.

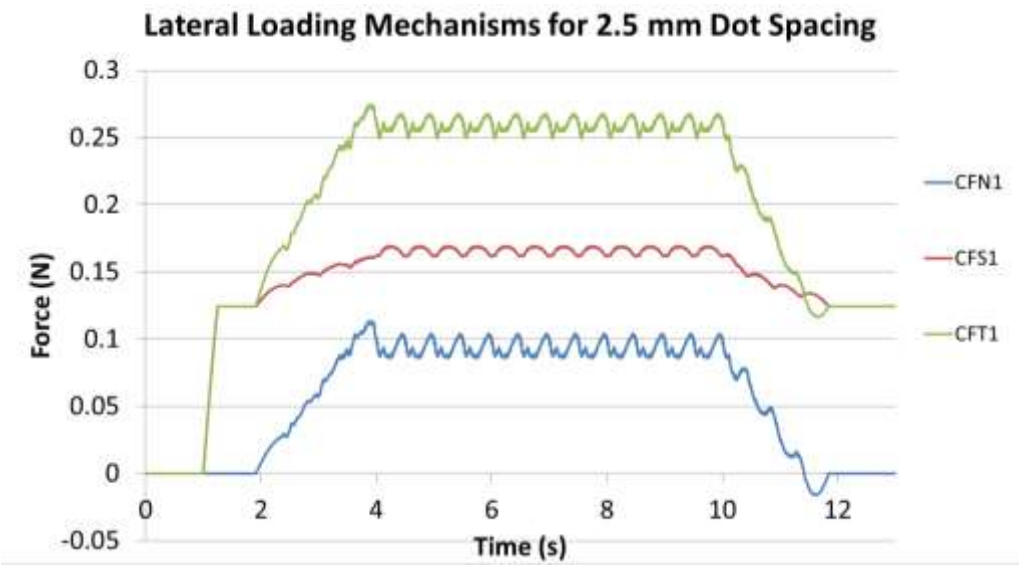

Figure 5.63. The lateral loading behavior decomposed by loading mechanism for the 2.5 mm ridged pattern.

5.3.3 Characterization of tactile graphics organized by perceptive uniqueness

The final phase of this study utilized similar principles in analyzing oscillating patterns in order to better understand the vibratory and friction effects observed when tactually scanning tactile graphics. To do so, a multi-axis tribometer was used to perform displacement controlled tests on polypropylene plaques of varying topographical features. In order to provide a baseline comparison to each of the patterned textures, silicone sliding over a smooth polypropylene surface was performed. Under the same normal loading conditions as the textured tests, a 3.0 N vertical load and 1 mm/s sliding speed yield a coefficient of friction of 0.6 between the silicone sphere and flat surface. Additionally, the maximum contact pressure for the sphere being loaded onto the flat polypropylene was calculated to be 612.4 kPa (Equation 2).

$$p_0 = \frac{1}{\pi}\left(\frac{6 \cdot E^2 \cdot F}{\left[\left(1-\upsilon\right)^2\right]^2 R^2}\right)^{1/3} \tag{3}$$

Where E is the silicone's modulus of elasticity, F is the vertical load, υ is the Poisson's ration of the silicone (assumed to be 0.48), and R is the sphere's radius.

At low loads, the tribometer's high limit load cell resolution was decreased due to system noise, and data was processed with a running average method to smooth out the curve and reduce the system noise. At a sampling rate of 1,000 Hz, the data's integrity was maintained by using a small subset range of 100 data points over 0.01 s. Figure 5.14 provides an example of reducing the input raw data to a useful periodic signal.

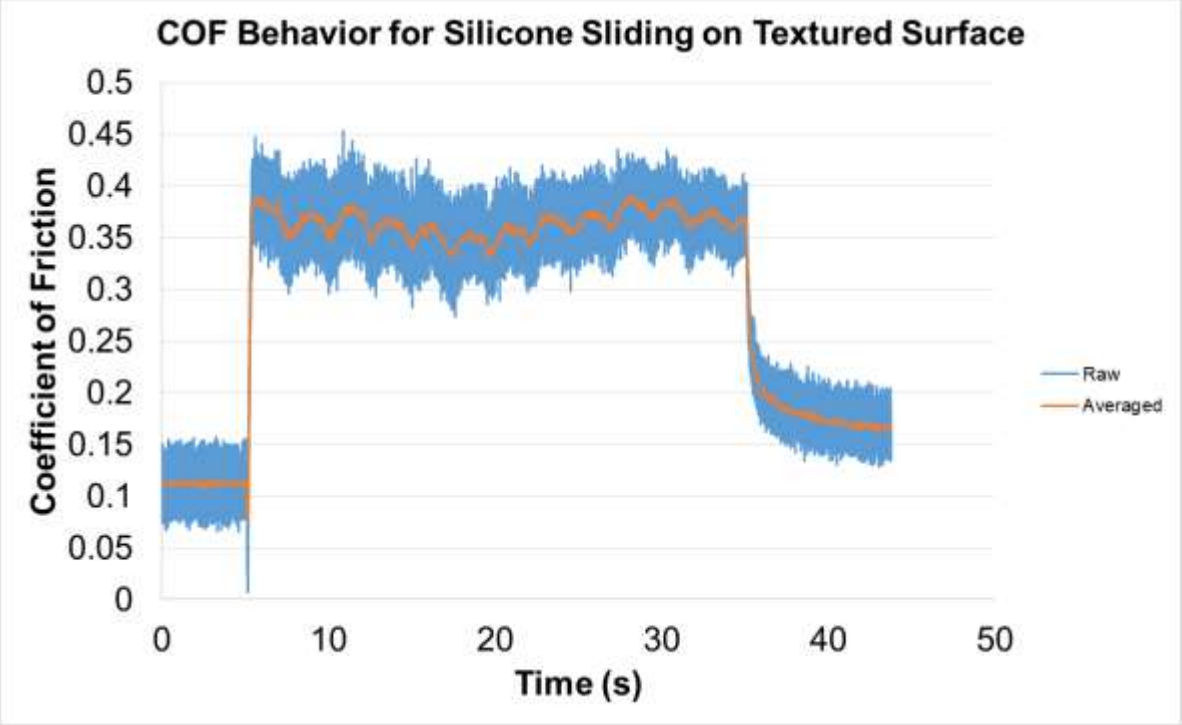

Figure 5.17. An example of raw data taken from a tactile graphic that is distorted with system noise (blue) and its periodic, filtered form (red).

It was hypothesized that a combination of experienced tactile frequency, COF magnitude, and vibratory tactile frequency play a role in tactile perception as defined by the Braille Authority of North America when designing tactile graphics. Based on testing and accompanying analysis, the samples all exhibited similar overall magnitudes in coefficient of friction under sliding with the silicone sphere. This alone implies that coefficient of friction alone is not a predictor of tactility. BANA defined samples A and B as perceptively similar to one another, yet their tactile frequencies and oscillating change in COF were quite different from one another. This finding was perplexing

due to the fact that samples C and D were far more similar in overall COF and oscillation, yet the tactile graphics guidelines state that they may be placed adjacent to one another due to perceptive uniqueness.

Table 5.1. Surface and tribological parameters defining the tactile graphics samples tested under loading conditions analogous to braille reading and tactile exploration.

Sample	Pitch (mm)	Expected Tactile Frequency (Hz)	Fourier Response (Hz)	Magnitude (COF)	Peak-to-Peak (COF)
A	0.6	1.67	1.6	0.45	0.005
B	1.45	0.69	0.67	0.47	0.013
C	1.74	0.57	0.56	0.44	0.014
D	2.34	0.43	0.4	0.38	0.016
E	Non-textured with non-directional 0.15 μm Ra surface roughness				0.6

For the grid-like textures, some trials exhibited significantly lower coefficients of friction and peak to peak values than the others, and this may have been attributed to the travel path of the silicone sphere. It was believed that for trials such as these, the sphere traveled along a ridge in the direction of sliding, and due to its stiffness, it did not deform around the ridge in the Y-direction. This lack of deformation simulated the sphere sliding on a smoother surface as opposed to a texture, and is one way that it may not have been perfectly representative of a human fingertip. And this claim was validated the trial's associated Fourier analysis. Here, the frequency response did not indicate any significant vibratory behavior.

The dependency of travel path on tactile frequency and COF may have been one of the reasons that the grid-like patterns were labeled as tactually unique from the parallel ridged textures and others listed in the graphics guidelines. The grid patterns (and others in their tactility group) were uniform in two directions of motion, whereas the ridges exhibit different frictional behaviors

depending on the direction of sliding. These geometric-based reasons appeared to be straightforward explanations for samples that were identifiably different, visually speaking, but it remains unclear why topographically similar textures with quantifiably similar tribological behaviors are perceived differently.

This question requires more thorough analysis and additional work to be performed in order to better relate the perceptibility of tactile graphics with that of tribological behavior and topographical parameters. One potential direction that could prove extremely useful would be to perform a multi-directional study on uniform and non-uniform spatial patterns (i.e. grids, ridges, dots, hashes, etc.), investigating the tactile frequencies, coefficients of friction, and oscillation COF of each surface, perhaps complemented with human perception evaluations to relate to the tribological testing. With an effective experimental design and data analysis, a tactually spatial exploratory study combined with EEG-ERP could provide a vital breakthrough in the ability to engineer for tactility.

5.4 Conclusions

Computational modeling and tribological tests were used to investigate more complex tactile configurations, exploring different tactile graphics and seeking to understand the relationship between their topographical features and pre-defined tactile uniqueness or similarity. Based on the findings, the following conclusions can be drawn:

- Two-dimensional computational modeling can effectively model the dot spacing effects of one-directional sliding over braille dot pairs and more complex dot configurations.
- For sufficiently small feature spacings, the soft body is unable to penetrate the feature gap, and frictional behavior resembles that of a single, independent feature; sufficiently large

spacings allow for complete penetration, resulting in cumulative frictional effects caused by each feature's interaction with the body.

- Axially uniform patterns produce a vibratory response in the loading behavior, and this causes the coefficient of friction to oscillate in the same manner, where the peak-to-peak values are dependent on the degree of body penetration between the features.
- Coefficient of friction alone is an insufficient tool to identify tactile graphics as perceptively unique, and further research is required to truly relate tribological parameters such as tactile frequency and oscillation COF to a surface's tactile attributes.

5.5 References

[1] Guidelines and Standards for Tactile Graphics, 2010. 2011, The Braille Authority of North America.

[2] Kenins, P., Influence of Fiber Type and Moisture on Measured Fabric-to-Skin Friction. Textile Research Journal. 64(12): p. 722-728.

[3] Sivamani, R.K., et al., Coefficient of friction: tribological studies in man – an overview. Skin Research and Technology. 9(3): p. 227-234.

[4] Sivamani, R.K., et al., Friction coefficient of skin in real-time. Skin Research and Technology, 2003. 9(3): p. 235-239.

[5] Gitis, N. and R. Sivamani, Tribometrology of Skin. Tribology Transactions. 47(4): p. 461-469.

[6] Gwosdow, A.R., et al., Skin Friction and Fabric Sensations in Neutral and Warm Environments. Textile Research Journal. 56(9): p. 574-580.

[7] Derler, S., U. Schrade, and L.C. Gerhardt, Tribology of human skin and mechanical skin equivalents in contact with textiles. Wear, 2007. 263(7–12): p. 1112-1116.

[8] Darden, M.A. and C.J. Schwartz, Investigation of skin tribology and its effects on the tactile attributes of polymer fabrics. Wear, 2009. 267(5): p. 1289-1294.

[9] Skedung, L., et al., Finger Friction Measurements on Coated and Uncoated Printing Papers. Tribol Lett. 37(2): p. 389-399.

[10] Skedung, L., et al., Tactile perception: Finger friction, surface roughness and perceived coarseness. Tribology International, 2011. 44(5): p. 505-512.

[11] Derler, S., et al., Friction of human skin against smooth and rough glass as a function of the contact pressure. Tribology International, 2009. 42(11): p. 1565-1574.

[12] Bobjer, O., S.-E. Johansson, and S. Piguet, Friction between hand and handle. Effects of oil and lard on textured and non-textured surfaces; perception of discomfort. Applied Ergonomics, 1993. 24(3): p. 190-202.

[13] Smith, A., et al., Role of friction and tangential force variation in the subjective scaling of tactile roughness. Exp Brain Res. 144(2): p. 211-223.

[14] Amaied, E., et al., Aging effect on tactile perception: Experimental and modelling studies. Wear, 2015. 332: p. 715-724.

[15] Darden, M.A. and C.J. Schwartz, Skin tribology phenomena associated with reading braille print: The influence of cell patterns and skin behavior on coefficient of friction. Wear, 2015.

[16] Darden, M.A. and C.J. Schwartz, Investigation of friction mechanisms during the sliding of elastomers against hard parallel-ridge textures. Tribology International, 2013. 63(0): p. 2-7.

CHAPTER 6: GENERAL CONCLUSIONS

Based on the research objectives described at the beginning of this dissertation, the conclusions from the current research work could be divided into three categories: 1) Pertaining to observing and detecting tactility, 2) Identifying the fundamental friction and loading mechanisms in skin-on-braille sliding, and 3) applying the mechanisms to relate them to tactility and perception.

The study described in Chapter 2 focused on observing and detecting tactility. This study aimed to determine if electrophysiological observation techniques such as electroencephalography (EEG) and event-related potential (ERP) could be applied to detecting and measuring tactile perception in the same way that they are implemented in studying the brain's neural response to visual or auditory cues. It was determined that EEG-ERP had the potential to be a useful tool in measuring tactile responses in real time, where both the parietal and central-parietal regions of the brain positively responded to the stimuli. But it was concluded that additional studies need to be performed to effectively characterize how the brain is expected to respond to a stimulus.

The fact that these techniques have not been extended to the tactile domain means that reference data and a priori knowledge regarding these applications do not exist, inhibiting the ability to effectively analyze acquired data. Many tactile evaluation studies involve human test groups who are professionally trained and have developed calibrated sensations. Combining the data taken from trained test groups with the accompanying EEG-ERP response data could lead to developing the very foundation of knowledge necessary to effectively quantifying and designing for tactility. Once this platform is developed, surface engineering and the design for haptic experience will no longer be such an inefficient trial-and-error "shotgun" approach, but can drastically broaden the potential of product design.

The second category, the identification of friction and loading mechanisms, was addressed in Chapters 3 and 4. Chapter 3 was a two-phase study that investigated the effect of braille dot size on friction mechanisms as well as the effect of braille dot spacing on friction behavior. Skin on braille sliding was found to resemble Hertzian contact mechanics, allowing it to be directly related to conventional friction models. The dot size study determined that contrary to previous friction models, deformation can play an enormously impactful role on sliding when investigated from macroscopic perspective. Sufficiently large surface features are capable of influencing sliding so significantly that friction effects due to adhesion are outweighed and can be neglected. The second phase determined that the spacing between features can significantly influence skin-on-braille sliding, where additional features additively affect the lateral loading and coefficient of friction. The study in Chapter 4 applied the models from Chapter 3 and involved developing a large-scale skin-on-braille testing apparatus to observe the specific loading mechanisms experienced during braille reading, as well as validating these claims with computational models. It was discovered that the introduction of a braille dot influences vertical and lateral loading through two means: due to contact pressures normal to the surface, or due to frictional stresses tangent to the surface. Loading due to contact pressures were the dominant mechanism in the vertical direction, and contact pressure and frictional stresses were equally contributory to lateral loading trends experienced as the finger slides over the dot feature.

This understanding of the frictional behavior and loading trends has highlighted the impact that macroscopic surface topographies have during soft-bodied sliding instances such as braille reading. If adhesion was found to be largely dominated by the deformation component of friction, it can be reasoned that under like material conditions, unique surface topographies would produce unique friction behaviors and loading profiles, all due to varying degrees of surface displacements

experienced at the interface. In the case of braille, if coding standards and limitations in perceptive resolution reduce the opportunity for innovating or redesigning the language to aid the reader, surface engineering techniques must be implemented to modulate frictions experienced during scanning. Further studies investigating the impact of how changing the surface topography affects soft-body surface displacements and the resulting tensile and compressive fluctuations would be most useful. It should also be noted that while the large-scale empirical and computational studies assumed plane strain mechanics, it would prove beneficial to perform a large-scale three-dimensional representation to verify the claims and determine if out-of-plane strain behaviors influence loading behaviors in any manner.

Lastly, Chapter 5 intended to apply the principles gained from Chapters 3 and 4 in order to quantify and better understand the tactile effects experienced in simple tactile graphics. Computational modeling and empirical testing were incorporated to investigate how topographical properties such as surface geometries and tribological effects such as oscillatory loading and period changes in coefficient of friction relate to tactile graphics of known perceived uniqueness. It was determined that while coefficient of friction is believed to be one component used to relate tactility to tribology, it alone cannot be used to make decisions that govern perception. As opposed to characterizing tactile graphics in one-directional sliding, future work that investigates spatial scanning of topographical surface could prove useful in determining how surface variability and directionality of known surfaces can affect perceived friction and its associated tactility.

APPENDIX: EXPLORING A HYPERELASTIC MATERIAL MODEL FOR COMPUTATIONAL SIMULATIONS OF SKIN ON BRAILLE

Throughout this dissertation, skin on the human fingertip was assumed to exhibit linear elastic behavior, represented by the polyurethane rubber's constant modulus of elasticity of 1.35 MPa and a Poisson's ratio of 0.48. While similarities were found between the empirical studies and the simplified assumptions, the sliding deformations behave in a more hyperelastic manner due to the increased magnitude of bulk deformation, where linear elastic behavior assumes small-scale deformation.

Following the completion of the presented work, the large-scale computational simulation from Chapter 4 was revisited in order to further investigate the sliding behavior under a more realistic material model. Like plastics and rubbers, the modulus of elasticity of skin does not remain constant under significant deformations. Instead, the stress-strain behavior exhibits linearity under small deformations stiffens and dampens to a plateau under increasing deformations. Modeling skin as a Neo-Hookean solid characterizes its material properties into two terms - the shear modulus, G, and the bulk modulus, K:

$$G = \frac{E}{2(1+\upsilon)} = 0.46MPa \tag{1}$$

$$K = \frac{E}{3(1-2\upsilon)} = 11.25MPa \tag{2}$$

Where E is the modulus of elasticity and υ is Poisson's ratio. The combination of these terms in a hyperelastic model take into consideration the bulk material's response to shear strain as well as its compressibility due to uniform pressure, generating a stiffness dampening effect.

Follow-up simulations replicating the same empirical sliding interactions with a Neo-Hookean material model were found to represent the loading and COF behavior of the tribometer testing results much more closely than the linear elastic assumption. The hyperelastic material model effectively represented the lateral loading behavior because the loading in the horizontal direction takes place independently of the sample's upper geometry and was solely determined by variations in stiffness due to the resulting bulk flow. Where the linear elastic model controlled the bulk flow over the contour rather consistently, the Neo-Hookean behavior allowed for more rapid changes in stiffness and Poisson-driven deformation. Conversely, the two-peak behavior observed during both the empirical study and the linear elastic model was nearly absent from the Neo-Hookean model. This variation in vertical loading behavior may be attributed to the difference in the soft-bodies' upper cross sections and the manner in which they were affixed and displaced. Unlike the linear elastic model, the hyperelastic soft body was never able to achieve full corner penetration prior to the dot due to deformation stiffening.

It should be noted that because the hyperelastic material model incorporates damping stiffness, vertical displacement was increased from 5 mm to 7 mm in order to replicate the tribometer test and achieve a similar degree of baseline surface contact when fully surrounding the dot contour.

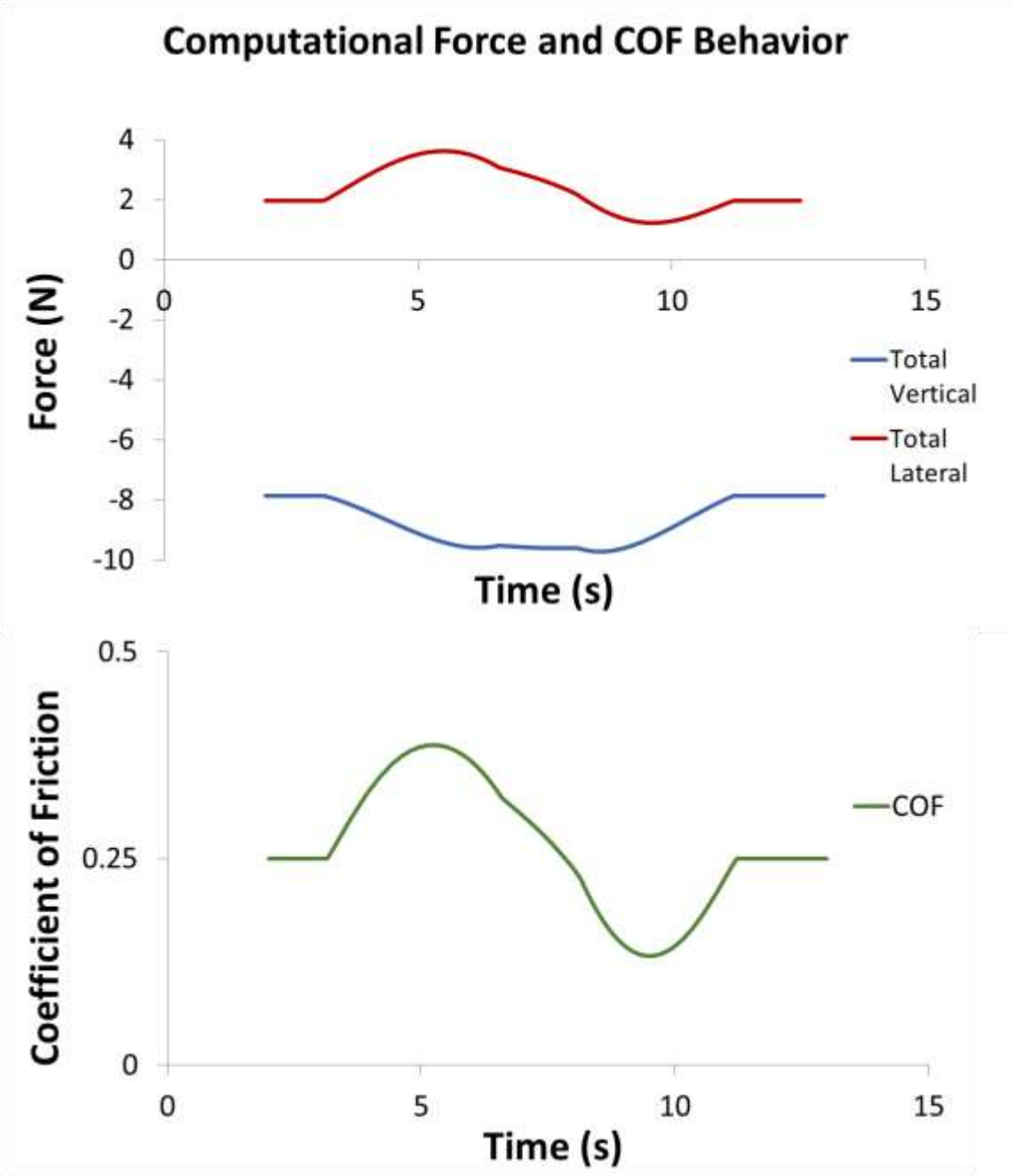

Figure A.1 The loading behavior from a simulation incorporating a Neo-Hookean hyper elastic material model more closely represents the data from the large-scale empirical testing.

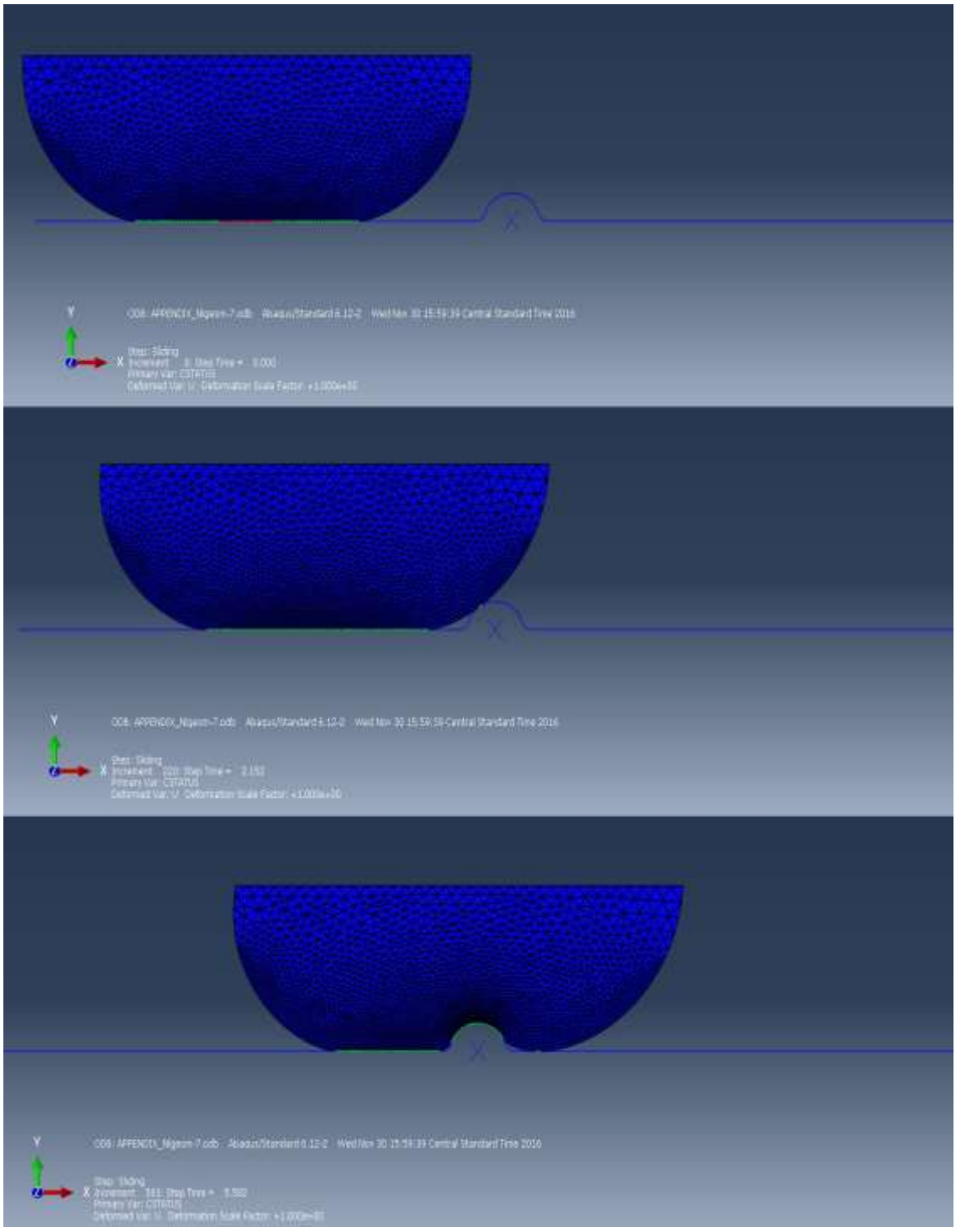

Figure A.2 The sliding storyboard for the hyperelastic simulation (from top to bottom): vertical displacement, onset dot contact, and onset contact with trailing baseline surface.

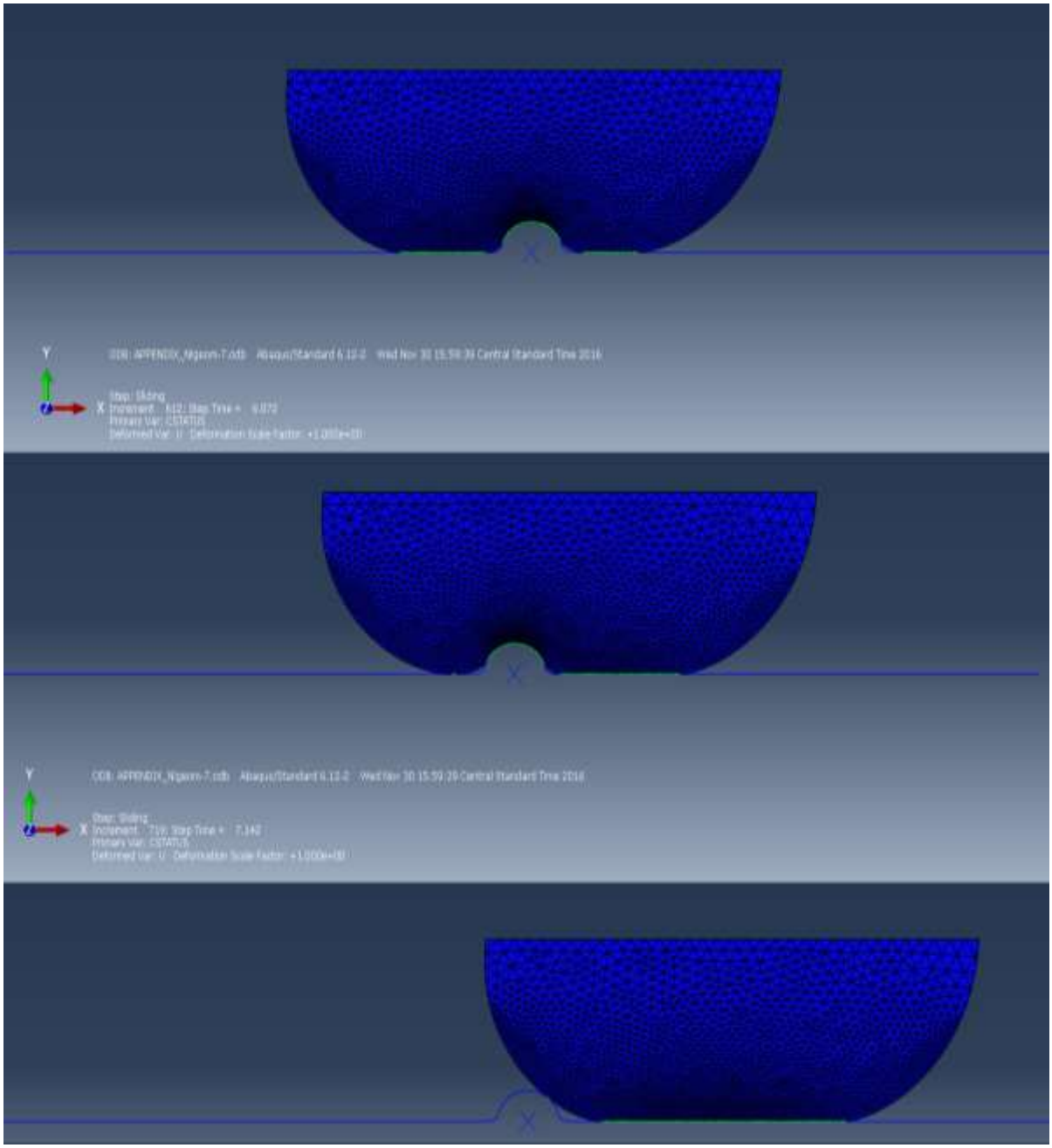

Figure A.3 The sliding storyboard for the hyperelastic simulation (from top to bottom): midpoint sliding, release of leading baseline surface, and release of dot contact.